NASA SP-8103

NASA
SPACE VEHICLE
DESIGN CRITERIA
(ENVIRONMENT)

THE PLANETS URANUS, NEPTUNE, AND PLUTO (1971)

NOVEMBER 1972

NATIONAL AERONAUTICS AND SPACE ADMINISTRATION

FOREWORD

NASA experience has indicated a need for uniform criteria for the design of space vehicles. Accordingly, criteria have been developed in the following areas of technology:

Environment
Structures
Guidance and Control
Chemical Propulsion

Individual components of this work are issued as separate monographs as soon as they are completed. A list of the titles that have been published to date can be found at the end of this monograph.

These monographs are to be regarded as guides to design and not as NASA requirements except as may be specified in formal project specifications. It is expected, however, that the monographs will be used to develop requirements for specific projects and be cited as the applicable documents in mission studies or in contracts for the design and development of space vehicle systems.

This monograph was prepared under the cognizance of the Goddard Space Flight Center with Scott A. Mills as program coordinator. The principal author was Frank Don Palluconi of the Jet Propulsion Laboratory. Valuable contributions were also made by A. J. Beck and Neil Divine of the Jet Propulsion Laboratory.

Comments concerning the technical content of these monographs will be welcomed by the National Aeronautics and Space Administration, Goddard Space Flight Center, Systems Reliability Directorate, Greenbelt, Maryland 20771.

October 1972

For sale by the National Technical Information Service, Springfield, Virginia 22151 – Price $3.00

CONTENTS

THE PLANETS URANUS, NEPTUNE, AND PLUTO (1971)

1. INTRODUCTION

The design of space vehicles which are intended to encounter and investigate the planets Uranus, Neptune, and Pluto requires both qualitative and quantitative descriptions of the expected environment. Although somewhat different data sets are required for the design of flyby, orbiter, atmospheric entry, and lander spacecraft, the paucity of present data permits inclusion of pertinent information for all four types of missions in one monograph.

In the process of evaluating information about these planets, assessments were made of the potential effects of environmental properties on vehicle performance so that appropriate descriptions for vehicle and subsystem design could be formulated. The design criteria presented are not specific to a particular mission and are given without reference to the circumstances of encounter except that encounter during the 1980's is assumed.

The information presented here reflects published information available through September 1971. Knowledge of the three planets is derived from data obtained at the angular and spectral resolution possible with Earth-based, aircraft, rocket, and balloon borne instrumentation and supplementary data from spacecraft observation of these planets and interplanetary particles and fields. Principally because of observational difficulties, the planets Uranus, Neptune, and Pluto have not shared in the revival of interest in planetology of the past 20 years. Consequently, a number of important properties such as magnetic field strength, trapped particles, and atmospheric composition and structure are either unknown or very uncertain. If the uncertainties in a given parameter are too large to be useful in spacecraft design, it is so stated and no criteria are given.

Section 2, State of the Art, discusses current understanding of the environment of Uranus, Neptune, and Pluto and forms the basis for the environments given in section 3, Criteria.

Other monographs in this series describe the environments of Mercury, Venus, Mars, Jupiter, and Saturn as well as terrestrial environments pertinent to space vehicle design. All are listed at the end of this monograph.

2. STATE OF THE ART

The observations and theory that are pertinent to the current state-of-the-art description of Uranus, Neptune, and Pluto are contained in this section. Appendix A explains notations and symbols, appendix B gives numerical constants and mathematical formulas, and appendix C is the glossary.

2.1 General Physical Properties

The general physical properties to be considered are the mass of the three planets and their radius, shape, mean density, rotational pole location, and mean orbital elements.

2.1.1 Mass

Mass determinations for the planets are usually reported as a ratio of the mass of the Sun to the mass of the planet, $M_\odot/M_p$. Table I contains recent individual determinations of this ratio for Uranus, Neptune, and Pluto and values taken from summaries by Klepczynski et al. (ref. 1) and Kovalevsky (refs. 2 and 3). The formal errors associated with the individual determinations listed in table I do not adequately reflect the systematic error in the theories used. Despite these difficulties the two independent summaries by Klepczynski et al. (ref. 1) and Kovalevsky (refs. 2 and 3) lead to values for the mass ratio which are in good agreement for Uranus and Neptune.

For this monograph, the nominal values given by Kovalevsky (ref. 3) for Uranus and Neptune will be adopted with uncertainty in the mass ratio for Neptune increased to that given by Kovalevsky (ref. 3) for Uranus. Although the recent determinations by Seidelmann et al. (ref. 7) and Gill and Gault (ref. 8) for the mass ratio of Neptune are in excellent agreement, the spread of older values in references 1, 2, and 3 indicates an uncertainty of ±200 is reasonable. Table I indicates the mass of Pluto is not well established. The investigations by Seidelmann et al. (ref. 10) and especially Ash et al. (ref. 11) demonstrate the sensitivity of the derived mass to the span and type of observation used. Here the range given by Ash et al. will be adopted with a central value obtained from the geometric mean of the limits.

The mass ratios adopted are:

$$M_\odot/M_U = 22{,}800 \pm 200$$

$$M_\odot/M_N = 19{,}300 \pm 200$$

$$^{*}M_\odot/M_P = 3{,}500{,}000 \times 1.7^{\pm 1}$$

With the constants given by Melbourne et al. (ref. 12) and Mechtly (ref. 13), the foregoing mass ratios can be converted to kilograms and the results of such computations have been

*In this notation 3.5×10^6 is the nominal value, $3.5 \times 10^6 \times 1.7^{+1}$ is the upper limit, and 3.5×1.7^{-1} is the lower limit.

TABLE I

RECENT ESTIMATES OF THE SYSTEM MASS RATIO, $M_\odot/M_p$, FOR URANUS, NEPTUNE, AND PLUTO

Source	Mass Ratio $M_\odot/M_p$	Satellite, Planet, or Technique Used
	URANUS	
Klepczynski et al. (ref. 4)	22,692 ± 33	Saturn (1913-1968)
Lieske et al. (ref. 5)	22,650 ± 100	Preliminary 9 planet integration with optical data (1910-1969)
Harris (1950) from Brouwer and Clemence (ref. 6)	22,934 ± 6	Uranian satellites
Klepczynski et al. (ref. 1)	22,800 ± 107	Weighted mean
Kovalevsky (ref. 3)	22,800 ± 200	Probable value
	NEPTUNE	
Lieske et al. (ref. 5)	19,500 ± 150	Preliminary 9 planet integration with optical data (1910-1969) plus radar and Mariner 5 data
Seidelmann et al. (ref. 7)	19,349 ± 28	Uranus (1781-1968)
Gill and Gault (ref. 8)	19,296 ± 9	Triton (1887-1958)
Klepczynski et al. (ref. 1)	19,325 ± 26	Weighted Mean
Kovalevski (ref. 3)	19,300 ± 100	Probable Value
	PLUTO	
Lieske et al. (ref. 5)	1,617,000 ± 120,000	Preliminary 9 planet integration with optical data (1910-1969)
Duncombe et al. (ref. 9)	1,812,000	Neptune (1846-1968)
Seidelmann et al. (ref. 10)	$(3 \pm 0.5) \times 10^6$	Neptune (1846-1968)
Ash et al. (ref. 11)	$(4 \pm 2) \times 10^6$	Numerical experiments and a priori density considerations

adopted as design criteria and are given in tables XII, XXIII, and XXXIV (sec. 3). Expressed in Earth masses, the masses of Uranus, Neptune, and Pluto are as follows:

$$M_U/M_\oplus = 14.60 \pm 0.13$$

$$M_N/M_\oplus = 17.25 \pm 0.18$$

$$M_P/M_\oplus = 0.095 \times 1.7^{\pm 1}$$

The uncertainties in the masses of Uranus and Neptune are quantitatively the largest among solar system planets and are both about 1 percent. These uncertainties are comparable to the mass of Pluto. Relative to its size, the mass of Pluto is more uncertain than any other planet and several major satellites.

2.1.2 Radius, Shape, and Mean Density

Discussion of these quantities is facilitated by comparing Uranus and Neptune, and treating Pluto separately. The radius values adopted for Uranus and Neptune should be associated with atmospheric parameters through the procedure given in section 2.3.7.

2.1.2.1 Uranus and Neptune

Table II gives a partial listing of the numerous attempts to measure the equatorial radius R_{eq}, polar radius R_{pl}, and oblateness (ϵ) of Uranus and Neptune. For Neptune, the results derived from the 1968 stellar occultation are superior to all other present determinations for two reasons. First, the systematic and random errors associated with the occultation result are smaller than other methods. Second, the radius derived from the occultation can be associated with atmospheric parameters such as number density more directly than radii obtained by other methods.

Comparison of the filar micrometer, discometer, and double image micrometer results for Uranus with those for Neptune indicates the relationships between these methods is the same for both planets. If the equatorial radius for Neptune that was derived from the occultation is accepted, scaling for Uranus can be accomplished as given in table III. The mean of 27,000 km for the equatorial radius of Uranus obtained from this procedure is appreciably larger than given by most references. This direct scaling procedure assumes that the linear difference between an optical measurement and the occultation result for Neptune can be transferred directly to Uranus. If on the other hand the angular difference rather than the linear difference is used, a mean of 26,300 km is obtained for the equatorial radius of Uranus.

From Earth, both Uranus and Neptune are faint objects with small, somewhat limb-darkened disks. This combination could reduce the apparent diameter as measured with micrometer and discometer devices. From table II it can be seen that the double image micrometer measurements depend on the size telescope used with the smaller aperture giving the smaller radius.

TABLE II

ESTIMATES OF THE RADIUS AND SHAPE OF URANUS AND NEPTUNE

Source	R_{eq} (km)*	$R_{p\ell}$ (km)	ϵ	Remarks
		URANUS		
Dollfus (ref. 14)	26,700 ± 2,100	26,200 ± 1,300	0.073 ± 0.015	Mean of filar micrometer measurements with telescopes $\geqslant$ 45 cm in diameter
Dollfus (ref. 14)	23,700			Mean of discometer results with 60 & 200 cm diameter telescopes
Dollfus (ref. 14)	24,600 ± 500			Mean of double image micrometer measurements with 60 cm diameter telescope
Dollfus (ref. 14)	25,400 ± 280	24,700 ± 280	0.030 ± 0.008	Mean of double image micrometer measurements with 107 cm diameter telescope adjusted for ϵ measured
West (ref. 15)			$0.06 \leqslant \epsilon \leqslant 0.10$	Extremes permitted by reduction from photographs
Danielson (ref. 16)	26,400 ± 1,000			Fit of infinite Rayleigh atmosphere to limb darkening curves obtained from the balloon Stratoscope II
		NEPTUNE		
Dollfus (ref. 14)	24,400 ± 1,400			Mean of filar micrometer measurements with telescopes $\geqslant$ 40 cm diameter
Dollfus (ref. 14)	22,700			Mean of discometer results 60 & 200 cm diameter telescopes
Dollfus (ref. 14)	22,500			Mean of double image micrometer measurements with 60 cm diameter telescopes

*When necessary, angular measurements of radius from original sources have been converted to linear measure.

TABLE II (Continued)

Source	R_{eq} (km)*	$R_{p\ell}$ (km)	ϵ	Remarks
NEPTUNE (Continued)				
Dollfus (ref. 14)	24,300 ± 400			Double image micrometer measurements 107 cm diameter telescope
Kovalevsky (ref. 17)	25,030 ± 80		< 0.0025	Derived from occulation timing at 0.5 light. No correction applied for relativity or refraction
Kovalevsky and Link (ref. 18)	25,130 ± 80			Derived from occultation timing at 0.5 light. Correction applied for relativity and refraction
Taylor (ref. 19)	25,230 ± 40	24,720 ± 40		Derived from occultation timing at 0.5 light. An oblateness $\epsilon = 0.02$ has been assumed and result includes relativistic correction
Freeman and Lyngå (ref. 20)	25,270 ± 40	24,610 ± 130	0.026 ± 0.008	Derived from occultation timing at 0.91 light. Result includes relativistic correction

*When necessary, angular measurements from original sources have been converted to linear measure.

Danielson (ref. 16) has compared densitometer tracings of photographs of the disk of Uranus obtained from a balloon flight with the scattered radiation expected from model atmospheres. This comparison leads to an equatorial radius of 26,400 km if an infinite Rayleigh atmosphere is assumed, and 27,400 km if a finite Rayleigh atmosphere with a deep reflection layer is assumed. Both results are uncertain to ±1000 km.

The foregoing arguments suggest taking the equatorial radius of Uranus as 27,000±1000 km, and this range will be adopted here.

The ground-based photography of West (ref. 15) and the filar micrometer measures reported by Dollfus (ref. 14) give an oblateness for Uranus of $0.06 \leqslant \epsilon \leqslant 0.10$. This result would place Uranus between Jupiter and Saturn in oblateness. If, however, polar limb darkening is

TABLE III

NEPTUNE – URANUS EQUATORIAL RADIUS COMPARISON

Method (Common to Neptune and Uranus)	*Equatorial Radius for Neptune (km)	**Ratio (Equatorial Radius of Neptune to Base Value)	*Equatorial Radius for Uranus (km)	Equatorial Radius for Uranus Implied by Using Ratio (km)
Filar Micrometer Mean with Telescopes $\geqslant$40 cm in Diameter	24,400	1.034	26,700	27,600
Discometer Mean with 60 cm & 200 cm Diameter Telescopes	22,700	1.111	23,700	26,300
Double Image Micrometer Mean with 60 cm Diameter Telescope	22,500	1.121	24,600	27,600
Double Image Micrometer Mean with 107 cm Diameter Telescope	24,300	1.038	25,400	26,400

*Equatorial radius values are taken directly from table II for both Uranus and Neptune.
**Base value of the equatorial radius for Neptune is taken from Taylor's (ref. 19) occultation result (25,230 km), based on 0.5 light.

greater than the equatorial limb darkening, such measurements lead to an exaggerated value of oblateness. Here, the mean value obtained by Dollfus (ref. 14) with a double image micrometer on a 107 cm diameter telescope will be adopted with an increase in the uncertainty, $\epsilon = 0.03 \pm 0.03$. If the uncertainties in R_{eq} and ϵ are considered as independent, a value of $R_{p\ell} = 26{,}000 \pm 1300$ km results for the polar radius of Uranus.

On the basis of these dimensions and the mass for Uranus given in section 2.1.1., the mean density can be computed with the formula $\overline{\rho} = 3M/4\pi R_{p\ell} R^2_{eq}$ to give ρ as 1.1 ± 0.1 g cm^{-3}. This value is intermediate between that for Jupiter and Saturn.

For Neptune, the value of 25,200 ±200 km for the equatorial radius will be adopted. This is essentially the value given by Taylor (ref. 19) on the basis of observations of an occultation

by Neptune and reduced with an assumed oblateness of 0.02. The uncertainty in equatorial radius adopted herein, however, has been increased to account for the uncertainty in Neptune's oblateness. The value of $\epsilon = 0.02$ used by Taylor (ref. 19) is based on a dynamic oblateness determination. If the oblateness were zero, Taylor's analysis and that of Kovalevsky and Link (ref. 13), given in table II, indicate the occultation radius would be approximately 100 km smaller. When the differences in reduction procedures are taken into account, the occultation results reported in table II are in good agreement.

The oblateness of Neptune inferred from the occultation results is shown in table II. Taylor (ref. 19) found a slightly better fit to the data when an oblateness of 0.02 was assumed. The value $\epsilon = 0.02 \pm 0.02$ will be adopted here to span the range suggested for Neptune. Use of this value leads to a polar radius, $R_{p\ell} = 24{,}700 \pm 500$ km, and with the mass value given in 2.1.1 to a mean density, $\bar{\rho} = 1.57 \pm 0.04$ g·cm^{-3}.

For both Uranus and Neptune, it is of importance in spacecraft design to associate the planetary radius with atmospheric parameters. This association can only be made after evaluation of the expected planetary atmospheres in section 2.7.

2.1.2.2 Pluto

An "extreme upper limit" of 6800 km to the diameter of Pluto has been given by Halliday et al. (ref. 21) on the basis of a near occultation of a star by Pluto. If a grazing occultation is assumed, these same observations lead to a diameter of 5800 km (ref. 21). Earlier, Kuiper (ref. 22) obtained a diameter of 5900 km on the basis of discometer measurements with the 200 inch Hale telescope. Although the mean error was estimated as 5 percent or 300 km, systematic effects could place the actual diameter outside this range.

The diameter of Pluto can be estimated from selected values for the visual geometric albedo or density. With the limits given for the mean opposition visual magnitude in table XXXVII (section 3.3.4), a visual geometric albedo of 0.1 corresponds to a maximum diameter of 6900 km and a visual geometric albedo of 1.0 to a minimum diameter of 2000 km. Likewise, with the limits for the mass ratio given in section 2.1.2, a density of 1 g cm^{-3} corresponds to a maximum diameter of 12,400 km and a density of 8 g· cm^{-3} to a minimum diameter of 4,300 km. Although these choices for visual geometric albedo and density are reasonable for solar system objects, such a priori estimates are only suitable for drawing general conclusions.

Here an upper limit to the diameter of 6800 km will be adopted based on the Halliday et al. (ref. 21) "extreme upper limit". The lower limit will be set at 4800 km to avoid unreasonably large densities. The central value is taken from the geometric mean of the limits which gives a diameter of $5700 \times 1.2^{\pm 1}$ km.

The derived value for the density permitted Pluto by the foregoing diameter and the mass given in section 2.1.1 is $5.9 \times 3^{\pm 1}$ g· cm^{-3}. Because the maximum density of objects in

the solar system is 8 g. cm^{-3} *, this computation suggests that future mass determinations for Pluto may lead to a smaller mass value than the one adopted in section 2.1.1.

2.1.3 Planetary Rotation and Orbits

2.1.3.1 Rotation Period

The most consistent determinations of the rotation period of Uranus and Neptune have come from spectrographic observations before 1931. These observations give no indication of the possible change in rotation period with planetary latitude or altitude.

For Uranus, Slipher (ref. 24) obtained a rotation period of $10^h.83$ and Moore and Menzel (ref. 25) a value of $10^h.84$. Numerous photometric observations (see Moore and Menzel (ref. 25) and Alexander (ref. 26) for references) lead to periods which are in substantial agreement with the foregoing values. Recent photometric studies (ref. 27) did not detect periodic variations which could be associated with rotation. Therefore, the period $10^h.8 \pm 1^h$ adopted here for Uranus has a range of $\pm 1^h$ to include the uncertainty in the spectroscopic measurements and the possibility of a latitude variation as large as that of Saturn.

For Neptune, the only spectrographic determination has been that of Moore and Menzel (ref. 28) which gave a rotation period of $15^h.8$. Photometric observation and dynamic arguments, based on an equatorial bulge, have led to periods ranging from 7.7^h to 19.1^h (refs. 28 and 29). Öpik (ref. 29) favors a period of $12^h.72$ on the basis of photometric observations. As in the case of Uranus, recent photometry of Neptune does not indicate the presence of periodic variations from which a period could be derived. In the absence of a modern confirmation of the photometrically derived period, the spectrographic result is preferred. The value $16^h \pm 2^h$ will be adopted here with the range of $\pm 2^h$ broad enough to include the possibility of variation in rotation rate with latitude.

The rotation period of Pluto has been established by photometry. The light curve given by Harris (ref. 30) shows a marked asymmetry with a total amplitude of 0.11 magnitudes. The period given by Hardie (ref. 31) is $6.3867^d \pm 0.0003^d$. Here the value $6.387^d \pm 0.001^d$ will be adopted.

2.1.3.2 Rotational Axis Orientation

The vector direction of the rotational axis for Uranus and Neptune has been established from observation of their satellites. With respect to the mean equinox and equator of 1950.0, the right ascension and declination of the North pole are given by Sturms (ref. 32) for Uranus as

$$\alpha_R = 76^\circ.761$$
$$\delta_R = 14^\circ.920$$

Uranus

*Density of iron meteorites, Allen (ref. 23).

and for Neptune by Gill and Gault (ref. 8) as

$$\left.\begin{aligned} \alpha_R &= 294^\circ.91 \\ \delta_R &= 40^\circ.53 \end{aligned}\right\} \text{Neptune}$$

The precessional rates of the rotational axis for Uranus and Neptune are not known.

The vector direction of the rotational axis of Pluto is not known. If it is assumed to be perpendicular to the orbital plane and the motion direct, the right ascension and declination with respect to the mean equinox and Earth equator of 1950.0 have been given by Sturms (ref. 32) as

$$\left.\begin{aligned} \alpha_R &= 313^\circ.89136 \\ \delta_R &= 66^\circ.36420 \end{aligned}\right\} \text{Pluto}$$

2.1.3.3 Orbital Elements

The orbital elements of Uranus, Neptune, and Pluto cannot be represented accurately in a simple way. The right ascension and declination, heliocentric positions, and osculating elements can be found in the appropriate year of the *American Ephemeris and Nautical Almanac* (published several years in advance of the year of intended use). Heliocentric co-ordinates referred to the Equinox of 1950.0 for the period 1960 to 1980 are tabulated in *Planetary Co-ordinates* (ref. 33). Mean orbital elements referred to the mean equinox and ecliptic of date for Uranus and Neptune are found in Melbourne et al. (ref. 12). Mean orbital elements for Uranus, Neptune, and Pluto with respect to the mean equinox and Earth equator of 1950.0 have been given by Sturms (ref. 32). The time dependence of the mean elements is expressed in polynominal form by Melbourne et al. (ref. 12) and Sturms (ref. 32). Precision trajectory computations can be carried out with the aid of the "JPL Development Ephemeris Number 69."*

Figure 1 shows a qualitative plot of the outer planet positions from 1970 to 1980 taken from *Planetary Co-ordinates* (ref. 33). The tick marks indicate the position of each planet at the beginning of the calendar year. Shortly after the start of 1979 the heliocentric distance of Pluto will be less than that of Neptune.

Orbital parameters for Uranus, Neptune, and Pluto are given in table IV. These parameters were taken from a tabulation provided by the British Astronomical Association's *Handbook for 1971* (ref. 34), and for Uranus and Neptune they are essentially the same as those which can be obtained from Melbourne et al. (ref. 12).

During the period 1971 to 1980 the heliocentric distance of Uranus will change from 18.3 AU to 18.8 AU and the corresponding orbital speeds vary from 7.1 km/sec to 7.0 km/sec. Because of its small eccentricity the heliocentric distance of Neptune will be 30.3 AU during this period and the orbital speed 5.4 km/sec. The heliocentric distance of

*O'Handley, D.A., Holdridge, D.B., Melbourne, W.G. and Mulholland, J.D., TR 32-1465, Jet Propulsion Laboratory, Pasadena, California, Dec. 15, 1969.

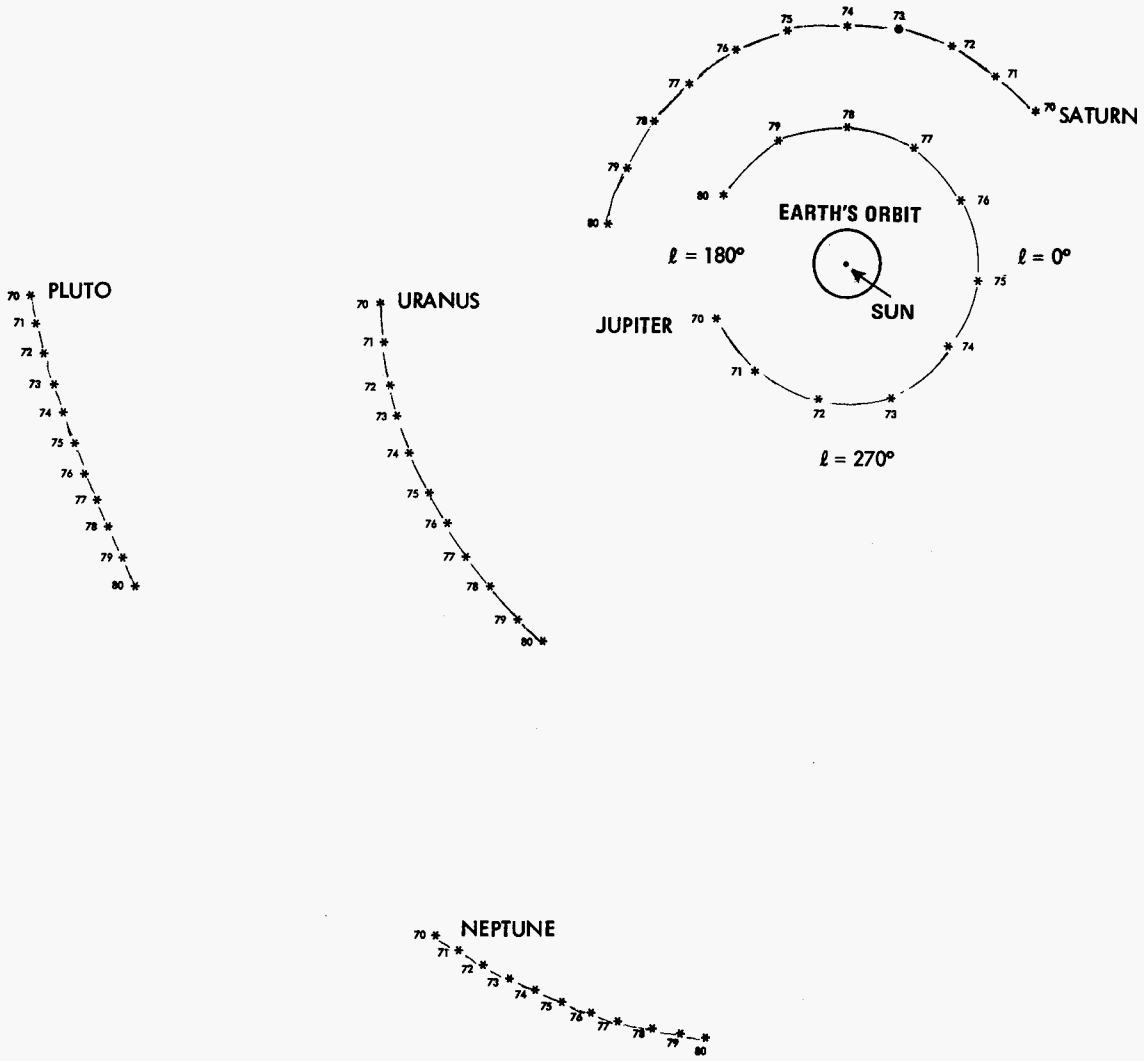

Figure 1.—Heliocentric longitude versus radial distance for the planets Jupiter, Saturn, Uranus, Neptune, and Pluto from the beginning of 1970 to the beginning of 1980. (Longitude with respect to the Earth equinox of 1950. 0).

TABLE IV

ORBITAL PARAMETERS FOR URANUS, NEPTUNE, AND PLUTO

Mean Elements for January 0.5 Ephemeris Time, 1971		
	Uranus	Neptune
Sidereal mean motion per tropical year	4°.2851	2°.1845
Period (tropical years)	84.013	164.795
Mean distance from Sun (AU)	19.181876	30.057912
Eccentricity	0.047239	0.0085832
Inclination to the ecliptic	0° 46′ 23″.3	1° 46′ 21″.8
Inclination of Equator to Orbit*	97° 53′	28° 43′
Osculating Elements at January 9.0 Ephemeris Time, 1971		
	Pluto	
Period (tropical years)	250.0	
Mean distance from Sun (AU)	39.7078	
Eccentricity	0.25306	
Inclination to the ecliptic	17°.144	
Inclination of Equator to Orbit	Unknown (sec. 2.1.3)	

*See *Explanatory Supplement to the Ephemeris*, p. 491 (ref. 73).

Pluto will change from 31.7 AU to 30.2 AU from 1971 to 1980 with the orbital velocity changing from 5.8 km/sec to 6.0 km/sec.

2.2 Gravitational Fields

The gravitational field of a planet can be conveniently obtained from a potential function U approximated by three terms in an infinite series expansion (ref. 12).

$$U = -\frac{GM_p}{R_{eq}}\left[\frac{R_{eq}}{R} + \frac{\sigma}{2}\left(\frac{R}{R_{eq}}\cos\phi\right)^2 - J_2\left(\frac{R_{eq}}{R}\right)^3 P_2(\sin\phi)\right]$$

The force per unit mass is obtained directly from the gradient of U. The term involving σ accounts for rotation with $\sigma = \omega_o{}^2 R_{eq}^3 / GM_p$ and is to be used when the coordinate system of interest rotates at angular speed ω_o. When a non-rotating coordinate system is used, σ is set to equal zero. J_2 is a gravitational coefficient and P_2 ($sin\ \phi$) is a Legendre polynominal that depends only on the planetocentric latitude ϕ. In this form the gravitational potential and field is independent of planetary longitude and symmetric about the planetary equator. Both of these assumptions are necessary because our understanding of the mass distribution for these planets is limited. Gravitational forces arising from the Sun, other planets, and planetary satellites are not included in the potential U and must be evaluated separately. Estimates of satellite mass are given in section 2.5.

The gravitational fields of Uranus, Neptune, and Pluto are considered herein for the cases of non-rotating (inertial) and corotating coordinates.

2.2.1 Inertial Coordinates

An inertial coordinate frame is appropriate for objects not constrained to share the planet's rotation. Then, as stated previously, $\sigma = 0$ in the foregoing expression for the gravitational potential U. The gravitational field then depends on the mass of the planet and the gravitational coefficient J_2. For Neptune, J_2 can be determined from observations of the satellites Triton and Nereid. With the latest value for the orbital precession rate and inclination of Triton (ref. 8), the radius adopted for Neptune in section 2.1.2, and the period and semimajor axis of Triton from reference 34, J_2 can be evaluated as 0.0038 ±0.0001. The uncertainty shown for Neptune's J_2 was obtained by assuming a ±200 km uncertainty in the radius of Neptune only. J_2 has been determined for Uranus by Dunham (ref. 35). Conversion of his result with the radius adopted for Uranus in section 2.1.2 gives $J_2 = 0.011 \pm 0.001$ where the uncertainty is entirely the result of the assumed 1000 km uncertainty in equatorial radius. The total contribution to the gravitational potential from the J_2 term for Uranus and Neptune is less than the uncertainty in this potential because of the uncertainty in the planetary masses.

In view of the uncertainty in the mass and radius of Pluto, it is not reasonable to consider higher order gravitational coefficients for this planet.

If the contribution to the gravitational potential from J_2 is neglected and the values for GM_p and R_{eq} in section 2.1 are used, the following expressions result in which the uncertainty reflects the uncertainty in mass and the neglected ϕ dependence.

$$U = -(215 \pm 2)\ (R_{eq}/R)\ km^2 \cdot s^{-2} \quad \text{Uranus}$$

$$U = -(273 \pm 3)\ (R_{eq}/R)\ km^2 \cdot s^{-2} \quad \text{Neptune}$$

$$U = -(13 \times 1.7^{\pm 1}) \ (R_{eq}/R) \ km^2 \cdot s^{-2} \ \text{Pluto}$$

On the basis of the foregoing potential values, the escape velocity, orbital velocity, and orbital period for an object near any of these planets can be computed; the results have been adopted as design criteria and are shown in tables XIII, XXIV, and XXXV (sec. 3).

2.2.2 Corotating Coordinates

A corotating coordinate frame is appropriate when the object of interest, e.g., a descending atmospheric probe, is constrained to rotate with the planet and requires that a value of σ appropriate to each planet be used in the foregoing expression for the gravitational potential U.

The non-spherical nature of this potential implies that the direction of the acceleration of gravity which defines the local vertical will not coincide with the radial direction except at the poles and equator. The planetographic latitude ϕ' is then defined as the angle between the direction of the acceleration of gravity and the equatorial plane. An approximate expression to first order in ϵ is given for the difference between planetographic and planetocentric latitude by $\phi' - \phi = \epsilon \sin 2\phi$.

The altitude z is defined in section 2.7.3 for Uranus and Neptune as the distance from the correspondence level. The distance from the center of the planet R in terms of z can be written as: $R = R_{eq} [1 - \epsilon(\sin \phi)^2 + (z - z_o)/R_{eq}]$ where z_o is a reference altitude given for each model atmosphere in sections 3.1.7 and 3.2.7.

For Pluto, z is measured from the surface of the planet and is related to R by $R = R_{eq} + z$ which can be obtained from the foregoing expression for R by setting ϵ and z_o equal to zero.

With the gravitational potential function and the value for GM_p, R_p, ϵ, J_2, and σ given in this and section 2.1, the polar and equatorial gravitation field can be computed; the results have been adopted as design criteria and are given in tables XIII, XXIV, and XXXV. Uncertainties in this table reflect the uncertainties in the basic quantities upon which the gravitational field depend. For the purpose of constructing model atmospheres, the acceleration of gravity is taken as the mean of the polar and equatorial field for each planet with the range that the extreme polar and equatorial fields permit. These values follow:

$$g = (810 \pm 140) \ cm \cdot s^{-2} \ \text{Uranus}$$

$$g = (1100 \pm 60) \ cm \cdot s^{-2} \ \text{Neptune}$$

For Pluto, the acceleration of gravity at its surface depends on the considerable uncertainty in mass and radius. Use of the central values and range for mass and radius given in sections 2.1.1 and 2.1.2, results in a range of values for Pluto's surface gravity of $470 \times 2.5^{\pm 1}$ $cm \cdot s^{-2}$.

2.3 Magnetic Fields

No data exist from which the magnetic fields of Uranus, Neptune, or Pluto can be established. Furthermore, existing data are not appropriate for setting firm upper limits.

2.3.1 Magnetic Fields of Uranus and Neptune

Of the four major outer planets, Jupiter, Saturn, Uranus, and Neptune, only the magnetic field of Jupiter and its corresponding dipole moment are reasonably well established (refs. 36, 37 and 38). The estimate of NASA SP-8069 (ref. 38) for Jupiter's field at one planetary radius on the magnetic equator is $1.2 \times 2^{\pm 1} \times 10^{-3}$T ($12 \times 2^{\pm 1}$ gauss), corresponding to a dipole moment of $4 \times 2^{\pm 1} \times 10^{27}$ A·m^2. This result came from extensive analysis of Jovian decametric and decimetric radiation. As stated in section 2.4.3, there has been no detection of decametric radiation from Uranus and Neptune and the brightness temperature measurements listed in table VII (sec. 2.4.3) do not lend themselves to the specification of planetary magnetic fields. One attempt to detect linear polarization in the emission from these planets at 3.12 cm has been made by Berge (ref. 39), but no linear polarization was established outside experimental uncertainties. No attempts to establish the extent of the source of radio emission have been reported. In short, the observational base from which Jupiter's magnetic field has been determined is almost entirely absent for Uranus and Neptune.

Analysis of the relevant magnetic field generation mechanisms (refs. 40 and 41) have not been applied to Uranus and Neptune. The difficulties of such analysis are indicated by Hide (ref. 42). Our lack of knowledge of the bulk composition and structure for these planets is a serious obstacle to the theoretical prediction of their magnetic fields.

Several scaling procedures have been suggested for estimating the fields of these planets (refs. 37, 40, and 43); the qualitative results with Jupiter as a base are shown in the first three entries of table V. The fourth entry is an estimate based on remnant core magnetism made by Pochtare (ref. 43). None of the procedures is based on a substantiated physical theory although the range shown in table V is not unreasonable for the general magnetic field of these two planets.

Because there are no valid reasons for accepting the results of any one of the scaling procedures in table V, the magnetic field strength, form (dipolar, quadrupolar, etc.), and orientation must be considered as unknown for both Uranus and Neptune. In specific regions near these planets, fields as large as 10^{-2} T (100 gauss) cannot be excluded. In the design of space vehicles intended to pass near these planets, consideration should be given to the possibility of such large fields.

2.3.2 Magnetic Field of Pluto

Pluto is smaller than Earth and rotates more slowly (secs. 2.1.2 and 2.1.3) so there may be insufficient motion to sustain a magnetic field even with a fluid, conducting core. Remnant magnetism (ref. 43) and other field generating mechanisms could be important. On the basis

TABLE V

ESTIMATES OF THE MAGNETIC FIELD OF URANUS AND NEPTUNE*

Principal Assumptions	Magnetic Flux Density in Magnetic Equator at one Planetary Radius	
	Uranus	Neptune
Magnetic Moment** Proportional to Volume	1.2×10^{-3} T (12 gauss)	1.2×10^{-3} T (12 gauss)
Magnetic Moment** Proportional to Rotational Angular Momentum	1.2×10^{-4} T (1.2 gauss)	1.1×10^{-4} T (1.1 gauss)
Magnetic Flux Density*** Proportional to Volume	7.0×10^{-5} T (0.7 gauss)	5.0×10^{-5} T (0.5 gauss)
Magnetic Flux Density Related to Remnant Magnetism of Core, Pochtarev (ref. 43)	1.5×10^{-6} T (0.015 gauss)	1.5×10^{-6} T (0.015 gauss)

*Mechanical quantities were taken from section 2.1, Allen (ref. 23), and NASA SP-8069 (ref. 38).
**Jovian magnetic moment of 4×10^{27} A·m^2 (4×10^{30} gauss·cm^3) assumed.
***Jovian magnetic equatorial field at one planetary radius of 1.2×10^{-3} T (12 gauss) assumed.

of current knowledge of Mars, Venus, Earth, and the Moon (which have been explored by spacecraft and have some similarity to Pluto), it is reasonable to adopt 1×10^{-4} T (1 gauss) as an upper limit magnetic field at the surface of Pluto.

2.4 Electromagnetic Radiation

Electromagnetic radiation in the vicinity of Uranus, Neptune, and Pluto is presented according to origin in three parts, solar radiation, reflected solar radiation, and thermal radiation.

2.4.1 Solar Radiation

In the vicinity of these planets and when unshadowed, the Sun is the dominant natural source of electromagnetic radiation for all wavelengths less than 10 μm. Values for the solar spectral irradiance H_λ (power per unit area and per unit wavelength interval) from 50 Å to 10 m and the integrated spectral irradiance H_e (power per unit area) are given in NASA SP-8005 (ref. 44) and apply at 1 AU outside the Earth's atmosphere. At the extremes of this range the emission is highly variable, but in the region of primary emission (0.3 μm to 4 μm) it is nearly constant with time. The spectral irradiance at 1 AU or solar constant H_e is

0.1353 ±0.0021 W· cm^{-2} (ref. 44). These quantities, H_λ and $H_\odot$, accurately vary as S^{-2} where S is distance from the Sun. Standard relationships for spectral intensity I_λ (power per unit area and per unit wavelength interval and per steradian), spectral flux F_λ, (power per unit area and per unit wavelength interval), and integrated flux F, (power per unit area), lead to the formulas adopted herein for solar radiation in tables XIV, XXV, and XXXVI (sec. 3).

2.4.2 Reflected Solar Radiation

Solar radiation reflected from Uranus has been observed only at phase angles less than 3° and for Neptune and Pluto only at phase angles less than 2°. This radiation is conventionally described in terms of astronomical magnitudes, color differences, and albedos. The definition of geometric albedo p_λ, given in appendix C, leads to formulas for the optical intensity and spectral flux reflected from these planets at zero phase and planetocentric distance R as follows

$$I_\lambda = p_\lambda H_\lambda / \pi R_{p_\odot}^2$$

$$F_\lambda = \frac{p_\lambda H_\lambda}{R_{p_\odot}^2 (R/R_{eq})^2}$$

where $R_{p\odot}$ is the distance from the planet to the Sun in AU. The phase dependence of these quantities (I_λ, F_λ) has not been established; but as the foregoing expressions refer to zero phase, they may be taken as upper limits.

Geometric albedos have been given by Harris (ref. 30) for Uranus, Neptune, and Pluto and by Appleby and Irvine (ref. 45) for Uranus. Fix et al. (ref. 46) gives relative albedos for Pluto. The results of the foregoing authors are based on modern photoelectric photometry. Accurate geometric albedos can be computed from this photometry only when the planetary dimensions and time-dependent brightness variations are known. The dimensions of all three planets are uncertain (sec. 2.1.2). In addition, because Uranus and Neptune have atmospheres with appreciable amounts of gas above any likely cloud layer, the selection of appropriate dimensions for computing geometric albedos is difficult. In particular, the adopted dimensions of section 2.1.2 are not directly suitable for the computation of geometric albedos as they encompass the high atmospheres of both planets through their relationship to stellar occultations.

To proceed further, dimensions for these planets must be assumed. For Uranus and Neptune, the radii obtained with a double image micrometer by Dollfus (refs. 14 and 47) will be used and for Pluto the radius adopted in section 2.1.2. The uncertainty in radius will be taken as ±1000 km for Uranus and ±500 km for Neptune. The resulting geometric albedos, sources of photometric data, and the planetary dimensions that were used are given in table VI. The uncertainty in geometric albedo shown in table VI results entirely from the assumed uncertainty in radius.

TABLE VI

GEOMETRIC ALBEDOS FOR URANUS, NEPTUNE, AND PLUTO

Effective Wavelength* μm	Source of Photometry	Calculated Geometric Albedo**		
		Uranus	Neptune	Pluto***
0.3147	Appleby & Irvine (ref. 45)	0.48 ±0.03	0.52 ±0.02	0.10 ±0.04
0.353 (U)	Harris (ref. 30)	0.48 ±0.03		
0.3590	Appleby & Irvine (ref. 45)	0.48 ±0.03		
0.3615 (U)	Appleby & Irvine (ref. 45)	0.48 ±0.03		
0.3926	Appleby & Irvine (ref. 45)	0.53 ±0.03		
0.4155	Appleby & Irvine (ref. 45)	0.53 ±0.03		
0.4400 (B)	Appleby & Irvine (ref. 45)	0.54 ±0.03		
0.4480 (B)	Harris (ref. 30)	0.54 ±0.03	0.55 ±0.02	0.11 ±0.05
0.4573	Appleby & Irvine (ref. 45)	0.56 ±0.03		
0.5012	Appleby & Irvine (ref. 45)	0.57 ±0.03		
0.5480 (V)	Appleby & Irvine (ref. 45)	0.48 ±0.03		
0.5540 (V)	Harris (ref. 30)	0.51 ±0.03	0.45 ±0.01	0.13 ±0.04
0.6264	Appleby & Irvine (ref. 45)	0.25 ±0.02		
0.6900 (R)	Harris (ref. 30)	0.29 ±0.02	0.22 ±0.01	0.16 ±0.06
0.7297	Appleby & Irvine (ref. 45)	0.07 ±0.01		
0.8200 (I)	Harris (ref. 30)	0.11 ±0.01	0.08 ±0.01	0.15 ±0.06
0.8595	Appleby & Irvine (ref. 45)	0.03 ±0.01		
1.0635	Appleby & Irvine (ref. 45)	0.05 ±0.01		

*Letter specifies pass bands which are discussed in the references cited and Newburn and Gulkis (ref. 49).

**The radii used were: Uranus R_{eq} = 25,400 ±1000 km, R_{pol} 24,700 ± 1000 km; Neptune $R_{eq} = R_{pol}$ = 24,300 ±500 km; Pluto $R_{eq} = 5700 \times 1.2^{\pm 1}$ km.

***Relative albedos at 21 wavelengths between 0.34 and 0.59 μm have also been given by Fix et al. (ref. 46).

The geometric albedos calculated from the photometry of Harris, and Appleby and Irvine are in good agreement for Uranus at wavelengths $\leqslant 0.554\ \mu m$. At longer wavelengths, the differences in bandpass coupled with CH_4 absorption features in the spectra can account for the apparent difference in geometric albedos, as pointed out by Appleby and Irvine (ref. 45). Table VI was used to establish the limiting values of geometric albedo plotted in figures 2, 5, and 8.

A photometric determination of the integrated geometric albedo p_g for Uranus has been given by Younkin and Münch (ref. 48) as $p_g = 0.32$. This value is uncertain, like the individual geometric albedos, because of the uncertainty in the planet's dimensions. However, p_g is unlikely to differ from the Younkin and Münch result by more than ±0.1. This

value, $p_g = 0.32 \pm 0.1$, and its substitution in the following expression for the integrated reflected solar flux F,

$$F = \frac{p_g H_\odot}{R_{p\odot}^2 (R/R_{eq})^2}$$

are adopted for both Uranus and Neptune. No integrated geometric albedos have been computed for Pluto. The relative albedos obtained by Fix et al. (ref. 46) slowly change over the wavelength region of maximum solar emission. As an estimate, the geometric albedo given in table VI for the visual V passband will be used for the integrated geometric albedo for Pluto with an uncertainty factor of $2^{\pm 1}$ ($p_g = 0.14 \times 2^{\pm 1}$).

Within the atmospheres of Uranus and Neptune, the foregoing intensities and fluxes likely represent upper limits on direct and reflected radiation from the Sun. Additional sources of radiation in this region (50 Å to 10 m) which might be expected are airglow, aurora, and lightning. Because these sources have not been observed, no description of the expected intensities is possible. Lightning discharge may occur in convective cloudforming regions with intensities comparable to those observed on Earth.

2.4.2.1 Magnitudes and Color

The brightness of Uranus and Neptune, their satellites, and Pluto can be specified by their magnitudes and colors. The values given by Harris have been adopted and are shown in tables XVI, XXVII, and XXXVII. When the geometry of illumination and observation is specified in terms of phase angle Ψ, $R_{p\odot}$, and observation distance Δ, the relationship

$$m_V = (m_o \pm \delta m_o) + 5 \log (R_{p\odot}\Delta) + (\Delta m)\Psi$$

applies with $R_{p\odot}$ and Δ in AU only and Ψ in degrees. The phase coefficient Δm for Uranus and Neptune has been investigated by Talley and Horak (ref. 50) and Harris (ref. 30). An observed Δm value of 0.00031 mag./degree for Uranus and 0.0006 mag./degree for Neptune have been reported by Sinton (ref. 51). As indicated by Harris (ref. 30), knowledge of this coefficient over the limited range of phase angle permitted by Earth observation (3° for Uranus and 2° for Neptune) does not permit extrapolation to much larger phase angles. The magnitude of the phase coefficient for the satellites of Uranus and Neptune and Pluto is not known. Here a value for Δm of $(0.01^{+0.01}_{-0.005})$ will be adopted for Uranus and Neptune and a value of $(0.03^{+0.05}_{-0.01})$ for the satellites and Pluto. The uncertainty for the satellites and Pluto includes the known phase variation for the Moon and the largest satellites of Jupiter (ref. 52). An alternate presentation of the visual magnitude of these objects has been given by Pace (ref. 53).

In addition to the phase variation, changes in brightness for these objects have been reported that are related to rotation and position in orbit. For Uranus, Alexander (ref. 26) and

Becker (ref. 54) report a 42-year variation in amplitude of ~ 0.3 mag., a 5.5 to 11.5-year variation of ~ 0.3 mag., and a variation with planetary rotation of ~ 0.15 mag. However, the most recent series of observations made at the Lowell Observatory from 1950 to 1966 and reported by Hardie and Giclas (ref. 27), Johnson and Iriarte (ref. 55), Sinton (ref. 51), Serkowski (ref. 56), and Jerzykiewicz & Serkowski (ref. 57) place the short and long term change in brightness at less than 0.1 mag. The Lowell Observatory results refer to blue magnitudes, whereas the variations reported by Becker and Alexander refer to visual magnitudes. Because this divergence of results has not been explained, the constant δm_o in the foregoing expression for m_V will be taken as ±0.3.

The Lowell Observatory series also included Neptune in blue magnitudes with a total long and short term variability of less than 0.1 mag. so a δm_o of ±0.1 mag. will be adopted for Neptune.

For Pluto, the total variation of brightness with rotation amounts to 0.11 mag. according to Walker and Hardie (ref. 58). Therefore, a δm_o of ±0.1 mag. has been adopted to span the expected change in brightness.

Of the satellites of Uranus and Neptune, only Triton changes appreciably in brightness; it has a total variation of 0.25 mag. with orbital position. Consequently, for the satellites of both planets, a δm_o of ±0.3 mag. is adopted to encompass any undiscovered brightness variations.

2.4.3 Intrinsic Thermal and Non-Thermal Radiation

The existing radiometer brightness temperature measurements for Uranus, Neptune, and Pluto are listed in table VII. There has been no successful radiometric detection of Pluto. Several attempts to detect decametric radiation from Uranus, reported by Brissenden and Erickson (ref. 59) and Smith (ref. 60), have not been successful.

The results tabulated in table VII are of mixed quality because of limitations of system sensitivity and calibration. The increase in brightness temperature with increasing wavelength (from 0.3 cm to 10 cm) for both Uranus and Neptune is similar to the change exhibited by both Jupiter and Saturn in this wavelength interval. Although alternate explanations are possible (sec. 2.6.4), the increase in brightness temperature with increasing wavelength likely represents atmospheric thermal radiation. It is then reasonable to interpret all these measures as disk brightness temperatures T_D. On this basis the ranges of disk brightness temperature were estimated for Uranus and Neptune and are given in figures 3 (sec. 3.1.4) and 6 (sec. 3.2.4) with liberal uncertainty and reasonable extrapolation in wavelength regions where no observations have been made.

The effective radiating temperature T_{eff} for Uranus, Neptune, their satellites, and Pluto is not known; considerable difficulties hamper experimental determinations of this parameter. For Uranus, a bolometric Bond albedo of 0.42 has been estimated by Younkin and Münch (ref. 48). Use of this value leads to an effective temperature of 56 K if it is assumed that Uranus radiates uniformly. If only one hemisphere radiates – an extreme case approached

TABLE VII

MEASURED BRIGHTNESS TEMPERATURES FOR URANUS, NEPTUNE, AND PLUTO

Brightness Temperature (K)	Wavelength	Source
	URANUS	
55 ± 3	17.5–25 μm	Low (ref. 61)
58^{+7}_{-6}	17.5–25 μm	Armstrong (ref. 62)
107 ±32	0.12 cm	Armstrong (ref. 62)
105 ±13	0.33 cm	Epstein et al. (ref. 63)
111 ± 7	0.35 cm	Pauliny-Toth and Kellermann (ref. 64)
131 ±15	0.822 cm	Kuzmin and Losovsky (ref. 65)
125 ±15	0.95 cm	Pauliny-Toth and Kellermann (ref. 64)
201 ±16	1.65 cm	Mayer & McCullough (ref. 66)
181 ± 7	1.95 cm	Pauliny-Toth and Kellermann (ref. 64)
212 ±16	2.7 cm	Mayer and McCullough (ref. 66)
169 ±20	3.12 cm	Berge (ref. 39) adjusted by Newburn and Gulkis (ref. 49)
170 ±20	3.75 cm	Klein & Seling (ref. 67) adjusted by Newburn and Gulkis (ref. 49)
210 ±17	6 cm	Mayer & McCullough (ref. 66)
180 ±40	11.13 cm	Gerard (ref. 68)
130 ±40	11.3 cm	Kellermann (ref. 69)
	NEPTUNE	
65	0.12 cm	Armstrong (ref. 62)
88 ± 5	0.35 cm	Pauliny-Toth & Kellermann (ref. 64)
134 ±18	0.95 cm	Pauliny-Toth & Kellermann (ref. 64)
194 ±24	1.65 cm	Mayer & McCullough (ref. 66)
172 ±22	1.95 cm	Pauliny-Toth & Kellermann (ref. 64)
225 ±20	2.7 cm	Mayer & McCullough (ref. 66)
137 ±40	3.12 cm	Berge (ref. 39) adjusted by Pauliny-Toth & Kellermann (ref. 64)
227 ±23	6 cm	Mayer & McCullough (ref. 66)
< 150	11.13 cm	Gerard (ref. 69)
	PLUTO	
300 ±1200, i.e., not detected	1.9 cm	Kellermann & Pauliny-Toth (ref. 70)

about 1985 when Uranus presents a rotational pole to the Sun – the foregoing albedo value leads to an effective temperature of 66 K. An effective temperature of 56 K is in accord with the two existing IR measurements by Low and Armstrong (table VII). It is possible, however, that Uranus radiates more energy than it receives from the Sun as is apparently the case for Jupiter and Saturn (ref. 71). For Uranus, a compromise T_{eff} of 61±5 K is adopted; this span takes into account the changing direction of the rotational axis to the Uranus-Sun line and some uncertainty in bolometric albedo but does not assume an internal source of energy.

For Neptune, use of the bolometric Bond albedo of 0.42 obtained by Younkin and Münch for Uranus (ref. 48) leads to an effective temperature of 45 K with the assumption of uniform emission from the whole planet. A bolometric Bond albedo between 0.2 and 0.6 leads to an effective temperature range of 45±3 K which is adopted here. As with Uranus, this value does not assume any internal source of energy.

Pluto and Triton (Neptune's largest satellite) are likely massive and cool enough to have atmospheres (secs. 2.7.4 and 2.5.1.2), but none have been detected. A tenuous atmosphere would limit backwarming of the surface. Bolometric Bond albedos are now known for Pluto or the satellites of Uranus and Neptune; however, for Pluto the bolometric Bond albedo is likely small ($\leq$0.2). The surface temperature for these objects depends on the illumination conditions, rotation rate, and surface thermal properties that could result in large temperature variations. The integrated thermal radiation from these objects will be dominated by the warmest surface region, near the sub-solar point. It is appropriate then to accept as an upper limit the subsolar point temperature with a bolometric Bond albedo of 0. These limiting values for Pluto and the satellites of Uranus and Neptune are:

T_{eff}	<72 K	Pluto at perihelion
T_{eff}	<72 K	Satellites of Neptune
T_{eff}	<90 K	Satellites of Uranus

It should be understood that even higher temperatures are possible if the emissivity is not unity.

2.5 Satellites and Meteoroids

2.5.1 Satellites

Uranus has five natural satellites, Neptune has two, and Pluto none. Limits to the photographic magnitude of any yet undiscovered satellite for these planets have been given by Kuiper (ref. 72). For Neptune, an upper limit of approximately 160 km was established for the diameter of any undiscovered satellites in the region from 15 to 1200 planetary radii with larger diameters possible inside and outside those regions. These limits to diameters of undiscovered satellites apply to the same regions around Uranus. Satellites with diameters smaller than the foregoing values are known to exist in the solar system (ref. 23) so undiscovered satellites for Uranus, Neptune, and even Pluto are possible.

Photometric information and surface temperature are discussed for the satellites of Uranus and Neptune in sections 2.4.2 and 2.4.3. Detailed orbital information on the satellites other than Miranda and Nereid is given in the *American Ephemeris* and *Nautical Almanac*; the 1961 *Explanatory Supplement to the Ephemeris* (ref. 73) gives orbital information on satellites other than Miranda.

2.5.1.1 The Satellites of Uranus

The five satellites of Uranus revolve in nearly circular orbits with negligible mutual inclinations (<1′ of arc) at distances between 4.8 to 21.6 R_{eq} from Uranus' center and with periods between 1.4 and 13.5 days according to Kuiper (ref. 74). The orbital plane is generally taken as coincident with the planetary equator, but Sandner (ref. 75) cites the lack of confirmation. Steavenson (ref. 76) has noted variations in the brightness of these satellites with position in orbit, but rotation rate and rotation axis orientation are not known. The orbital properties and estimates of radius and mass are given in table XVII. The radius was estimated from the photo-visual magnitudes given by Harris (ref. 30) and a range of geometric albedo (0.08 – 0.65) suggested by Dollfus (ref. 47). The mass estimates given in table XVII were taken from the provisional satellite to planet mass ratios given by Kuiper (ref. 74). Because these ratios depend on an assumed equality of albedo and density for the five satellites (ref. 74), the implied mass in grams is taken as an order of magnitude estimate only. Two relationships that exist between the mean motions n_i of these satellites (ref. 74) are given by

$$n_5 - 3n_1 + 2n_2 = 0^\circ.079$$

$$n_1 - n_2 - 2n_3 + n_4 = 0^\circ.0034$$

where the subscript 1 refers to Ariel, 2 to Umbriel, 3 to Titania, 4 to Oberon, and 5 to Miranda.

2.5.1.2 The Satellites of Neptune

Neptune's two satellites stand in marked contrast to the regularity of the Uranian system. Triton circles Neptune in an orbit of negligible eccentricity at a distance of 14.1 R_{eq} with a period of 5.89 days (ref. 77). This motion is retrograde with respect to Neptune's rotation; the inclination of the orbital plane being approximately 161° to the planet's equator leads to precession of Triton's orbital pole (360° in 580.8 years) (ref. 8). The mass ratio of Triton to Neptune has been given by Alden (ref. 78), and Kovalevsky (ref. 3) quotes a second value by Nicholson et al. (1931). These two results differ by a factor of three which may be taken as a measure of the uncertainty in Triton's mass. On the basis of these results, Triton rivals Jupiter's Ganymede and Saturn's Titan for being the solar system's most massive satellite. Dollfus (ref. 47) indicates that G. P. Kuiper directly determined the diameter of Triton with a discometer. The diameter given by Dollfus (ref. 47) from this measurement is 3770 km with an estimated uncertainty of ±1300 km. At Triton's mean distance from the Earth, the

foregoing diameter corresponds to an angular diameter of less than 0.2". Triton is known to exhibit brightness variations which correlate with orbital position (ref. 30). If this correlation is real, it may imply synchronous rotation. Arguments given by Kuiper (ref. 79) indicate Triton might possess a tenuous atmosphere. A recent attempt (ref. 80) to detect methane established an upper limit for methane abundance, but no methane was found. Other less easily detectable gases are possible, but no limits on their abundance have been given.

Neptune's second satellite, Nereid, moves in an orbit of large eccentricity ($\simeq 0.75$) at a mean distance from the planet of 221 R_{eq} with a period of 359.9 days. Nereid's eccentricity is the largest among known natural satellites. The motion of Nereid is direct with respect to planetary rotation and the orbit is inclined approximately 28° to the planetary equator (ref. 77). Neither the mass nor the dimensions of this satellite are known. Here, the diameter has been estimated by assuming a range of geometric albedo (0.08 to 0.65) as was done for the satellites of Uranus. An extreme upper limit to the mass was estimated by combining the largest diameter given by the foregoing argument with a density of 8 g/cm^3, the upper limit density for meteoric material (ref. 23). These orbital and physical properties for Neptune's two satellites are given in table XXVIII (sec. 3).

2.5.2 Meteoroids

The planetary and interplanetary meteoroid environment from 0.1 to 30 AU has been specified in NASA SP-8038 (ref. 81). This range effectively includes Uranus, Neptune, and Pluto after 1979. The cometary meteoroid model given in NASA SP-8038 is recommended for use near any of these three planets in conjunction with the mass and radius values given in sections 2.1.1 and 2.1.2.

2.6 Charged Particles

2.6.1 Galactic Cosmic Rays

As observed near and from the Earth, galactic cosmic ray intensities are modulated by the interplanetary magnetic field (refs. 82, 83 and 84). In general, it is expected that this modulation reduces the intensities more severely at lower energies, closer to the Sun, and during intervals of greater solar activity. Quantitative predictions of the intensities near Uranus, Neptune, and Pluto have not been made. The approach adopted here is to specify fluxes in the observed energy range (0.1 and 10^{10} GeV) between zero and a spectrum extrapolated from the highest energies of cosmic rays observed for the most abundant particle kinds at times near minimum solar activity. This spectrum can be approximated for the flux of particles with kinetic energy greater than E by

$$\phi_E = K (E + M_o c^2)^{-1.5}$$

where $M_o c^2$ is the particle rest energy and E is the particle kinetic energy in GeV (both $M_o c^2$ and E in GeV per nucleon for alpha-particles). The summary by Haffner (ref. 85) gives

$K \simeq 2.5\ cm^{-2} \cdot s^{-1}$ for protons and $K \simeq 0.25\ cm^{-2} \cdot s^{-1}$ for alpha particles; Fanselow (ref. 86) gives $K \simeq 0.02\ cm^{-2} \cdot s^{-1}$ for electrons.

2.6.2 Solar Protons

Protons of energy greater than 1 MeV constitute a major component of solar cosmic rays. Their intensity near the Earth varies over several orders of magnitude, has both directional and isotropic components, and is positively correlated with flare activity. The intensity variation with heliocentric distance S has not been measured and depends on the configuration of the interplanetary magnetic field and the form and location of the heliosphere boundary. Because solar proton emission is sporadic and the radial dependence is not known, the fluxes adopted here for the vicinity of Uranus, Neptune, and Pluto are between 0 and 1.0 times the near-Earth values specified by McDonald (ref. 87).

2.6.3 Solar Wind

The properties of the solar wind are summarized by Dessler (ref. 88), Parker (ref. 89), and by Hundhausen (ref. 90) and the references therein. On the basis of data from spacecraft (for values of S in the range 0.8 to 1.5 AU), protons and electrons have observed concentrations of approximately $8\ S^{-2}\ cm^{-3}$ (for S in AU), and are streaming radially away from the Sun at speeds near 320 km/sec during quiescent solar conditions (ref. 90). Increased solar activity can result in temporary inceases up to factors of 10 in concentration and 3 in speed. The applicable theory suggests that extrapolation of these conditions towards the heliosphere boundary is justified.

The location of the heliosphere boundary, the shape of the corresponding solar cavity, and the nature of the boundary itself are all subjects of current controversy. Distances to the heliopause of from 5 AU (ref. 91) to 300 AU (ref. 89) are found in the current literature with arguments leading to intermediate values from 30 to 100 AU being given by Brandt (ref. 82), Semar (ref. 92), Blum and Fahr (ref. 93), and McDonough and Brice (ref. 94). If the wind terminated in a strong shock (as would be likely if the boundary were as near as 30 AU), Brandt (ref. 82) argues the solar wind particle speed will drop by a factor of four, the density will increase by the same amount, and the temperature of the solar wind protons and perhaps electrons will rise to 10^6 or 10^7°K. Current estimates of interstellar conditions (refs. 89 and 94) imply it is quite unlikely the heliosphere boundary is as near as the orbit of Uranus.

The position adopted here is to assume there exists some chance that the heliosphere boundary will be encountered on a mission to Neptune or Pluto. Interior to the boundary, the solar wind properties will be extrapolated from observations at 1 AU; beyond the boundary the arguments of Brandt (ref. 82) will be used.

2.6.4 Trapped Radiation Belts

On the basis of its radio emission, Jupiter is known to possess extensive trapped radiation belts containing relativistic electrons (refs. 36, 37 and 38). It is appropriate to consider the existence of such energetic particle belts for Uranus, Neptune, and Pluto.

2.6.4.1 Comparison of Uranus and Neptune with Jupiter

The sources of information describing the radio emission of Uranus and Neptune are contained in table VII (sec. 2.4.3); a comparison of selected data for these two planets and Jupiter is made in table VIII. This comparison indicates three deficiencies in the existing measurements for Uranus and Neptune. First, polarization measurements have been made at only a single frequency (3.12 cm) where for Jupiter the radiation is thought to be mainly of thermal origin and unpolarized. Second, no source extent measurements have been made. Third, there are no measurements at all beyond 11.13 cm for Uranus and 6 cm for Neptune.

For Jupiter, synchrotron emission is believed to be the dominant source of radiation for wavelengths greater than 10 cm and thermal emission the dominant source at wavelengths less than 6 cm (ref. 36). Thus, the existing measurements for Uranus and Neptune would not likely provide evidence of a synchrotron source.

The comparison in table VIII of the 8.6 mm and 10.4 cm Jovian brightness temperatures with those of Uranus and Neptune indicates rough agreement in magnitude and the general trend of increasing temperature with wavelength. This agreement is consistent with what would be expected of thermal emission from planetary atmospheres in which NH_3 is the principal opacity source (ref. 65). Law and Staelin (ref. 95) and Gulkis et al. (ref. 96) discuss NH_3 as an opacity source in the atmospheres of Jupiter and Saturn. There is some tendency in the disk brightness temperatures for Uranus and Neptune (table VII) to flatten out or decrease at the longest wavelengths observed. This is particularly evident in the self-consistent results reported by Mayer and McCullough (ref. 66). It would be premature to conclude this trend is real. If it were real, it would not indicate a synchrotron source. However, it might indicate the presence and amount of NH_3 and H_2O and provide associated information on pressure-temperature structure of these atmospheres. Radio emission from an extensive ionosphere could be made to mimic the longer wavelength brightness temperatures, but simple computation with the formulas provided by Gulkis et al. (ref. 96) demonstrates the required emission measurement (integral of electron density squared through the source) is unreasonably large.

The Jovian spectral flux density is observed to be nearly constant at $(6.7 \pm 1) \times 10^{-26}$ $W \cdot m^{-2} \cdot Hz^{-1}$ (ref. 36) from 10 to 100 cm. It is worth considering what the corresponding flux density would be if the Jovian source were scaled to the dimensions and mean opposition distance of Uranus and Neptune. If the effective emitting region varies as the equatorial radius cubed, the result is as follows:

at the distance of Uranus

$$\left[\frac{4.04}{18}\right]^2 \left[\frac{2.7}{7.14}\right]^3 (6.7) \times 10^{-26} W \cdot m^{-2} \cdot Hz^{-1} = 0.02 \times 10^{-26} W \cdot m^{-2} \cdot Hz^{-1}$$

TABLE VIII

SELECTED UHF RADIATION DATA FOR JUPITER, URANUS, AND NEPTUNE

JUPITER			URANUS			NEPTUNE		
Reference	Wavelength	Characteristic	Reference	Wavelength	Characteristic	Reference	Wavelength	Characteristic
Carr & Gulkis (ref. 36)	10-100 cm	22% linear polarization (approx. East-West)	Berge (ref. 39)	3.12 cm	No polarization established outside experimental uncertainty	Berge (ref. 39)	3.12 cm	No polarization established outside experimental uncertainty
Dickel (ref. 97)	6 cm	8.6% degree of polarization						
Berge (ref. 98)	10.4 cm	Most emission definitely external to disk			Emission source extent not established			Emission source extent not established
Branson (ref. 99)	21 cm	Same as above						
Dickel (ref. 97)	6 cm	Flux at 4.04 AU $(10.8 \pm 0.6) \times 10^{-26}$ W·m^{-2}·Hz^{-1}	Mayer & McCullough (ref. 66)	6 cm	Flux at 18 AU $(0.05 + 0.004) \times 10^{-26}$ W·m^{-2} Hz^{-1}	Mayer & McCullough (ref. 66)	6 cm	Flux at 29 AU $(0.02 \pm 0.002) \times 10^{-26}$ W·m^{-2}·Hz^{-1}
Carr & Gulkis (ref. 36)	10-100 cm	$(6.7 \pm 1) \times 10^{-26}$ W·m^{-2}·Hz^{-1}	Gerard (ref. 69)	11.13 cm	$(0.01 \pm 0.003) \times 10^{-26}$ W·m^{-2} Hz^{-1}			
Braun & Yen (ref. 100)	8.6 mm	Brightness temperature (all flux assigned to disk): 149 ±15 K	Pauliny-Toth & Kellermann (ref. 64)	9.5 mm	Brightness temperature (all flux assigned to disk): 125 ±15 K	Pauliny-Toth & Kellermann (ref. 64)	9.5 mm	Brightness temperature (all flux assigned to disk): 134 ±18 K
Dickel (ref. 97)	6 cm	369 ±6 K	Mayer & McCullough (ref. 66)	6 cm	210 ±17 K	Mayer & McCullough (ref. 66)	6 cm	227 ±23 K
Mayer (ref. 101)	10.3 cm	640 ±57 K	Gerard (ref. 68)	11.13 cm	180 ±40 K			
Berge* (ref. 98)	10.4 cm	260 K						
Mayer (ref. 101)	21 cm	3,000 K						

*Brightness temperature with non-thermal contribution removed.

at the distance of Neptune

$$\left[\frac{4.04}{29}\right]^2 \left[\frac{2.52}{7.14}\right]^3 (6.7) \times 10^{-26} \mathrm{W \cdot m^{-2} Hz^{-1}} = 0.006 \times 10^{-26} \mathrm{W \cdot m^{-2} Hz^{-1}}$$

Comparison of the Uranus result with the spectral flux density given in table VII at 11.13 cm indicates that Uranus is a somewhat weaker source than a scaled Jupiter model even if all the Uranian emission were considered as nonthermal. No such comparison is possible for Neptune because measurements do not extend to 10 cm.

The foregoing considerations lead to two conclusions. First, radio emission measurements do not establish either planet as a synchrotron source. Second, the existing measurements are in rough agreement with what would be expected of thermal emission from these atmospheres.

2.6.4.2 A Limiting Model for Neptune

It is not possible to construct a unique limiting model of the fluxes and energies of electrons and protons in the environment of Neptune because the necessary observations have not been made. The arguments given in the preceding section indicate Neptune could possess radiation belts comparable to Jupiter in energy and flux so as a limit to the radiation belts at Neptune, the nominal model developed for Jupiter and contained in NASA SP-8069 (ref. 38) will be adopted. Formulas describing this model are given in table IX. The latitude dependence contained in the Jovian model [NASA SP-8069] has been dropped because the orientation of the magnetic axis to the rotation axis is not known. Therefore, it is appropriate that the magnetic shell parameter L in the formulas given in table IX be interpreted simply as the distance from Neptune in units of Neptune's equatorial radius R_{eq} (sec. 2.1.2).

2.6.4.3 Uranus and Pluto

As with Neptune, there have been a few observations of Uranus appropriate for obtaining evidence of trapped radiation belts. There is some evidence (sec. 2.6.4.1) that at the longest wavelength of observation, 11.3 cm, Neptune's emission is less intense than that expected of a scaled Jovian source. This evidence is considerably weakened, however, when it is recognized that emission by the synchrotron mechanism strongly depends on the magnetic field strength and particle energy in accordance with the formulas given by references 37 and 102. A minor decrease in either the magnetic field or electron energy used for the nominal Jovian model of NASA SP-8069 (ref. 38) would substantially reduce the synchrotron emission at 11 cm.

The principal difference between Uranus and Neptune lies in the probable orientation of Uranus' magnetic axis. In 1985, Uranus' rotational axis will point within 10° of the Sun-Uranus direction. If Uranus has a polodial magnetic field, it is likely the magnetic axis lies within 20° of the rotational axis as is the case for the Earth and Jupiter (refs. 23, 36 and

TABLE IX

FORMULAS FOR UPPER LIMIT MODEL OF TRAPPED CHARGED PARTICLE RADIATION NEAR NEPTUNE AND URANUS

Parameter	Location	Characteristic Energy, E_o (MeV)	Flux Parameter Φ_o ($cm^{-2} \cdot s^{-1}$)
Electrons	$1 < L < 2$	6.2	2×10^7
	$2 < L$	$0.51 \left[\left(\frac{1377}{L^3} + 1\right)^{1/2} - 1\right]$	$\frac{1.7 \times 10^{10}}{L^6} \left(\frac{1377}{L^3} + 1\right)^{-1/2}$
Protons	$1 < L$	$938 \left[\left(\frac{1.06}{L^3} + 1\right)^{1/2} - 1\right]$	$\frac{4.7 \times 10^8}{L^6} \left(\frac{1.06}{L^3} + 1\right)^{-1/2}$
Distribution with Energy	$\Phi_E < \Phi_o \left(1 + \frac{E}{E_o}\right) \exp\left(-\frac{E}{E_o}\right)$		

37). Thus, solar wind electrons and protons streaming radially away from the Sun will approach the planet roughly parallel to magnetic field lines. With this geometry and the energies of solar wind electrons and protons, the trapping and acceleration of particles to MeV energies is not likely.

Whereas radiation belts with fluxes and energies comparable to Jupiter may be present at Uranus, the argument given here indicates the particle energies may be less.

It is possible that any Uranian radiation belts could be populated by cosmic ray neutron albedo decay or that particle lifetimes are long enough to allow residual belts to remain from periods of favorable orientation of the magnetic field with the solar wind. Primarily to indicate that this possibility exists, the same limiting model presented in section 2.6.4.2 and table IX for Neptune will be adopted for Uranus.

The absence of any relevant observations, uncertainties in the properties of the solar wind at Pluto's heliocentric distance, and insufficient information about Pluto's magnetic field preclude any discussion of trapped radiation and no model will be adopted.

2.6.5 Magnetosphere and Ionosphere

The size, shape, and charged particle content of the magnetospheres of Uranus, Neptune, and Pluto are not known because information is lacking on their magnetic fields (sec. 2.3)

and the properties of the solar wind (sec. 2.6.3). The sunward magnetosphere boundary could be as near to the planet as the ionosphere (small magnetic field and peak solar wind); or beyond 100 R_{eq} for Uranus and Neptune (10^{-3} T equatorial dipole field at 1 R_{eq} and nominal solar wind) and beyond 50 R_{eq} for Pluto (10^{-4} T equatorial surface field and nominal solar wind).

Observations of these planets give little indication of limits for the concentration and energy of magnetosphere plasma. Equating the plasma energy density to the planetary magnetic field energy density (ref. 38) will not provide useful plasma limits in the absence of a reasonable way for determining an upper limit magnetic field. Apart from the foregoing broad range for the sunward magnetosphere boundary, no attempt will be made to estimate the shape or plasma content for the magnetospheres of these planets.

No data observed for Uranus, Neptune, and Pluto have been related to the characteristics of the ionosphere. Theories on Jupiter's ionosphere have been published, but they have not been extended to Uranus and Neptune. Peak electron and proton densities of $10^{6 \pm 1}$ cm^{-3} derived for Jupiter by Gross and Rasool (ref. 103), Hunten (ref. 104), and Shimizu (ref. 105) may be representative for Uranus and Neptune. Atmospheric temperatures close to the exospheric value derived for Saturn by McGovern (ref. 106) are also reasonable. If the solar UV radiation responsible for maintenance of the ionosphere is absorbed principally at the same optical depth for Uranus and Neptune as for Jupiter, the corresponding pressure level will be roughly 2.5 times smaller (the ratio of gravitational accelerations at the equatorial radius R_{eq}). Thus, the 3 dyn/cm^2 level appropriate for Jupiter (ref. 103) suggests 1 dyn/cm^2 as a reasonable total gas pressure at the peak of the ion and electron concentrations for Uranus and Neptune. With the assumption of comparable temperatures, the ionospheric scale height for these two planets should be 2.5 times that for Jupiter, i.e., near 250 km. On this basis the description adopted herein for the ionosphere of Uranus and Neptune has a temperature of 150 ±50 K and equal electron and proton concentrations given by $N_o = 10^{6 \pm 1} \exp\left[-\frac{z-z_1}{250}\right]$ cm^{-3} for $z > z_1 = 300 \pm 200$ km and $N_o = 0$ for $z < z_1$. The range of values for z_1 is large enough to include several regions of local maximum electron density.

The absence of atmosphere for Pluto (sec. 2.7.4) would preclude the existence of an ionosphere. If there is a tenuous atmosphere, the ionosphere could extend to the surface of the planet. An upper limit to the positive ion and electron concentration of 10^6 cm^{-3} on the basis of peak concentrations for Earth (ref. 107) will be adopted. Because the temperature, dominant positive ion, and surface gravity are not known, a temperature of 150 ±50 K and a scale height of 200 km will be assumed. The concentration of equal numbers of electrons and positive ions is then given by $N_o \leq 10^6 \exp\left[-\frac{z}{200}\right]$ cm^{-3} with z in kilometers.

2.7 Atmospheres

Because of their similarity, the atmospheres of Uranus and Neptune are considered together; the atmosphere of Pluto is considered separately.

2.7.1 Composition of the Atmosphere of Uranus and Neptune

On the basis of planetary evolution, Kuiper (ref. 79) suggested that both Uranus and Neptune had lost appreciable amounts of H_2 and He. Although this conclusion is qualified by the uncertainty in basic assumptions, it has received indirect confirmation from attempts to construct overall models of Uranus and Neptune.

The compositions of Uranus and Neptune have been discussed by a number of authors, De Marcus (ref. 108), Porter (ref. 109), Reynolds and Summers (ref. 110) and Ramsey (ref. 111). Although the models developed by these authors strongly depend on meager observational data which has changed,* one general conclusion is apparent. Uranus and Neptune are far too massive on the basis of their radii to be composed predominantly of H_2. The conclusion by all authors is that Uranus and Neptune are not composed of a homogeneous solar-like mixture. This has led to models composed of mixtures given such names as "Mud", "CHONNE", "Ice", "Rock", and "Homall", all of which represent mixtures of elements and molecules with mean molecular weights greater than either H_2 or He. It is not possible to determine the composition of the outermost regions of these planets (their atmospheres) from any of the foregoing planetary models.

The presence of two molecules, molecular hydrogen (H_2) and methane (CH_4) is established in the atmospheres of Uranus and Neptune (refs. 79, 112, 113, 114, 115 and 116). The presence of ammonia (NH_3) is suggested for both planets on the basis of the trend of radio brightness temperatures as a function of wavelength. However, no specific spectral features attributable to NH_3 have been found at any wavelength for either planet. An analysis of a pressure-induced H_2 feature in the spectrum of Uranus and Neptune by Herzberg (ref. 112) leads to an estimate of the helium to hydrogen mixing ratio. However, the technique used has recently been questioned (refs. 117 and 118). In view of current evidence, the existence of helium in these atmospheres is not established.

McElroy (ref. 117) has summarized the existing abundance determinations on the basis of the absorption spectra of H_2 and CH_4. His summary and a subsequent article by Belton et al. (ref. 119) conclude that for Uranus sufficient hydrogen is present to require consideration of Rayleigh scattering in the line formation process. The quadrupole lines used in this analysis have not been reported for Neptune. The presence of large amounts of hydrogen in the atmosphere of Uranus and Neptune is accepted.

The amount of methane in the atmosphere of Uranus and Neptune has been estimated by Kuiper (ref. 79), Owen (ref. 116), and Teifel and Kharitonova (ref. 120). Kuiper's and Owen's estimates are based on a direct comparison of planetary and laboratory spectra. The large amounts estimated may result, in part, from comparison with laboratory spectra obtained at temperatures higher than expected in the line-forming regions of these planets.

*Section 2.1.2 gives recent radius determinations.

Teifel and Kharitonova (ref. 120) argue that Kuiper's estimates are too large by a factor of 100 because of the effects of scattering on an already-saturated band. The strong temperature dependence of the saturation vapor pressure of CH_4 make even this amount difficult to reconcile with the expected low atmospheric temperatures. Several possible explanations of the apparent CH_4 abundance are:

1) The atmospheric temperatures in the line-forming region are higher than expected.

2) Methane clouds are thin or non-existent so observation is below the region where methane is saturated.

3) The methane mixing ratio is large enough to drive the methane cloud base to higher temperatures and permit larger amounts of CH_4 above the cloud base.

The third of these explanations is judged the most likely and has been used to set the CH_4 mixing ratio in the models presented in section 2.7.3.

The foregoing arguments indicate that apart from the definite existence of H_2 and CH_4 the composition of the atmospheres of Uranus and Neptune is not known. The approach taken here is to assume that apart from CH_4 the nominal composition of the atmospheres of these two planets consists essentially of solar elements formed into the kinds of molecules expected in a hydrogen-reducing atmosphere. For the nominal model, the number fraction of CH_4 is taken as 0.03, approximately fifty times larger than would be given by a solar mixture. The abundance of elements in the Sun is taken from compilations by Lewis (ref. 121) and Hauge and Engvold (ref. 122). The resulting number fractions of atoms and molecules are given in tables X and XI and apply in the completely-mixed region of the atmosphere below the clouds. The uncertainty in composition is taken into account by two additional models given in tables X and XI. The Warm Model was derived from the Nominal by reducing the number fraction of all constituents other than H_2 by three; an atmosphere with 95% H_2 resulted. The Cool Model was derived by fixing the number fraction of He at 0.6 and increasing the constituents of the Nominal other than H_2 by three; a molecular hydrogen to helium ratio of approximately two was the result.

Only species with a number percent based on solar composition that is greater than 0.01 percent have been considered explicitly in tables X and XI. For some purposes, estimates of constituents present in trace amounts is required. Lewis (refs. 121 and 123) has provided a study of the compounds expected in the atmosphere of Jupiter which can be applied to Uranus and Neptune in conjunction with the models presented in section 2.7.3.

2.7.2 Pressure and Temperature Structure of the Atmospheres of Uranus and Neptune

For discussion, the atmospheres of Uranus and Neptune are divided into two parts, upper and lower separated by the tropopause.

2.7.2.1 Lower Atmosphere

In the lower atmosphere the primary contribution of the solar input is absorbed. A measurement of the total radiation emitted in the thermal infrared (1.24μm - 1000μm) would establish the presence or absence of an internal source of energy, but such broadband measurements have not been made for either planet. Two measurements over restricted bandwidths have been made for Uranus. Low (ref. 61) reported a brightness temperature of 55 ±3 K at 20μm with a 17.5 to 25μm bandwidth. Ney and Maas (ref. 124), on the basis of a single observation, reported a brightness temperature of 270 K at 3.6μm with a 1μm bandwidth. The effective temperature expected for Uranus at mean distance from the Sun,

TABLE X

COMPOSITION AND STRUCTURE PARAMETERS
FOR URANUS MODEL ATMOSPHERES

Parameter		Cool Model	Nominal Model	Warm Model
Fraction by Number	H_2	0.30559	0.85853	0.95285
	He	0.60000	0.11000	0.03667
	CH_4^*	0.09000	0.03000	0.01000
	H_2O^*	0.00300	0.00100	0.00033
	NH_3^*	0.00045	0.00015	0.00005
	Ne	0.00039	0.00013	0.00004
	Others	0.00057	0.00019	0.00006
Mean Molecular Weight, μ (g/mol)		4.55	2.68	2.24
Acceleration of Gravity, g (cm/s^2)		950	810	670
Troposphere lapse rate parameters				
	β_o	0.220	0.230	0.288
	K_1 (K)	97	484	450
	K_2 (K)	71	282	324
Correspondence level Temperature (K)		84	84	84
Correspondence level Pressure (atm)		3.0	1.0	0.3
Tropopause temperature (K)		47	54	60

*In unsaturated region of atmosphere.

TABLE XI

COMPOSITION AND STRUCTURE PARAMETERS
FOR NEPTUNE MODEL ATMOSPHERES

Parameters		Cool Model	Nominal Model	Warm Model
Fraction by Number	H_2	0.30559	0.85853	0.95285
	He	0.60000	0.11000	0.03667
	CH_4^*	0.09000	0.03000	0.01000
	H_2O^*	0.00300	0.00100	0.00033
	NH_3^*	0.00045	0.00015	0.00005
	Ne	0.00039	0.00013	0.00004
	Others	0.00057	0.00019	0.00006
Mean Molecular Weight, μ (g/mol)		4.55	2.68	2.24
Acceleration of Gravity, g (cm/s^2)		1160	1100	1040
Troposphere lapse rate parameters				
	β_o	0.220	0.23	0.288
	K_1 (K)	97	484	450
	K_2 (K)	71	282	324
Correspondence level Temperature (K)		57	57	57
Correspondence level Pressure (atm)		3	1.0	0.3
Tropopause temperature (K)		38	42	50

*In unsaturated region of atmosphere.

with the assumption of uniform temperature, is 64 K for a bolometric Bond albedo of 0 and 56 K for a bolometric Bond albedo of 0.4. A bolometric Bond albedo of 0.4 is near the value suggested for Uranus by Younkin and Münch (ref. 48). Thus, it can be seen that Low's result of 55 ±3 K is consistent with the temperatures expected with solar input only. The Ney and Maas result is especially difficult to understand. With the amounts of CH_4 suggested for the atmosphere of Uranus, absorption near 3.6μm should be dominated by CH_4 bands as is the case for Jupiter (ref. 125). Thus, the 3.6μm measurement should refer to regions higher in the atmosphere (than the one at 20μm) where the temperatures would be expected to be lower than the 270 K which was obtained.

For Uranus, there have been some additional "rotational" temperature estimates based on CH_4 and H_2 spectra (refs. 114, 115, 119 and 120). These results, however, are beset with

difficulties which render them unsuitable for determining atmospheric structure. The existing observations do not establish the structure of the atmosphere of either Uranus and Neptune or whether they are radiating more energy than they receive from the Sun.

Trafton (ref. 126) has developed model atmospheres for both Uranus and Neptune with H_2 and He as sources of thermal opacity. Although new information on the radius of these planets has been published (sec. 2.1.2) which affect the acceleration of gravity, Trafton's models represent the best published estimate of the lower atmosphere. Recently, Fox and Ozier (ref. 127) have pointed out the importance of pressure-induced methane in assessing thermal opacity sources for the outer planets. This source of opacity was not considered by Trafton. However, in the regions where an increase in opacity would be most important, the temperatures are so low that methane could only be a trace constituent. If, however, either planet were to possess an appreciable internal source of energy which would elevate atmospheric temperatures, methane could be an important thermal opacity source. Trafton found that his models for both Uranus and Neptune became unstable against convection at some depth in the radiative zone. If an internal heat source is present, convection may dominate the transport process to great depth. In the absence of such an energy source, the atmospheric temperature gradient would be expected to diminish at depths below which scattered sunlight does not penetrate.

2.7.2.2 Upper Atmosphere

For the upper atmosphere, the region above the tropopause, Trafton's models are nearly isothermal because he did not consider opacity sources other than H_2 and He. If CH_4 is present in this region and consideration is given to photochemical processes and energy deposition from short wavelength solar radiation, the possibility of a temperature inversion exists. Considerable analysis of this region in the atmospheres of Jupiter and Saturn has been done by Gross and Rasool (ref. 103), Hunten (ref. 104), Lewis and Prinn (ref. 128), Shimizu (ref. 105), and McGovern (ref. 106). For Neptune some evidence for higher temperatures in this region can be found in the pressure scale height derived from the 1968 stellar occultation by Neptune. Freeman and Lyngå (ref. 20) report a scale height of 28.9 ±2.6 km with larger values suggested by Kovalevsky and Link (ref. 18) and Guinan and Shaw (ref. 129). A scale height of 28.9 km corresponds to a ratio of temperatures to mean molecular weight of 38 $K/g \cdot mol^{-1}$. Assumption of $\mu = 2\ g \cdot mol^{-1}$ as the minimum mean molecular weight implies the temperature is greater than or equal to 76 K. This result refers to heights in the atmosphere where the pressure is less than 10^{-4} atm and is most simply explained by a temperature inversion at some height above the tropopause. No similar observation has been made for Uranus.

2.7.3 Models for the Atmosphere of Uranus and Neptune

The only published numerical models of the atmosphere of Uranus and Neptune are those of Trafton (ref. 126). These models do not completely tabulate the basic parameters of altitude, temperature, pressure, and density nor fully consider the possible range of atmospheric composition and the implications of the stellar occultation by Neptune. Therefore,

new sets of models have been developed for this monograph. These models assume hydrostatic equilibrium, the ideal gas law, and a smoothly-varying lapse rate throughout the tropospheric region. Changes in the tropospheric lapse rate from the convective value are expected from radiative processes and from cloud condensation effects, but these changes have not been taken into account because their effect would not be significant in comparison to the other large uncertainties.

The Nominal Models were constructed with the parameters given in tables X and XI. The convective troposphere's lapse rate depends on both composition and temperature. The correspondence level pressure and temperature for both Uranus and Neptune were taken directly from Trafton's 1967 models. The correspondence level also serves as the zero reference for the altitude scale. The change in mean molecular weight resulting from condensation was roughly accounted for above the base of the CH_4 clouds. The tropopause temperature was computed from $(1/2)^{1/4}\ T_{eff}$ where T_{eff} was computed at mean distance for each planet with an assumed bolometric Bond albedo of 0.4. Above the tropopause, an inversion layer of constant, $(P/T)(dT/dP) = \beta$, was used. β was determined by the requirement that the scale height be comparable to that given by Freeman and Lyngå (ref. 20) at a number density of 2×10^{12} cm^{-3}. The upper limit to these atmospheres was set at 10^{-7} atm, above which diffusive separation is likely and atomic hydrogen will become increasingly important. The lower limit was set at 10^{3} atm, at or below which the assumption of the ideal gas law is likely to break down.

The limiting models given in tables X, and XI are "cool" and "warm" in the sense that for a given pressure of the nominal model they provide extremes in temperature and density. The values selected for these models represent reasonable limits to the nominal values.

The specific numerical values calculated from these models are based on the atmospheric relationships given in appendix B and are tabulated in tables XX, XXI, XXII, XXXI, XXXII, and XXXIII (sec. 3). In each model the zero of altitude is taken at the correspondence level. The range in atmospheric variables between the Cool and Warm Models is intended to cover variations expected with changes in planetary longitude, latitude, and in the case of Uranus, season. For some purposes it is desirable to associate the planetary radius given in section 2.1.2 with the altitude scale of the model atmospheres. The values selected in section 2.1.2 correspond to occultation results, i.e., to low density regions of the atmosphere. The most direct procedure for associating the radial distance R with the altitude z is by

$$R = R_{eq}\,[1 + (z - z_o)/R_{eq} - \epsilon(\sin\phi)^2]$$

where z_o is the altitude in each model that corresponds to a total number density of $\sim 1 \times 10^{13}$ cm^{-3}.

2.7.4 The Atmosphere of Pluto

The most complete discussions of a possible Pluto atmosphere have been given by Kuiper (ref. 79) and Urey (ref. 130). At present there is no evidence that this planet has an atmosphere. The maximum sub-solar point temperature possible for Pluto at perihelion with

an assumed bolometric Bond albedo of 0.0 and unit emissivity is 72 K. The average temperature over the illuminated hemisphere is likely to be more than 10 K lower. Even at 72 K, only H_2, He, and Ne will remain unsaturated. These gases would not be expected to produce detectable absorptions. The other possible gases that would be saturated are N_2, O_2, CH_4, and A as well as some unlikely candidates like NO and CO. Kuiper suggested that the λ^{-4} Rayleigh law of scattering might be used to detect the presence of a thin atmosphere through the expected enhancement in the ultraviolet. Neither the geometric albedos given by Harris (ref. 30) nor the recent relative albedos by Fix et al. (ref. 46) show this type of increase. With a reasonable pressure scale height and surface temperature, Kuiper calculated the amount of methane the atmosphere of Pluto could support. The resulting column number density was 3×10^{19} molecules/cm^2 or about the same number of molecules contained in a column 1 cm $\times$ 1 cm^2 at the surface of the Earth. This amount is too small to be detected readily by spectroscopic means.

Because there is no information as to the kind and amount of material in Pluto's atmosphere and because there are appreciable uncertainties in its mass and radius (secs. 2.1.1 and 2.1.2), no model of Pluto's atmosphere will be constructed for this monograph.

3 CRITERIA

This section provides descriptions of the environment of Uranus, Neptune, and Pluto for use in the design of spacecraft operating near these planets. Here, in contrast to the State-of-the Art section, each planet will be treated separately. The preceding State-of-the-Art section contains a discussion of the investigations made in arriving at the adopted values. The uncertainties, ranges, or limits given herein represent extreme possible design values on the basis of current data and investigations. However, the real environment may be quite different in some cases.

3.1 Uranus

3.1.1 General Physical Properties

Values and uncertainties for Uranus' mass, radius, shape rotation rate, and several orbital parameters are given in table XII. This planet may be somewhat flattened and should be taken as an oblate spheroid. The planet is axially symmetric about the rotational axis, and the spheroid radius R_s depends on latitude ϕ through the relationship $R_s(\phi) = R_{eq}[1 - \epsilon(\sin\phi)^2]$. This radius is not to be associated with any cloud level and can be connected with the properties of the model atmospheres only by the relationship given in section 3.1.7. No solid surface has been identified, and none is expected at pressures less than 10^3 atm, the high pressure limit of section 3.1.7. The inclination of the rotational axis is such that the North rotational pole will be within 10° of the Uranus-Sun direction in 1985.

TABLE XII

PHYSICAL PROPERTIES OF URANUS

Parameters	Values
Range of distance from the Sun 1971-1980	18.3 to 18.8 AU
Mean distance from the Sun*	19.1819 AU
Heliocentric orbital speed 1971-1980	7.1 - 7.0 km s^{-1}
Period of revolution about the Sun	84.01 tropical years
Inclination of orbital plane to ecliptic plane*	0° 46' 23.''3
Inclination of equatorial plane to orbital plane*	97° 53'
Right ascension of North rotational pole*	α_R = 76.°76
Declination of North rotation pole*	δ_R = 14.°92
Mass of Uranus and satellites	$M_U = (8.72 \pm 0.08) \times 10^{25}$ kg
Gravitational constant of Uranus and satellites	$GM_U = (5.82 \pm 0.05) \times 10^6$ $km^3 \cdot s^{-2}$
Equatorial radius	R_{eq} = 27000 ±1000 km
Polar radius	R_{pl} = 26000 ±1300 km
Mean density	$\bar{\rho}$ = 1.1 ±0.1 g·cm^{-3}
Optical flattening or oblateness	ϵ = 0.03 ±0.03
Period of rotation	$T_o = 10^h.8 \pm 1^h$
Angular rotation rate	$\omega_o = (1.6 \pm 0.2) \times 10^{-4}$ rad·s^{-1}

*These parameters vary with time; the values given here are for qualitative purposes only. Values for particular times should be obtained from the references of section 2.1.3.

3.1.2 Gravity Field

Table XIII gives parameters and their uncertainties for Uranus' gravitational field.

TABLE XIII

GRAVITY FIELD AND RELATED PARAMETERS FOR URANUS

Gravitational potential at distance R from planet in a coordinate system not rotating	$-(215 \pm 2)\ (R_{eq}/R)\ km^2 \cdot s^{-2}$
Equatorial gravitational acceleration at $R = R_{eq}$ with rotation at ω_o (including uncertainty in R_{eq})	$730 \pm 60\ cm \cdot s^{-2}$
Polar gravitational acceleration at $R = R_{p\ell}$ (including uncertainty in $R_{p\ell}$)	$860 \pm 90\ cm \cdot s^{-2}$
Range of gravitational acceleration at $R = R_s$ (including rotation at ω_o)	$810 \pm 140\ cm \cdot s^{-2}$
Equatorial deflection from planocentric direction	$\phi' - \phi = (1\overset{\circ}{.}7 \pm 1\overset{\circ}{.}7)\ sin\ 2\phi$
Escape speed at distance R from planet (from above potential, at R_{eq})	$(20.8 \pm 0.1) \left(\frac{R_{eq}}{R}\right)^{1/2}\ km \cdot s^{-1}$
Orbital speed at distance R with semi-major axis a	$(14.7 \pm 0.1) \left(\frac{2R_{eq}}{R} - \frac{R_{eq}}{a}\right)^{1/2}\ km \cdot s^{-1}$
Period of object in orbit with semi-major axis a	$(3.21 \pm 0.01)\ (a/R_{eq})^{3/2}$ hours

3.1.3 Magnetic Field

Limits for the magnetic field strength, form (dipolar, quadrupolar, etc.), or orientation with respect to the rotational axis have not been established for Uranus. However, the presence of fields as large as 10^{-2} T (100 gauss) cannot be excluded in some regions near the planet so that this possibility should be considered in spacecraft design.

3.1.4 Electromagnetic Radiation

Outside of Uranus' atmosphere for which the tropopause is taken as the appropriate limit (sec. 3.1.7), the formulas in table XIV specify the ranges of intensity, flux, and temperature associated with conditions of maximum illumination. During partial illumination or eclipse, the values for intensities and fluxes of direct and reflected solar radiation may decrease to zero. The wavelength determines which radiation sources in table XIV should be considered. The ranges of geometric albedo and disk brightness temperature are given in figures 2 and 3.

TABLE XIV

ELECTROMAGNETIC RADIATION PARAMETERS NEAR URANUS WITH MAXIMUM ILLUMINATION

Parameters	Direct Sunlight* $1\ \text{Å} < \lambda < 100$ cm	Reflected Sunlight* $0.1\ \mu\text{m} < \lambda < 1.0\ \mu\text{m}$	Thermal Radiation** $10\ \mu\text{m} < \lambda < 100$ cm
Intensity — Power/(Area-wavelength-solid angle)	$I_\lambda = \dfrac{H_\lambda}{6.8 \times 10^{-5}\ \text{sr}}$	$I_\lambda = \dfrac{p_\lambda H_\lambda}{\pi R_{p\odot}^2}$	$I_\lambda = B_\lambda (T_D)$
Power/(Area-frequency-solid angle)			$I_\nu = B_\nu (T_D)$
Flux — Power/(Area-wavelength)	$F_\lambda = \dfrac{H_\lambda}{S^2}$	$F_\lambda = \dfrac{p_\lambda H_\lambda}{R_{p\odot}^2 (R/R_{eq})^2}$	$F_\lambda = \dfrac{\pi B_\lambda (T_D)}{(R/R_{eq})^2}$
Power/(Area-frequency)			$F_\lambda = \dfrac{\pi B_\nu (T_D)}{(R/R_{eq})^2}$
Integrated Flux — Power/Area	$F = \dfrac{(1.353 \pm 0.021) \times 10^{-1}}{S^2} \left(\dfrac{W}{cm^2}\right)$	$F = \dfrac{(4.3 \pm 1.4) \times 10^{-2}}{R_{p\odot}^2 (R/R_{eq})^2} \left(\dfrac{W}{cm^2}\right)$	*** $F = \dfrac{(7.9 \pm 3) \times 10^{-5}}{(R/R_{eq})^2} \left(\dfrac{W}{cm^2}\right)$
Effective Temperature			*** $T_{eff} = 61 \pm 5$ K

*Solar spectral irradiance from NASA SP-8005 (ref. 44), S and $R_{p\odot}$ in AU only, and geometric albedo p_λ from figure 2.
**Disk Brightness Temperature T_D from figure 3, and Planck functions B_λ (t) and B (t) from Allen (ref. 23) or elsewhere.
***With the assumption that Uranus does not have an internal energy source.

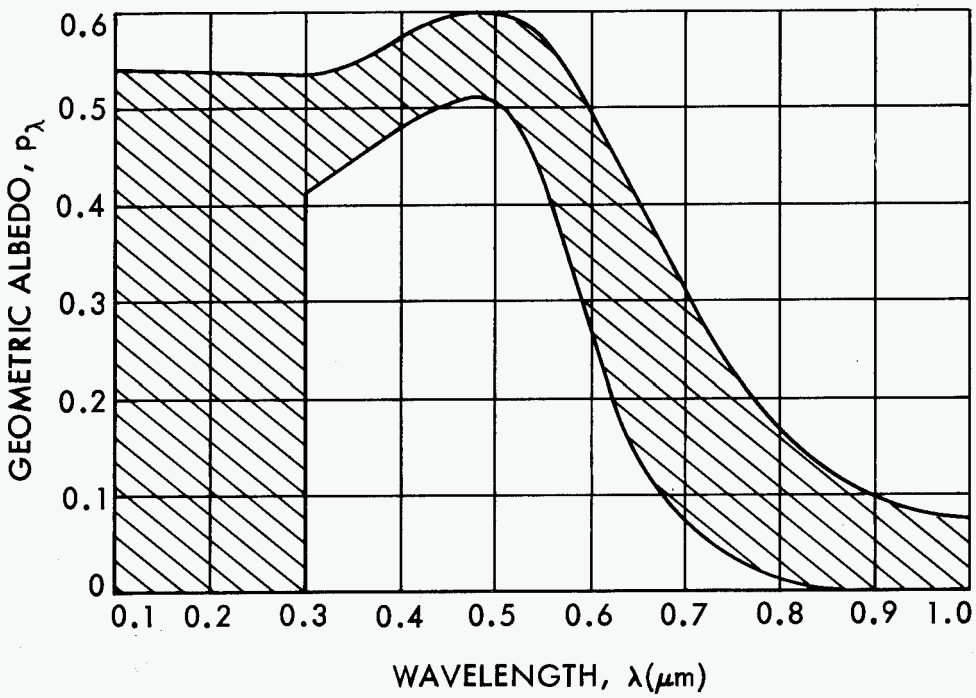

Figure 2.—Ranges of geometric albedo for Uranus.

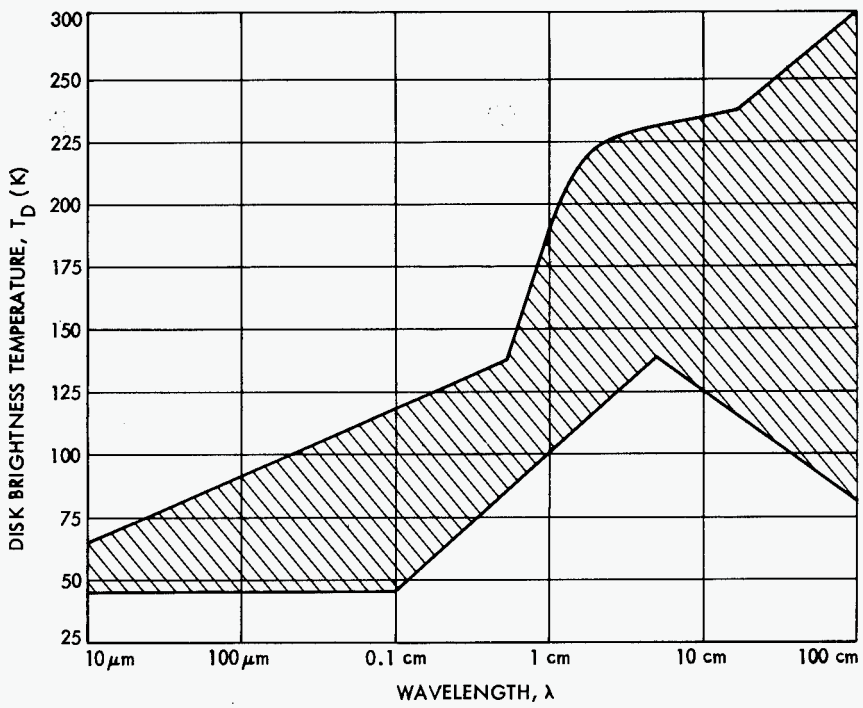

Figure 3.—Ranges of disk brightness temperature as a function of wavelength for Uranus.

TABLE XV

THERMAL RADIATION PARAMETERS BELOW THE TROPOPAUSE IN THE ATMOSPHERE OF URANUS FOR 10 $\mu m < \lambda < 100$ cm

Intensities*	$I_\lambda = B_\lambda(t)$ $I_\nu = B_\nu(t)$
Fluxes*	$F_\lambda = \pi B_\lambda(t)$ $F_\lambda = \pi B_\nu(t)$
Integrated Fluxes**	$F = \begin{cases} (7.9 \pm 3) \times 10^{-5} \left(\frac{W}{cm^2}\right) & \text{for } T < 61 \text{ K} \\ \left(\frac{T}{61}\right)^4 (7.9 \pm 3) \times 10^{-5} \left(\frac{W}{cm^2}\right) & \text{for } T > 61 \text{ K} \end{cases}$
Brightness Temperature	t = larger of T and T_D

*t is the larger of the disk brightness temperature shown in figure 3 and the local tropospheric temperature T (sec. 3.1.7); Planck functions $B_\lambda(t)$ and $B_\nu(t)$ from Allen (ref. 23) or elsewhere.
**With the assumption that Uranus does not have an internal radiation source.

The value and range shown for the thermal component of integrated flux F is predicted on the assumption that Uranus does not possess an internal energy source.

Below the tropopause, the maximum contribution of the Sun is identical to that given in table XIV. Table XIV also gives the values for reflected solar radiation which should be considered omni-directional to account for atmospheric scattering.

With the parameters in table XVI, Ψ in degrees, and both $R_{p,e}$ and Δ in AU, the visual magnitude of Uranus and its satellites is specified by $m_V = (m_o \pm 0.3) + 5\,log\,(R_{p,e}\,\Delta) + \Delta m \Psi$ where $\Delta m = (0.01\ ^{+0.01}_{-0.005})$ for the planet and $\Delta m = (0.03\ ^{+0.05}_{-0.01})$ for the satellites.

TABLE XVI

MAGNITUDES AND COLORS FOR THE SUN, URANUS, AND URANIAN SATELLITES

Object	Absolute Visual Magnitude	Mean Opposition Visual Magnitude	Brightness Differences between Photometric Passbands*			
	m_O	$\bar{m}$	U-B	B-V	V-R	R-I
Sun	-26.81	–	0.14	0.63	0.45	0.29
Uranus	-7.19	+5.52	0.28	0.56	-0.15	-0.80
Ariel I	+1.7	+14.4	–	–	–	–
Umbriel II	+2.6	+15.3	–	–	–	–
Titania III	+1.30	+14.01	0.25	0.62	0.52	0.41
Oberon IV	+1.49	+14.20	0.25	0.65	0.49	0.33
Miranda V	+3.8	+16.5	–	–	–	–

*For photometric definitions see appendix C.

3.1.5 Satellites and Meteoroids

Orbital and physical properties of Uranus' five satellites are given in table XVII. Their photometric properties are given in section 3.1.4. All of them except Miranda can be located from information in the appropriate year of the *American Ephemeris and Nautical Almanac* and the *Explanatory Supplement to the Ephemeris* (ref. 73). Rotation rate and rotation axis orientation are not known for any of these satellites. Surface temperatures are not known but are likely to be less than 90 K (the sub-solar point temperature for a black non-conducting object at Uranus' distance from the Sun of unit emissivity) with temperatures as low as 3 K possible for unilluminated regions.

The meteoroid environment near Uranus should be obtained from the cometary meteoroid model and procedures of NASA SP-8038 (ref. 81) with the mass and radius values given in 3.1.1.

TABLE XVII

ORBITAL AND PHYSICAL PROPERTIES OF URANUS' SATELLITES

Satellite	Range of Distance for Uranus' Center (km)	Ratio of Mean Distance to Uranus' Equatorial Radius	Orbital Period (days)	Orbital Speed (km/s)	Range of Planetocentric Latitude* (degrees)	Radius** (km)	Mass (kg)
V Miranda	$(129.8 \pm 1) \times 10^3$	4.8	1.413	7	< 0.02	140–400	$9 \times 10^{19 \pm 1}$
I Ariel	$(190.9 \pm 1) \times 10^3$	7.1	2.520	6	< 0.02	370–1100	$1 \times 10^{21 \pm 1}$
II Umbriel	$(266.0 \pm 1) \times 10^3$	9.9	4.144	5	< 0.02	240–700	$5 \times 10^{20 \pm 1}$
III Titania	$(436.0 \pm 1) \times 10^3$	16.1	8.706	4	< 0.02	440–1300	$4 \times 10^{21 \pm 1}$
IV Oberon	$(583.4 \pm 1) \times 10^3$	21.6	13.46	3	< 0.02	400–1200	$3 \times 10^{21 \pm 1}$

*Orbital plane taken as identical to equatorial plane; all five satellite orbits are inclined less than 1' of arc with respect to one another.
**Range possible assuming visual geometric albedo between 0.08 and 0.65.

TABLE XVIII

PARAMETERS FOR CHARGED PARTICLES NEAR URANUS

Particle	Location	Temperature, Energy, or Velocity	Number Density or Flux
Galactic Cosmic Rays	Everywhere	$0.1 < E < 10^{10}$ GeV (GeV/nucleon for alphas)	$\Phi_E = K(E + M_o c^2)^{-1.5}$ Electrons– $0 \leq K \leq 0.02$ cm$^{-2}\cdot$s^{-1} Protons– $0 \leq K \leq 2.5$ cm$^{-2}\cdot$s^{-1} Alphas– $0 \leq K \leq 0.25$ cm$^{-2}\cdot$s^{-1}
Solar Cosmic Ray Protons	Everywhere	$10 < E < 10^4$ MeV	Sporadic, with fluxes between 0 and 1.0 times those specified in NASA TR R-169 (ref. 87)
Solar Wind (Electrons and Protons)	Beyond Magnetosphere	V = 320 km/s (up to 960 km/sec, at peak solar activity)	$N_o = 0.02$ cm^{-3} (up to 0.2 cm^{-3} at peak solar activity)
Trapped Radiation (Electrons and Protons)	$1 < L < 2$	6.2 MeV	$\Phi_o = 2 \times 10^7$ cm$^{-2}\cdot$s^{-1}
Trapped Radiation (Electrons)	$2 < L$	$(0.51)\left[\left(\frac{1377}{L^3}+1\right)^{1/2}-1\right]$ MeV	$\Phi_o = \frac{1.7\times10^{10}}{L^6}\left(\frac{1377}{L^3}+1\right)^{-1/2}$ cm$^{-2}\cdot$s^{-1}
Trapped Radiation (Protons)	$1 < L$	$(938)\left[\left(\frac{1.06}{L^3}+1\right)^{1/2}-1\right]$ MeV	$\Phi_o = \frac{4.7\times10^{8}}{L^6}\left(\frac{1.06}{L^3}+1\right)^{1/2}$ cm$^{-2}\cdot$s^{-1}
Distribution with Energy (Electrons and Protons)	$1 < L$	–	$\Phi_E < \Phi_o (1 + E/E_o) \exp(-E/E_o)$
Ionosphere (Electrons and Protons)	For $z > z_1$, where $z_1 = 300 \pm 200$ km	$T = 150 \pm 50$ K	$N_o = (10^{6\pm1}$ cm$^{-3}) \exp\left(-\frac{z-z_1}{250}\right)$ z in km
Magnetospheric Plasma (Electrons and Protons)	Within Magnetosphere	$10^{-2} < E < 10^6$ eV	Not established

3.1.6 Charged Particles and Magnetosphere

Table XVIII presents formulas and parameters for galactic cosmic rays, solar cosmic ray protons, the solar wind, and ionosphere as well as a limiting model for trapped radiation. The sunward magnetosphere boundary may be as near to the planet as the ionosphere or farther than 100 R_{eq}. Uranus' magnetic axis may point in the direction of the solar wind about 1985.

3.1.7 Atmospheric Structure

The Nominal Model atmosphere of Uranus given in table XXI contains values for the temperature T, density ρ, altitude z, logarithmic lapse rate β, lapse rate dT/dz, pressure and density scale heights H_p and H_ρ, and cloud mass w as functions of pressure P for 10^{-7} atm $\leq P \leq$ 1000 atm. Tables XX and XXII give Cool and Warm Model atmospheres which cover the uncertainty in construction of the Nominal Model and variations with planetary latitude, time of day, local features, and seasons. These models represent cool and warm extremes at given pressures only. The compositions for all three models are given in table XIX which does not take into account condensation. The amount of a condensable (CH_4, NH_3,

TABLE XIX

COMPOSITION FOR URANUS MODEL ATMOSPHERES

Parameter	Cool Model	Nominal Model	Warm Model
Fraction by Number			
H_2	0.30559	0.85853	0.95285
He	0.60000	0.11000	0.03667
CH_4^*	0.09000	0.03000	0.01000
H_2O^*	0.00300	0.00100	0.00033
NH_3^*	0.00045	0.00015	0.00005
Ne	0.00039	0.00013	0.00004
Others	0.00057	0.00019	0.00006
Mean Molecular Weight μ	4.55	2.68	2.24

*In unsaturated region of atmosphere.

or H_2O) that can be present above a cloud base in gas form can be computed with the aid of the saturation vapor pressure formulas and constants given in appendix B. For all models, the zero of altitude is arbitrarily set at the correspondence level. The distance from Uranus' center R to any altitude z in the models is given by

$$R = R_{eq}[1 + (z - z_o)/R_{eq} - \epsilon(sin\ \phi)^2]$$

where $R_{eq} = 27000 \pm 1000$ km, $\epsilon = 0.03 \pm 03$, and z_o is a reference altitude given separately for each model in tables XX, XXI, and XXII. Although all models indicate the presence of CH_4 clouds, it should not be assumed that the limb of the planet is defined by these clouds at any wavelength. Interpolation between tabulated values should be carried out with the formulas in appendix B.

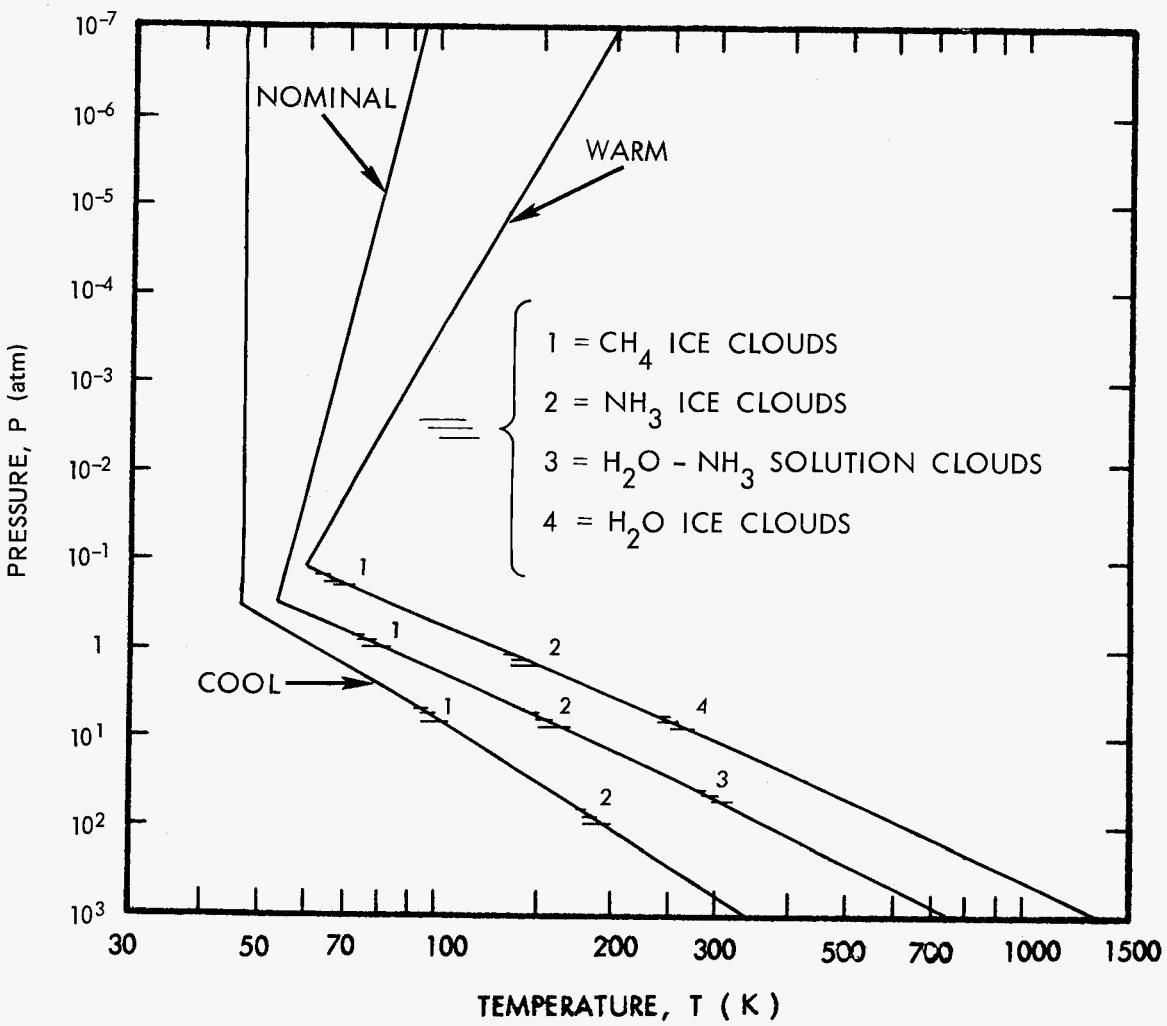

Figure 4.—Pressure versus temperature for Uranus model atmospheres.

TABLE XX

VALUES AT SELECTED PRESSURES FOR WARM, EXTENDED URANUS MODEL ATMOSPHERE

P (atm)	T (K)	ρ ($g \cdot cm^{-3}$)	z (km)	β	dT/dz (K/km)	H_p (km)	H_ρ (km)	w (mg/l)	Remarks
10^{-7}	200.0	1.28×10^{-11}	1003	-0.086	0.145	119	109		z_o Reference Level
10^{-6}	164.0	1.55×10^{-10}	755	-0.086	0.145	97.2	89.5		
10^{-5}	134.6	1.90×10^{-9}	552	-0.086	0.145	79.8	73.4		
10^{-4}	110.4	2.31×10^{-8}	385	-0.086	0.145	65.4	60.2		
10^{-3}	90.6	2.82×10^{-7}	248	-0.086	0.145	53.7	49.4		
10^{-2}	74.3	3.43×10^{-6}	136	-0.086	0.145	44.0	40.5		
0.03	67.6	1.11×10^{-5}	90.3	-0.086	0.145	40.0	36.8		
0.12	60.0	5.35×10^{-5}	36.8	0.383	-0.690	34.9	56.6	0.3	Tropopause
0.15	65.0	6.40×10^{-5}	27.8	0.381	-0.688	36.0	58.2	1.3	
0.18	69.7	7.17×10^{-5}	20.9	0.390	-0.686	38.6	62.3	4.4	CH_4 Cloud Base
0.3	84.0	9.75×10^{-5}	0.0	0.377	-0.680	46.6	75.7		Correspondence Level
1.0	131.5	2.07×10^{-4}	-70.8	0.368	-0.663	72.9	115	0.005	
1.14	138.0	2.25×10^{-4}	-80.6	0.367	-0.661	76.5	121	0.02	
1.29	144.4	2.44×10^{-4}	-90.2	0.365	-0.659	80.0	126	0.07	NH_3 Ice Cloud Base
3.0	195.9	4.18×10^{-4}	-169.3	0.358	-0.646	109	169		
4.71	230.0	5.59×10^{-4}	-222.3	0.354	-0.638	127	197	0.08	
5.96	250.0	6.51×10^{-4}	-253.8	0.351	-0.634	139	214	0.6	
6.80	261.7	7.09×10^{-4}	-272.3	0.350	-0.631	145	223	1.7	H_2O Ice Cloud Base
10.0	299.4	9.12×10^{-4}	-332.3	0.346	-0.625	166	254		
30.0	435.3	1.88×10^{-3}	-554.6	0.336	-0.606	241	363		
100	648.1	4.21×10^{-3}	-910.7	0.325	-0.587	359	532		
300	922.3	8.88×10^{-3}	1394	0.317	-0.572	511	748		
1000	1345.8	2.03×10^{-2}	2132	0.310	-0.559	745	1080		

TABLE XXI

VALUES AT SELECTED PRESSURES FOR NOMINAL URANUS MODEL ATMOSPHERE

P (atm)	T (K)	ρ ($g \cdot cm^{-3}$)	z (km)	β	dT/dz (K/km)	H_p (km)	H_ρ (km)	w (mg/l)	Remarks
10^{-7}	94.7	2.87×10^{-11}	532	−0.0377	0.0819	43.6	42.0		z_o Reference Level
10^{-6}	86.8	3.13×10^{-10}	436	−0.0377	0.0819	40.0	38.5		
10^{-5}	79.6	3.41×10^{-9}	346	−0.0377	0.0819	36.7	35.3		
10^{-4}	73.0	3.72×10^{-8}	267	−0.0377	0.0819	33.6	32.4		
10^{-3}	66.9	4.06×10^{-7}	193	−0.0377	0.0819	30.8	29.7		
10^{-2}	61.4	4.43×10^{-6}	125	−0.0377	0.0819	28.3	27.2		
0.03	58.9	1.38×10^{-5}	94.8	−0.0377	0.0819	27.1	26.1		
0.10	56.2	4.83×10^{-5}	62.9	−0.0377	0.0819	25.9	25.0		
0.30	54.0	1.49×10^{-4}	35.4	0.368	−0.80	24.9	39.4		Tropopause
0.49	65.0	2.19×10^{-4}	21.5	0.364	−0.84	28.0	44.0	1.3	
0.73	75.0	3.17×10^{-4}	9.6	0.360	−0.94	28.7	44.9	14.5	
0.93	81.9	3.71×10^{-4}	2.3	0.357	−0.93	31.4	48.9	54.9	CH_4 Ice Cloud Base
1.00	84.0	3.89×10^{-4}	0.0	0.357	−0.93	32.2	50.0		Correspondence Level
3.0	123.5	7.93×10^{-4}	−43.2	0.345	−0.90	47.3	72.2		
4.80	145.0	1.08×10^{-3}	−67.3	0.339	−0.88	55.6	84.0	0.1	
5.85	155.0	1.23×10^{-3}	−78.6	0.336	−0.88	59.4	89.5	0.4	
6.69	162.2	1.34×10^{-3}	−86.9	0.335	−0.87	62.1	93.4	1.12	NH_3 Ice Cloud Base
10.00	185.3	1.76×10^{-3}	−113.6	0.329	−0.86	71	106		
30.0	264.1	3.71×10^{-3}	−207.3	0.315	−0.82	101	148		
32.2	270.0	3.89×10^{-3}	−214.5	0.314	−0.82	103	151	3.3	
42.7	295.0	4.73×10^{-3}	−245.2	0.311	−0.81	113	164	15.0	
48.4	306.6	5.16×10^{-3}	−295.5	0.309	−0.81	118	170	28.0	Solution Cloud Base H_2O–NH_3
100	382.3	8.54×10^{-3}	−355.9	0.300	−0.78	146	209		
300	527.8	1.86×10^{-2}	−545.1	0.287	−0.75	202	284		
1000	740.5	4.41×10^{-2}	−835.2	0.275	−0.72	284	392		

TABLE XXII

VALUES AT SELECTED PRESSURES FOR COOL, DENSE URANUS MODEL ATMOSPHERE

p (atm)	T (K)	ρ (g·cm^{-3})	z (km)	β	dT/dz (K/km)	H_p (km)	H_ρ (km)	w (mg/l)	Remarks
10^{-7}	47.0	8.68×10^{-11}	220	0.0	0.0	12.3	12.3		z_o Reference Level
10^{-6}	47.0	8.68×10^{-10}	192	0.0	0.0	12.3	12.3		
10^{-5}	47.0	8.68×10^{-9}	164	0.0	0.0	12.3	12.3		
10^{-4}	47.0	8.68×10^{-8}	135	0.0	0.0	12.3	12.3		
10^{-3}	47.0	8.68×10^{-7}	107	0.0	0.0	12.3	12.3		
10^{-2}	47.0	8.68×10^{-6}	78.7	0.0	0.0	12.3	12.3		
0.03	47.0	2.60×10^{-5}	65.2	0.0	0.0	12.3	12.3		
0.10	47.0	8.68×10^{-5}	50.4	0.0	0.0	12.3	12.3		
0.33	47.0	2.86×10^{-4}	35.8	0.268	-1.02	12.3	16.8		Tropopause
1.00	63.1	6.80×10^{-4}	20.0	0.262	-1.05	15.6	21.2	0.7	
3.00	84.0	1.62×10^{-3}	0.0	0.257	-1.09	19.7	26.5	71.6	Correspondence Level
3.93	90.0	1.98×10^{-3}	-5.5	0.256	-1.08	21.1	28.4	179.2	
4.85	95.0	2.50×10^{-3}	-9.8	0.254	-1.16	20.7	27.8	350.0	
6.25	101.3	3.42×10^{-3}	-14.6	0.253	-1.32	19.5	26.1	734.8	CH_4 Ice Cloud Base
10	114.0	4.86×10^{-3}	-24.3	0.251	-1.30	21.9	29.3		
30	149.8	1.11×10^{-2}	-52.0	0.246	-1.28	28.8	38.2	0.2	
39.2	160.0	1.35×10^{-2}	-60.0	0.245	-1.27	30.8	40.8	0.8	
63.6	180.0	1.96×10^{-2}	-75.8	0.243	-1.26	34.6	45.7	10.0	
80.7	190.7	2.35×10^{-2}	-84.3	0.242	-1.26	36.7	48.4	31.4	NH_3 Ice Cloud Base
100	200.8	2.76×10^{-2}	-92.3	0.241	-1.25	38.6	50.9		
300	261.1	6.37×10^{-2}	-141	0.237	-1.23	50.2	65.9		
1000	346.7	1.6×10^{-1}	-211	0.234	-1.21	66.7	87.0		

3.2 Neptune

3.2.1 General Physical Properties

Values and uncertainties for Neptune's mass, radius, shape, rotation rate, and several orbital parameters are given in table XXIII. This planet may be somewhat flattened and should be

TABLE XXIII

PHYSICAL PROPERTIES OF NEPTUNE

Parameters	Values
Range of distance from the Sun 1971–1980	30.3 AU (essentially constant)
Mean distance from the Sun*	30.0579 AU
Heliocentric orbital speed 1971–1980	5.4 $km \cdot s^{-1}$ (essentially constant)
Period of revolution about the Sun	164.80 tropical years
Inclination of orbital plane to ecliptic plane*	1° 46′ 21.″8
Inclination of equatorial plane to orbital plane*	28° 48′
Right ascension of North rotational pole*	$\alpha_R = 294.^{\circ}9$
Declination of North rotation pole*	$\delta_R = 40.^{\circ}53$
Mass of Neptune and satellites	$M_N = (1.03 \pm 0.01) \times 10^{26}$ kg
Gravitational constant of Neptune and satellites	$GM_N = (6.87 \pm 0.07) \times 10^6$ $km^3 \cdot s^{-2}$
Equatorial radius	$R_{eq} = 25200 \pm 200$ km
Polar radius	$R_{p\ell} = 24700 \pm 500$ km
Mean density	$\bar{\rho} = 1.57 \pm 0.04$ $gr \cdot cm^{-3}$
Optical flattening or oblateness	$\epsilon = 0.02 \pm 0.02$
Period of rotation	$T_o = 16^h \pm 2^h$
Angular rotation rate	$\omega_o = (1.1 \pm 0.1) \times 10^{-4}$ $rad \cdot s^{-1}$

*These parameters vary with time; the values given here are for qualitative purposes only. Values for particular times should be obtained from the references of 2.1.3.

taken as an oblate spheroid. The planet is axially symmetric about the rotational axis, and the spheroid radius R_s depends on latitude ϕ through the relationship $R_s(\phi) = R_{eq}[1-\epsilon(\sin\phi)^2]$. This radius is not to be associated with any cloud level and can be connected with the properties of the model atmospheres only by the relationship given in section 3.2.7. No solid surface has been identified, and none is expected at pressures less than 10^3 atm, the high pressure limit of section 3.2.7.

3.2.2 Gravity Field

Table XXIV gives parameters and their uncertainties for Neptune's gravitational field.

3.2.3 Magnetic Field

Limits for the magnetic field strength, form (dipolar, quadrupolar, etc.), or orientation with respect to the rotational axis have not been established for Neptune. However, the presence

TABLE XXIV

GRAVITY FIELD AND RELATED PARAMETERS FOR NEPTUNE

Gravitational potential at distance R from planet in a coordinate system not rotating	$-(273 \pm 3)\,(R_{eq}/R)\ km^2 \cdot s^{-2}$
Equatorial gravitational acceleration at $R = R_{eq}$ with rotation at ω_o (including uncertainty in R_{eq})	$1060 \pm 20\ cm \cdot s^{-2}$
Polar gravitational acceleration at $R = R_{pc}$ (including uncertainty in R_{pc})	$1110 \pm 50\ cm \cdot s^{-2}$
Range of gravitational acceleration at $R = R_s$ (including rotation at ω_o)	$1100 \pm 60\ cm \cdot s^{-2}$
Equatorial deflection from planocentric direction	$\phi' - \phi = (1^\circ.1 \pm 1^\circ.1)\ sin\ 2\phi$
Escape speed at distance R from planet (from above potential at R_{eq})	$(23.4 \pm 0.1)\left(\frac{R_{eq}}{R}\right)^{1/2}\ km \cdot s^{-1}$
Orbital speed at distance R with semi-major axis a	$(16.5 \pm 0.1)\left(\frac{2R_{eq}}{R} - \frac{R_{eq}}{a}\right)^{1/2}\ km \cdot s^{-1}$
Period of object in orbit with semi-major axis a	$(2.66 \pm 0.01)\,(a/R_{eq})^{3/2}$ hours

of fields as large as 10^{-2}T (100 gauss) cannot be excluded in some regions near the planet so that this possibility should be considered in spacecraft design.

3.2.4 Electromagnetic Radiation

Outside of Neptune's atmosphere, for which the tropopause is taken as the appropriate limit (sec. 3.2.7), the formulas in table XXV specify the ranges of intensity, flux, and temperature associated with conditions of maximum illumination. During partial illumination or eclipse, the values for intensities and fluxes of direct and reflected solar radiation may decrease to zero. The wavelength determines which radiation sources in table XXV should be considered. The ranges of geometric albedo and disk brightness temperature are given in figures 5 and 6. The value and range shown for the thermal component of integrated flux F are predicted on the assumption that Neptune does not possess an internal energy source.

Below the tropopause, the maximum contribution of the Sun is identical to that given in table XXV. Table XXV also gives the values for reflected solar radiation which should be considered omnidirectional to account for atmospheric scattering.

With the parameters in table XXVII, Ψ in degrees, and $R_{p\odot}$ and Δ in AU, the visual magnitude of Neptune is specified by

$$m_V = (m_o \pm 0.1) + 5\,log(R_{p\odot}\Delta) + (0.1^{+0.01}_{-0.005})\Psi$$

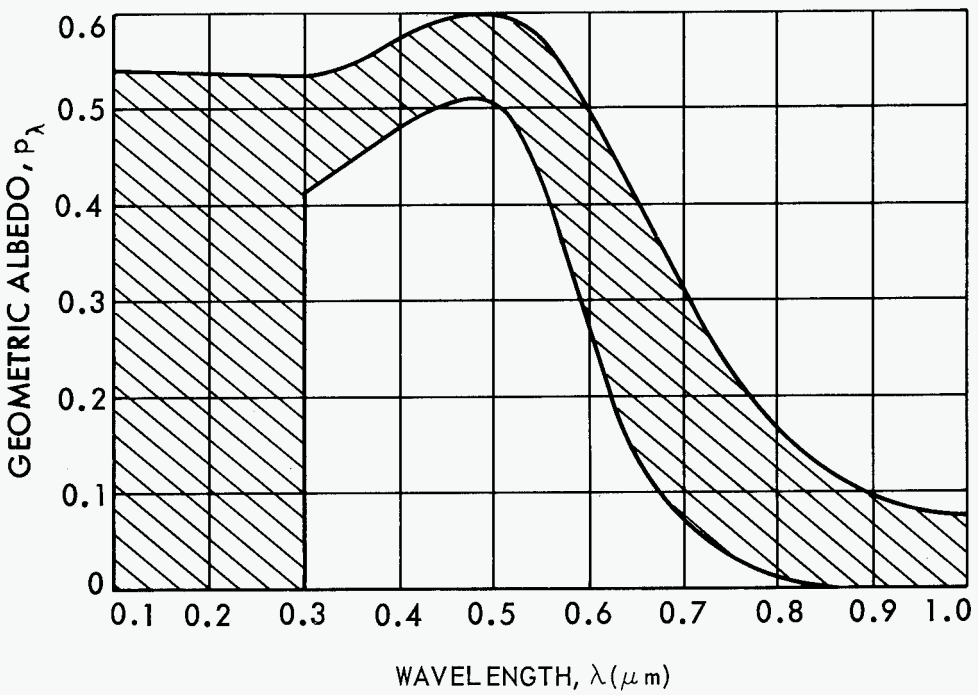

Figure 5.—Ranges of geometric albedo for Neptune.

TABLE XXV

ELECTROMAGNETIC RADIATION PARAMETERS NEAR NEPTUNE WITH MAXIMUM ILLUMINATION

Parameters	Direct Sunlight* $1\ \text{Å} < \lambda < 100$ cm	Reflected Sunlight* $0.3\ \mu\text{m} < \lambda < 1.0\ \mu\text{m}$	Thermal Radiation** $10\ \mu\text{m} < \lambda < 100$ cm
Intensity — Power/(Area-wavelength-solid angle)	$I_\lambda = \dfrac{H_\lambda}{6.8 \times 10^{-5}\ \text{sr}}$	$I_\lambda = \dfrac{p_\lambda H_\lambda}{\pi R_{p\odot}^2}$	$I_\lambda = B_\lambda (T_D)$
Power/(Area-frequency-solid angle)			$I_\nu = B_\nu (T_D)$
Flux — Power/(Area-wavelength)	$F_\lambda = \dfrac{H_\lambda}{S^2}$	$F_\lambda = \dfrac{p_\lambda H_\lambda}{R_{p\odot}^2 (R/R_{eq})^2}$	$F_\lambda = \dfrac{\pi B_\lambda (T_D)}{(R/R_{eq})^2}$
Power/(Area-frequency)			$F_\nu = \dfrac{\pi B_\nu (T_D)}{(R/R_{eq})^2}$
Integrated Flux — Power/(Area)	$F = \dfrac{(1.353 \pm 0.021) \times 10^{-1}}{S^2} \left(\dfrac{W}{cm^2}\right)$	$F = \dfrac{(4.3 \pm 1.4) \times 10^{-2}}{R_{p\odot}^2 (R/R_{eq})^2} \left(\dfrac{W}{cm^2}\right)$	*** $F = \dfrac{(2.3 \pm 1) \times 10^{-5}}{(R/R_{eq})^2} \left(\dfrac{W}{cm^2}\right)$
Effective Temperature			*** $T_e = 45 \pm 3$K

*Solar spectral irradiance from NASA SP-8005 (ref. 44), S and $R_{p\odot}$ in AU only, and geometric albedo p_λ from figure 5.

**Disk Brightness Temperature T_D from figure 6, and Planck functions B_λ (t) and B_λ (t) from Allen (ref. 23) or elsewhere.

***With the assumption that Neptune does not have an internal radiation source.

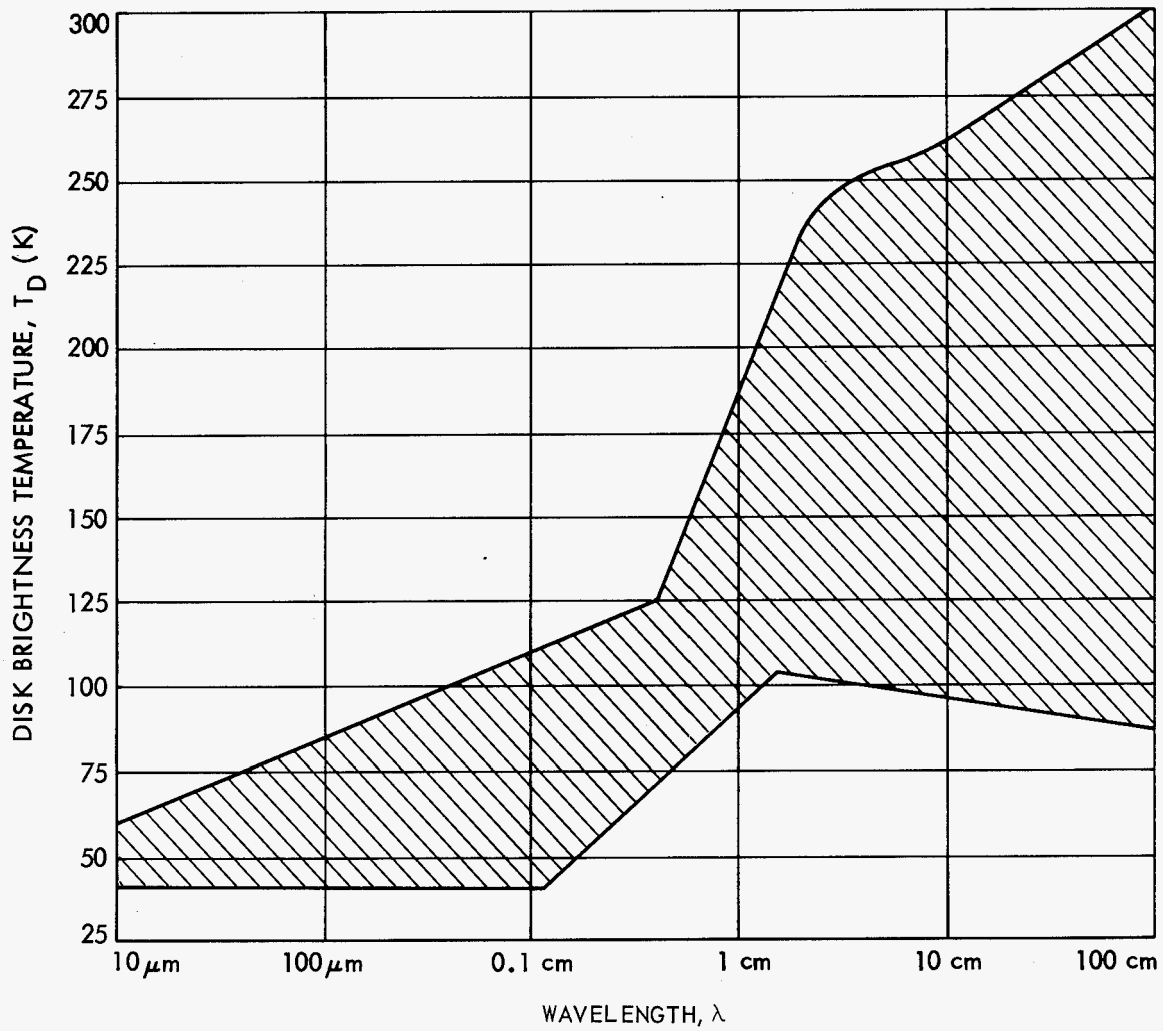

Figure 6.—Ranges of disk brightness temperature as a function of wavelength for Neptune.

and the visual magnitude of its two satellites by

$$m_V = (m_o \pm 0.3) + 5\,log(R_p \Delta) + (0.03^{+0.05}_{-0.01})\Psi$$

3.2.5 Satellites and Meteoroids

Orbital and physical properties of Neptune's two satellites, Triton and Nereid, are given in table XXVIII. Their photometric properties are given in section 3.2.4. Information permitting the location of Triton can be found in the appropriate year of the *American Ephemeris and Nautical Almanac*, and the *Explanatory Supplement to the Ephemeris* (ref. 73) gives similar information for both Triton and Nereid. Rotation rate and rotation axis orientation are not known although there is slim evidence that Triton rotates in a synchronous manner.

Triton may have a thin atmosphere, but none has been defined by observation. Its surface temperatures are not known but are likely to be less than 72 K (the subsolar point temperature for a black, nonconducting object at Neptune's distance from the Sun with unit emissivity) with temperatures as low as 3 K possible for unilluminated regions.

TABLE XXVI

THERMAL RADIATION PARAMETERS BELOW THE TROPOPAUSE IN THE ATMOSPHERE OF NEPTUNE FOR $10\ \mu m < \lambda < 100$ cm

Intensities*	$I_\lambda = B_\lambda(t)$ $I_\nu = B_\nu(t)$
Fluxes*	$F_\lambda = \pi B_\lambda(t)$ $F_\lambda = \pi B_\nu(t)$
Integrated Fluxes**	$F = \begin{cases} (2.3 \pm 1) \times 10^{-5} \left(\frac{W}{cm^2}\right) & \text{for } T < 45\ K \\ \left(\frac{T}{45}\right)^4 (2.3 \pm 1) \times 10^{-5} \left(\frac{W}{cm^2}\right) & \text{for } T > 45\ K \end{cases}$
Brightness Temperature	t = larger of T and T_D

*t is the larger of the disk brightness temperature shown in figure 6 and the local tropospheric temperature T (sec. 3.2.7); Planck functions $B_\lambda(t)$ and $B_\nu(t)$ from Allen (ref. 23) or elsewhere.

**With the assumption that Neptune does not have an internal energy source.

TABLE XXVII

MAGNITUDES AND COLORS FOR THE SUN, NEPTUNE, AND NEPTUNE'S SATELLITES

Object	Absolute Visual Magnitude	Mean Opposition Visual Magnitude	Brightness Differences between Photometric Passbands*			
	m_o	$\bar{m}$	U-B	B-V	V-R	R-I
Sun	-26.81	–	0.14	0.63	0.45	0.29
Neptune	-6.87	+7.84	0.21	0.41	-0.33	-0.80
Triton I	-1.16	+13.55	0.40	0.77	0.58	0.44
Nereid II	4.0	+18.7	–	–	–	–

*For photometric definitions see appendix C.

The meteoroid environment near Neptune should be obtained from the cometary meteoroid model and procedures of NASA SP-8038 (ref. 81) with the mass and radius values given in section 3.2.1.

3.2.6 Charged Particles and Magnetosphere

Table XXIX presents formulas and parameters for galactic cosmic rays, solar cosmic ray protons, the solar wind, and the ionosphere as well as a limiting model for energetic trapped radiation. The sunward magnetosphere boundary may be as near to the planet as the ionosphere or farther than 100 R_{eq}. There is a slim chance that the heliosphere boundary may form closer to the Sun than Neptune's orbit. If this is the case, a strong shock is likely and the estimate of solar wind radial velocity should be decreased by a factor of four, the number density estimates increased by four, and electron and proton temperatures of 10^6 to 10^7 K considered.

3.2.7 Atmospheric Structure

The Nominal Model atmosphere of Neptune given in table XXXII contains values for the temperature T, density ρ, altitude z, logarithmic lapse rate β, lapse rate dT/dz, pressure and density scale heights H_p and H_ρ, and cloud mass w as functions of pressure P, for 10^{-7} atm $\leqslant P \leqslant$ 1000 atm. Tables XXXI and XXXIII give Cool and Warm Model atmospheres which

TABLE XXVIII

ORBITAL AND PHYSICAL PROPERTIES OF NEPTUNE'S SATELLITES

Parameter	Triton	Nereid
Range of Distance from Neptune's Center (km)	$(355.4 \pm 1) \times 10^3$	$(5565 \pm 4170) \times 10^3$
Ratio of Mean Distance to Neptune's Equatorial Radius	14.1	221
Orbital Period (days)	5.877	359.9
Orbital Speed (km/s)	4.4	0.4 to 2.9
Range of Planetocentric Latitude (degrees)	$\pm 19°$*	$\pm 28°$
Radius (km)	1890 ±700	130 – 360**
Mass (kg)	$(1.4 \times 3^{\pm 1}) \times 10^{23}$	$< 2 \times 10^{21}$

*Motion of Triton is retrograde with respect to planetary rotation.
**Range possible with an assumed visual geometric albedo between 0.08 and 0.65.

TABLE XXIX

PARAMETERS FOR CHARGED PARTICLES NEAR NEPTUNE

Particles	Location	Temperature Energy or Velocity	Number Density, Flux, or Flux Parameter
Galactic Cosmic Rays	Everywhere	$0.1 < E < 10^{10}$ GeV (GeV/nucleon for alphas)	$\Phi_E = K (E + M_o c^2)^{-1.5}$ Electrons– $0 \leqslant K \leqslant 0.02$ cm$^{-2}\cdot$s^{-1} Protons– $0 \leqslant K \leqslant 2.5$ cm$^{-2}\cdot$s^{-1} Alphas– $0 \leqslant K \leqslant 0.25$ cm$^{-2}\cdot$s^{-1}
Solar Cosmic Ray Protons	Everywhere	$10 < E < 10^4$ MeV	Sporadic, with fluxes between 0 and 1.0 times those specified in NASA TR R-169 (ref. 87)
Solar Wind (Electrons and Protons)	Beyond Magnetosphere	V^* = 320 km/s (up to 960 km/sec at peak solar activity	$N_o{}^*$ = 0.008 cm^{-3} (up to 0.08 cm^{-3} at peak solar activity)
Trapped Radiation (Electrons and Protons)	$1 < L \leqslant 2$	6.2 MeV	$\Phi_o = 2 \times 10^7$ cm$^{-2}\cdot$s^{-1}
Trapped Radiation (Electrons)	$2 < L$	$(0.51)\left[\left(\frac{1377}{L^3}+1\right)^{1/2}-1\right]$ MeV	$\Phi_o = \frac{1.7\times10^{10}}{L^6}\left(\frac{1377}{L^3}+1\right)^{-1/2}$ cm$^{-2}\cdot$s^{-1}
Trapped Radiation (Protons)	$1 < L$	$(938)\left[\left(\frac{1.06}{L^3}+1\right)^{1/2}-1\right]$ MeV	$\Phi_o = \frac{4.7\times10^{8}}{L^6}\left(\frac{1.06}{L^3}+1\right)^{1/2}$ cm$^{-2}\cdot$s^{-1}
Trapped Radiation Distribution with Energy (Electrons and Protons)	$1 < L$	–	$\Phi_E < \Phi_o (1 + E/E_o) \exp(-E/E_o)$
Ionosphere (Electrons and Protons	For $z > z_1$, where z_1 = 300 ±200 km	T = 150 ±50 K	$N_o = (10^{6\pm1}$ cm$^{-3}) \exp\left(-\frac{z-z_1}{250}\right)$ z in km
Magnetospheric Plasma (Electrons and Protons)	Within Magnetosphere	$10^{-2} < E < 10^6$ eV	Not established

*See sec. 3.2.6 for change, if Neptune lies beyond heliosphere boundary.

cover the uncertainty in construction of the Nominal Model and variations with planetary latitude, time of day, and local features. These models represent cool and warm extremes at given pressures only. The compositions for all three models are given in table XXX which does not take into account condensation. The amount of a condensable (CH_4, NH_3 or H_2O) that can be present above a cloud base in gas form can be computed with the formulas and constants given in appendix B. For all models the zero of altitude is arbitrarily set at the correspondence level. The distance from Neptune's center R to any altitude z in the models is given by

$$R = R_{eq} [1 + (z - z_o)/R_{eq} - \epsilon(\sin \phi)^2]$$

where $R_{eq} = 25{,}200 \pm 200$ km, $\epsilon = 0.02 \pm 0.02$, and z_o is a reference altitude given separately for each model in tables XXXI, XXXII, and XXXIII. Although all models indicate the presence of CH_4 clouds, it should not be assumed that the limb of the planet is defined by these clouds at any wavelength. Interpolation between tabulated values should be carried out with the aid of formulas in appendix B.

TABLE XXX

COMPOSITION OF NEPTUNE MODEL ATMOSPHERES

Parameter	Cool Model	Nominal Model	Warm Model
Fraction by Number			
H_2	0.30559	0.85853	0.95285
He	0.60000	0.11000	0.03667
CH_4^*	0.09000	0.03000	0.01000
H_2O^*	0.00300	0.00100	0.00033
NH_3^*	0.00045	0.00015	0.00005
Ne	0.00039	0.00013	0.00004
Others	0.00057	0.00019	0.00006
Mean Molecular Weight μ	4.55	2.68	2.24

*In unsaturated region of atmosphere

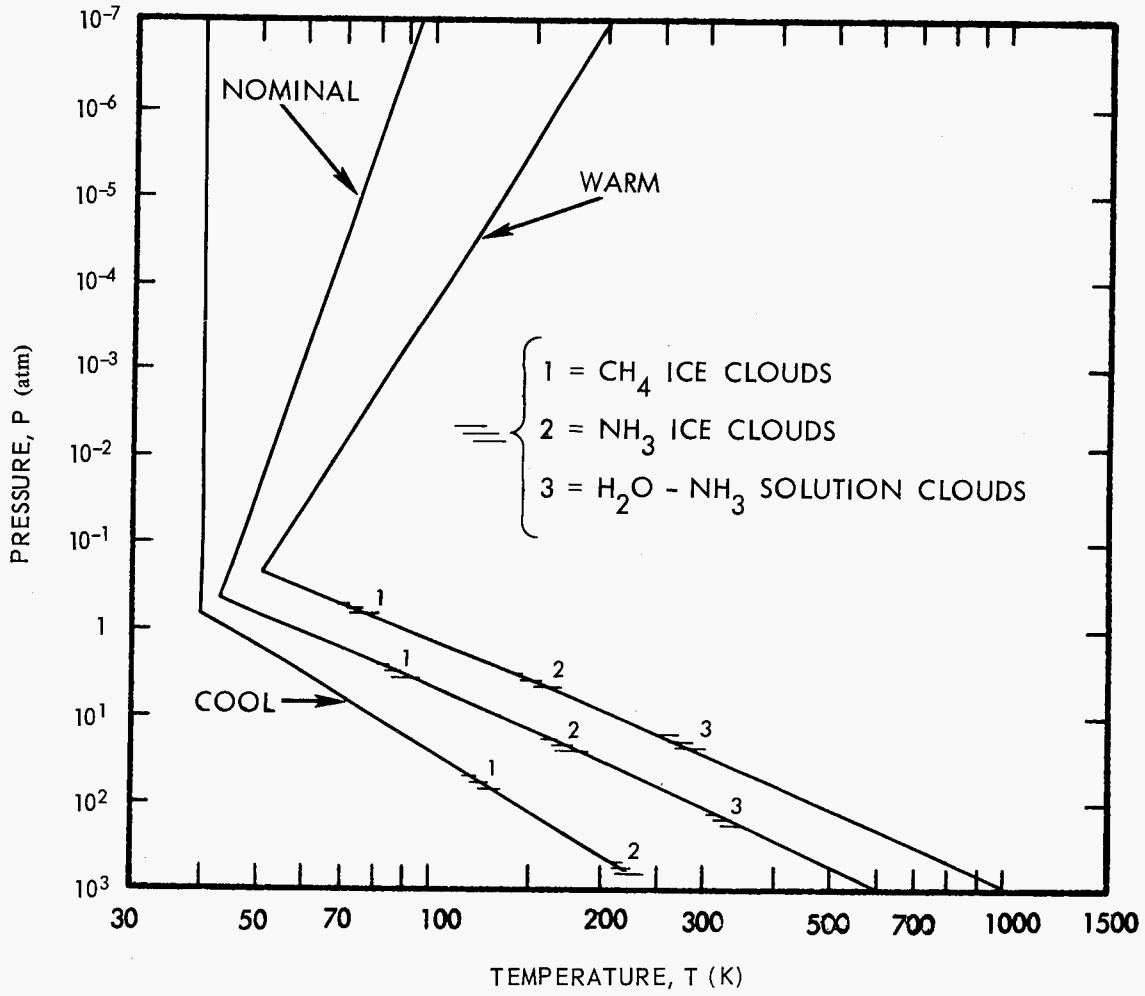

Figure 7.—Pressure versus temperature for Neptune model atmospheres.

TABLE XXXI

VALUES AT SELECTED PRESSURES FOR WARM, EXTENDED NEPTUNE MODEL ATMOSPHERE

P (atm)	T (K)	ρ ($g \cdot cm^{-3}$)	z (km)	β	dT/dz (K/km)	H_p (km)	H_ρ (km)	w (mg/l)	Remarks
10^{-7}	200.0	1.28×10^{-11}	604	-0.095	0.251	75.7	69.1		z_o Reference Level
10^{-6}	160.0	1.60×10^{-10}	447	-0.095	0.251	60.8	55.5		
10^{-5}	128.8	1.99×10^{-9}	322	-0.095	0.251	48.9	44.6		
10^{-4}	103.4	2.48×10^{-8}	221	-0.095	0.251	39.3	35.8		
10^{-3}	83.1	3.09×10^{-7}	139	-0.095	0.251	31.5	28.8		
10^{-2}	66.7	3.84×10^{-6}	74.2	-0.095	0.251	25.3	23.1		
0.03	60.2	1.28×10^{-5}	47.8	-0.095	0.251	22.8	20.9		
0.1	53.7	4.78×10^{-5}	21.8	-0.095	0.251	20.4	18.6		
0.21	50.0	1.10×10^{-4}	6.9	0.385	-1.01	19.0	30.8		Tropopause
0.3	57.0	1.35×10^{-4}	0.0	0.383	-1.01	21.6	35.0	0.1	Correspondence Level
0.42	65.0	1.67×10^{-4}	-7.9	0.381	-1.01	24.6	39.8	1.3	
0.6	74.6	2.22×10^{-4}	-16.9	0.379	-1.06	26.6	42.9	13.5	CH_4 Ice Cloud Base
1.0	90.0	3.03×10^{-4}	-31.5	0.376	-1.05	32.1	51.5		
3.29	140.0	6.41×10^{-4}	-79.6	0.366	-1.03	50.0	78.9	0.03	
4.13	152.2	7.41×10^{-4}	-91.5	0.364	-1.02	54.3	85.5	0.25	NH_3 Ice Cloud Base
10	209.3	1.30×10^{-3}	-148.1	0.356	-1.00	74.7	116		
14.7	240.0	1.67×10^{-3}	-179.1	0.352	-0.99	85.7	132	0.2	
18.5	260.0	1.94×10^{-3}	-199.4	0.350	-0.98	92.8	143	1.4	
21.9	275.8	2.17×10^{-3}	-215.6	0.349	-0.98	98.5	151	4.9	Solution Cloud Base H_2O-NH_3
30	307.6	2.66×10^{-3}	-248.4	0.345	-0.97	110	168		
100	463.1	5.89×10^{-3}	-411.9	0.334	-0.94	165	248		
300	664.9	1.23×10^{-2}	-630.9	0.325	-0.91	237	352		
1000	977.6	2.79×10^{-2}	-980.0	0.316	-0.88	349	510		

TABLE XXXII

VALUES AT SELECTED PRESSURES FOR NOMINAL, NEPTUNE MODEL ATMOSPHERE

P (atm)	T (K)	ρ ($g \cdot cm^{-3}$)	z (km)	β	dT/dz (K/km)	H_p (km)	H_ρ (km)	w (mg/l)	Remarks
10^{-7}	93.0	2.95×10^{-11}	343	−0.052	0.155	31.3	29.7		z_o Reference Level
10^{-6}	82.5	3.32×10^{-10}	276	−0.052	0.155	27.7	26.4		
10^{-5}	73.2	3.74×10^{-9}	215	−0.052	0.155	24.6	23.4		
10^{-4}	65.0	4.22×10^{-8}	162	−0.052	0.155	21.8	20.7		
10^{-3}	57.6	4.76×10^{-7}	115	−0.052	0.155	19.4	18.4		
10^{-2}	51.1	5.36×10^{-6}	72.6	−0.052	0.155	17.2	16.3		
0.03	48.3	1.70×10^{-5}	54.2	−0.052	0.155	16.2	15.4		
0.1	45.4	6.04×10^{-5}	35.3	−0.052	0.155	15.2	14.5		
0.3	42.8	1.19×10^{-4}	19.0	−0.052	0.155	14.4	13.7		
0.44	42.0	2.86×10^{-4}	13.6	0.373	−1.11	14.1	22.5		Tropopause
1.0	57.0	4.81×10^{-4}	0.0	0.367	−1.09	19.2	30.3		Correspondence Level
1.43	65.0	6.04×10^{-4}	−7.4	0.364	−1.08	21.8	34.3	1.3	
2.13	75.0	7.89×10^{-4}	−16.5	0.360	−1.09	24.9	38.9	15	
3.0	84.8	1.06×10^{-3}	−24.9	0.357	−1.17	25.9	40.3	90	
3.47	89.4	1.27×10^{-3}	−28.5	0.356	−1.26	25.2	39.1	182	CH_4 Ice Cloud Base
10.0	129.3	2.53×10^{-3}	−60.8	0.343	−1.22	36.5	55.5		
17.1	155.0	3.59×10^{-3}	−82.2	0.336	−1.19	43.7	65.9	0.4	
20.5	165.0	4.07×10^{-3}	−90.6	0.334	−1.18	46.6	70.0	1.7	
22.8	170.9	4.36×10^{-3}	−95.6	0.333	−1.18	48.2	72.2	3.6	NH_3 Ice Cloud Base
30	187.0	5.24×10^{-3}	−109	0.329	−1.17	52.8	78.7		
93.9	270.0	1.14×10^{-2}	−182	0.314	−1.11	76.2	111	3.3	
154.2	315.0	1.60×10^{-2}	−223	0.308	−1.09	88.9	128	42	
184.6	332.9	1.81×10^{-2}	−240	0.306	−1.08	93.9	135	96	Solution Cloud Base H_2O-NH_3
300	385.6	2.54×10^{-2}	−289	0.300	−1.06	109	155		
1000	548.4	5.95×10^{-2}	−446	0.286	−1.01	155	217		

TABLE XXXIII

VALUES AT SELECTED PRESSURES FOR COOL, DENSE NEPTUNE MODEL ATMOSPHERE

P (atm)	T (K)	ρ ($g \cdot cm^{-3}$)	z (km)	β	dT/dz (K/km)	H_p (km)	H_ρ (km)	w (mg/l)	Remarks
10^{-7}	38.0	1.07×10^{-10}	143	0	0	8.2	8.2		z_o Reference Level
10^{-6}	38.0	1.07×10^{-9}	125	0	0	8.2	8.2		
10^{-5}	38.0	1.07×10^{-8}	106	0	0	8.2	8.2		
10^{-4}	38.0	1.07×10^{-7}	87.0	0	0	8.2	8.2		
10^{-3}	38.0	1.07×10^{-6}	68.2	0	0	8.2	8.2		
10^{-2}	38.0	1.07×10^{-5}	49.4	0	0	8.2	8.2		
0.03	38.0	3.21×10^{-5}	40.5	0	0	8.2	8.2		
0.1	38.0	1.07×10^{-4}	30.6	0	0	8.2	8.2		
0.3	38.0	3.21×10^{-4}	21.7	0	0	8.2	8.2		
0.66	38.0	7.10×10^{-4}	15.2	0.272	-1.27	8.2	11.2		Tropopause
1.00	42.5	9.59×10^{-4}	11.6	0.270	-1.26	9.1	12.5		
3.00	57.0	2.14×10^{-3}	0.0	0.265	-1.23	12.2	16.6		Correspondence Level
10.0	78.1	5.23×10^{-3}	-17.3	0.258	-1.21	16.7	22.5	25	
26.3	100.0	1.15×10^{-2}	-34.4	0.253	-1.27	20.0	26.8	636	
61.6	123.9	2.76×10^{-2}	-49.4	0.249	-1.58	19.5	26.0	5326	CH_4 Ice Cloud Base
100	139.7	3.97×10^{-2}	-59.4	0.247	-1.57	22.0	29.2		
300	182.8	9.10×10^{-2}	-67.2	0.243	-1.54	28.8	38.0	14	
534.8	210.2	1.4×10^{-1}	-105	0.240	-1.53	33.1	43.6	184	NH_3 Ice Cloud Base

3.3 Pluto

3.3.1 General Physical Properties

Values and uncertainties for Pluto's mass, radius, rotation rate, and several orbital parameters are given in table XXXIV. The uncertainty in equatorial radius is large enough to span any irregularities of shape. The value of equatorial radius shown is associated with a solid surface.

TABLE XXXIV

PHYSICAL PROPERTIES OF PLUTO

Parameters	Values
Range of distance from the Sun 1971–1980	31.7 to 30.2 AU
Mean distance from the Sun*	39.708 AU
Heliocentric orbital speed 1971–1980	5.8 to 6.0 $km \cdot s^{-1}$
Period of revolution about the Sun	250.0 tropical years
Inclination of orbital plane to ecliptic plane*	$17^{\circ}.144$
Inclination of equatorial plane to orbital plane*	unknown
Mass of Pluto	$M_P = (5.7 \times 1.7^{\pm 1}) \times 10^{23}$ kg
Gravitational constant of Pluto	$GM_P = (3.8 \times 1.7^{\pm 1}) \times 10^4$ $km^3 \cdot s^{-2}$
Equatorial radius	$D_{eq} = 5700 \times 1.2^{\pm 1}$ km
Polar radius	$D_{p\ell} = 5700 \times 1.2^{\pm 1}$ km
Mean density	$\overline{\rho} = 5.9 \times 3^{\pm 1}$ $g \cdot cm^{-3}$
Period of rotation	$T_o = 6.387 \pm 0.001$ days
Angular rotation rate	$\omega_o = (1.139 \pm 0.002) \times 10^{-5}$ $rad \cdot s^{-1}$

*These parameters vary with time and are given here for qualitative purposes only. Values for particular times are given in the references of section 2.1.3.

TABLE XXXV

GRAVITY FIELD AND RELATED PARAMETERS FOR PLUTO

Gravitational potential at distance R from planet in a coordinate system not rotating	$-(13 \times 1.7^{\pm 1})\ (R_{eq}/R)\ km^2 \cdot s^{-2}$
Range of gravitational acceleration at $R = R_s$ including rotation at ω_o	$470 \times 2.5^{\pm 1}\ cm \cdot s^{-2}$
Escape speed at distance R from planet (from above potential at R_{eq})	$(5.2 \times 1.3^{\pm 1}) \left(\frac{R_{eq}}{R}\right)^{1/2}\ km \cdot s^{-1}$
Orbital speed at distance R with semi-major axis a	$(3.6 \times 1.3^{\pm 1}) \left(\frac{2R_{eq}}{R} - \frac{R_{eq}}{a}\right)^{1/2}\ km \cdot s^{-1}$
Period of object in orbit with semi-major axis a	$(0.77 \times 1.3^{\pm 1})\ (a/R_{eq})^{3/2}$ hours

3.3.2 Gravity Field

Table XXXV gives parameters and their uncertainties for Pluto's gravitational field.

3.3.3 Magnetic Field

Neither the strength of Pluto's magnetic field nor its form (dipolar, quadrupolar, etc.) is known. A field of 10^{-3} T (1 gauss) is adopted as an upper limit to the surface field on the basis of analogy with the terrestrial planets that have been explored by spacecraft, Mars, Earth, and Venus.

3.3.4 Electromagnetic Radiation

The formulas in table XXXVI specify the ranges of intensity, flux, and temperature associated with conditions of maximum illumination from the Sun and Pluto. During partial illumination or eclipse, the values for intensities and fluxes of direct and reflected solar radiation may decrease to zero. The wavelength region of interest determines which radiation sources in table XXXVI should be considered. The ranges of geometric albedo are shown in figure 8. The upper limit to the planetary thermal contribution is set by $T_{eff} = 72$ K, which is the maximum subsolar point temperature expected for Pluto at perihelion. The dark-side temperature could range down to a few degrees kelvin because of Pluto's long rotation period and the unknown direction of the rotational axis (sec. 2.1.3).

TABLE XXXVI

ELECTROMAGNETIC RADIATION PARAMETERS NEAR PLUTO WITH MAXIMUM ILLUMINATION

Parameters	Direct Sunlight* $1\,\text{Å} < \lambda < 100$ cm	Reflected Sunlight* $0.3\,\mu\text{m} < \lambda < 1.0\,\mu\text{m}$	Thermal Radiation** $1\,\mu\text{m} < \lambda < 100$ cm
Intensity — Power/(Area-wavelength-solid angle)	$I_\lambda = \dfrac{H_\lambda}{6.8 \times 10^{-5}\ \text{sr}}$	$I_\lambda = \dfrac{p_\lambda H_\lambda}{\pi R_{p\odot}^2}$	$I_\lambda = B_\lambda (T_D)$
Power/(Area-frequency-solid angle			$I_\nu = B_\nu (T_D)$
Flux — Power/(Area-wavelength)	$F_\lambda = \dfrac{H_\lambda}{S^2}$	$F_\lambda = \dfrac{p_\lambda H_\lambda}{R_{p\odot}^2 (R/R_{eq})^2}$	$F_\lambda = \dfrac{\pi B_\lambda (T_D)}{(R/R_{eq})}$
Power/(Area-frequency)			$F_\nu = \dfrac{\pi B_\nu (T_D)}{(R/R_{eq})^2}$
Integrated Flux — Power/Area	$F = \dfrac{(1.353 \pm 0.021) \times 10^{-1}}{S^2} \left(\dfrac{W}{cm^2}\right)$	$F = \dfrac{(1.9 \times 2^{\pm 1}) \times 10^{-2}}{R_{p\odot}^2 (R/R_{eq})^2} \left(\dfrac{W}{cm^2}\right)$	$F < \dfrac{(15) \times 10^{-5}}{(R/R_{eq})^2} \left(\dfrac{W}{cm^2}\right)$
Brightness Temperature			$T_D < 72$ K
Effective Temperature			$T_{eff} < 72$ K

*Solar spectral irradiance from NASA SP-8005 (ref. 44), S and $R_{p\odot}$ in AU only, and geometric albedo p_λ from figure 8.
**Planck functions B_λ (t) and B_ν (t) from Allen (ref. 81) or elsewhere.

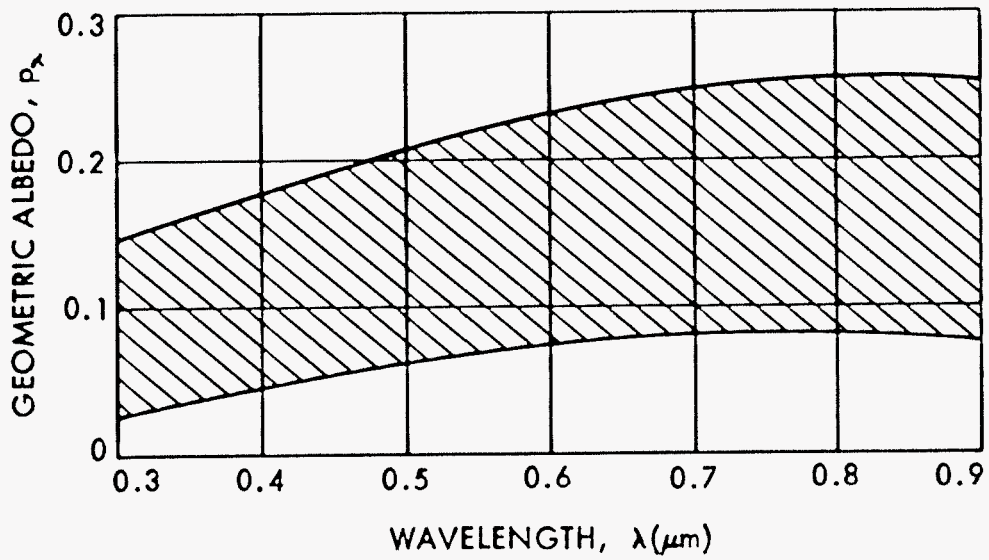

Figure 8.—Ranges of geometric albedo for Pluto.

TABLE XXXVII

MAGNITUDE AND COLORS FOR THE SUN AND PLUTO

Object	Absolute Visual Magnitude	Mean Opposition Visual Magnitude	Brightness Differences between Photometric Passbands*			
	$m_\odot$	$\bar{m}$	U-B	B-V	V-R	R-I
Sun	-26.81	–	0.14	0.63	0.45	0.29
Pluto	-1.01	+14.90	0.27	0.80	0.63	0.28

*For photometric definitions see appendix C.

With the parameters in table XXXVII, Ψ in degrees, and $R_{p\odot}$ and Δ in AU, the visual magnitude of Pluto is specified by

$$m_V = (m_\odot \pm 0.1) + 5 \log (R_{p\odot} \Delta) + (0.03^{+0.05}_{-0.01}) \Psi$$

The known total variation with rotation of 0.11 magnitudes in the visual as observed from Earth is taken into account in the foregoing expression.

TABLE XXXVIII

PARAMETERS FOR CHARGED PARTICLES NEAR PLUTO

Particle	Location	Temperature, Energy or Velocity	Number Density or Flux
Galactic Cosmic Rays	Everywhere	$0.1 < E < 10^{10}$ GeV (GeV/Nucleon for alphas)	$\phi_E = K (E + M_o e^2)^{-1.5}$ Electrons- $0 \leqslant K \leqslant 0.02$ cm$^{-2}\cdot$s^{-1} Protons- $0 \leqslant K \leqslant 2.5$ cm$^{-2}\cdot$s^{-1} Alphas- $0 \leqslant K \leqslant 0.25$ cm$^{-2}\cdot$s^{-1}
Solar Cosmic Ray Protons	Everywhere	$10 < E < 10^4$ MeV	Sporadic, with fluxes between 0 and 1.0 times those specified in NASA TR R-169 (ref. 87)
Solar Wind (Electrons and Protons)	Beyond Magnetosphere	V^* = 320 km/s (up to 960 km/sec at peak solar activity)	$N_o{}^*$ = 0.008 cm^{-3} (up to 0.08 cm^{-3} at peak solar activity)
Ionosphere (Electrons and Protons)	For $z > 0$	T = 150 ±50 K	$N_o \leqslant 10^6 \exp(-z/200)$ cm^{-3} z in km
Magnetospheric Plasma (Electrons and Protons)	Within Magnetosphere	$10^{-2} < E < 10^6$ eV	Not established
Energetic Trapped Radiation (Electrons and Protons)	Within Magnetosphere	$E > 10^6$ eV	Not established

*See sec. 3.3.6 for change, if Pluto lies beyond heliosphere boundary.

3.3.5 Satellites and Meteoroids

Pluto has no known satellites. The meteoroid environment near Pluto should be obtained from the cometary meteoroid model and procedures of NASA SP-8038 (ref. 81) with the mass and radius values given in section 3.3.1.

3.3.6 Charged Particles and Magnetosphere

Table XXXVIII presents formulas and parameters for galactic cosmic rays, solar cosmic ray protons, and the solar wind as well as a limiting model for the ionosphere. The sunward magnetosphere boundary may be as near to the planet as the ionosphere or surface or farther than 50 R_{eq}. There is a slim chance that the heliosphere boundary may lie inside the orbit of Pluto. If this is the case, a strong shock is likely and the estimates of solar wind radial velocity should be decreased by a factor of four, the number density estimates increased by four, and electron and proton temperatures of 10^6 to 10^7 K considered.

3.3.7 Atmospheric Structure

No observation has established the presence of an atmosphere for Pluto. The candidate species are H_2, He, and Ne in an unsaturated state and N_2, O_2, CH_4, A, NO, and CO in a saturated condition. In the absence of sufficient information, no models are provided.

REFERENCES

1. Klepczynski, W. J.; Seidelmann, P. K.; and Duncombe, R. L.: The Masses of the Principal Planets. Celestial Mechanics, vol. 4, no. 2, 1971, pp. 253-272.

2. Kovalesvky, J.: Détermination des Masses des Planèts. Celestial Mechanics, vol. 4, no. 2, 1971, pp. 213-223.

3. Kovalevsky, J.: Determination Des Masses Des Planetes Et Satellites. Surfaces and Interiors of Planets and Satellites, A. Dollfus (ed.), Academic Press, New York, 1970, pp. 1-44.

4. Klepczynski, W. J.; Seidelmann, P. K.; and Duncombe, R. L.: The Masses of Saturn and Uranus. Astronomical J., vol. 75, no. 6, 1970, pp. 739-742.

5. Lieske, J. H.; Melbourne, W. G.; O'Handley, D. A.; Holdridge, D. B.; Johnson, D. E.; and Sinclair, W. S.: Simultaneous Solution for the Masses of the Principal Planets from Analysis of Optical, Radar, and Radio Tracking Data. Celestial Mechanics, vol. 4, no. 2, 1971, pp. 233-245.

6. Brouwer, D.; and Clemence, G. M.: Orbits and Masses of Planets and Satellites. Planets and Satellites, G. Kuiper and B. Middlehurst (ed.), University of Chicago Press, 1961, pp. 31-94.

7. Seidelmann, P. K.; Duncombe, R. L.; and Klepczynski, W. J.: The Mass of Neptune and the Orbit of Uranus. Astronomical J., vol. 74, no. 6, 1969, pp. 776-778.

8. Gill, J. R.; and Gault, B. L.: A New Determination of the Orbit of Triton, Pole of Neptune's Equator, and Mass of Neptune. Astronomical J., vol. 73, 1968, p. 595, (abstract).

9. Duncombe, R. L.; Klepczynski, W. J.; and Seidelmann, P. K.: Mass of Pluto. Science, vol. 162, no. 3855, 1968, pp. 8000-8002.

10. Seidelmann, P. K.; Klepczynski, W. J.; and Duncombe, R. L.: Determination of the Mass of Pluto. Astronomical J., vol. 76, no. 5, 1971, pp. 488-492.

11. Ash, M. E.; Shapiro, I. I.; and Smith, W. B.: The System of Planetary Masses. Science, vol. 174, 1971, pp. 551-556.

12. Melbourne, W. G.; Mulholland, J. D.; Sjogren, W. L.; and Sturms, F. M.: Constants and Related Information for Astrodynamic Calculations, 1968. Tech. Rep. 32-1306, Jet Propulsion Lab., Pasadena, Calif., 1968.

13. Mechtly, E. A.: The International System of Units Physical Constants and Conversion Factors Revised. Office of Technology Utilization, NASA, Washington, D.C. 1969.

14. Dollfus, A.: New Optical Measurements of the Diameters of Jupiter, Saturn, Uranus, and Neptune, Icarus, vol. 12, 1970, pp. 101-117.

15. West, F. R.: Polar Flattening of Uranus. Transactions of the American Geophysical Union, vol. 49, 1968, p. 707 (abstract).

16. Danielson, R. E.: Private Communication, February 3, 1971.

17. Kovalevsky, J.: New Determination of the Diameter of Neptune. Comptes Rendus, Series B, Physical Sciences, vol. 267, no. 12, 1968, pp. 594-596.

18. Kovalevsky, J.; and Link, F.: Diameter, Flattening, and Optical Properties of the Upper Atmosphere of Neptune as Derived from the Occultation of the Star BD-17° 4388. Astronomy and Astrophysics, vol. 2, 1969, pp. 398-412.

19. Taylor, G. E.: The Occultation of B.D. -17° 4388 by Neptune on 1968 April 7. Royal Astronomy Society Monthly Notices, vol. 147, 1970, pp. 27-33.

20. Freeman, K. C.; and Lyngå, G.: Data for Neptune from Occultation Observations. Astrophys. J., vol. 160, no. 2, 1970, pp. 767-780.

21. Halliday, I.; Hardie, R. H.; Franz, O. G.; and Priser, J. B.: An Upper Limit for the Diameter of Pluto. Astronomical Society of the Pacific, Pub., vol. 78, no. 461, 1966, pp. 113-124.

22. Kuiper, G. P.: The Diameter of Pluto. Astronomical Society of the Pacific, Pub., vol. 62, 1950, pp. 133-137.

23. Allen, C. W.: Astrophysical Quantities. The Athlone Press, University of London, 1963.

24. Slipher, V. M.: Detection of the Rotation of Uranus. Lowell Obs. Bull., vol. II, no. 53, 1909 through 1916, pp. 19-20.

25. Moore, J. H.; and Menzel, D. H.: The Rotation of Uranus. Astronomical Society of the Pacific, Pub., vol. 42, 1930, pp. 330-335.

26. Alexander, A. F. O'D.: The Planet Uranus, American Elsevier Publishing Co., 1965.

27. Hardie, R. H.; and Giclas, H. L.: A Search for Solar Variation. Astrophysical J., vol. 122, 1955, pp. 460-465.

28. Moore, J. H.; and Menzel, D. H.: Preliminary Results of Spectrographic Observations for Rotation of Neptune. Astronomical Society of the Pacific, Pub., vol. 40, 1928, pp. 234-238.

29. Öpik, E.: Variability and Period of Rotation of Neptune. Astronomical J. (Irish), vol. 3, 1954-55, pp. 255-256.

30. Harris, D. L.: Photometry and Colorimetry of Planets and Satellites, Planets and Satellites, G. Kuiper and B. Middlehurst (eds.), University of Chicago Press, 1961, pp. 272-342.

31. Hardie, R.: A Re-Examination of the Light Variation of Pluto. Astronomical J., vol. 70, 1965, p. 140.

32. Sturms, F. M. Jr.: Polynomial Expressions for Planetary Equators and Orbit Elements with Respect to the Mean 1950.0 Coordinate System. Technical Report 32-1508, Jet Propulsion Laboratory, Pasadena, California, 1971.

33. Woolley, R. v.d. R.: Planetary Coordinates 1960-1980. Her Majesty's Stationery Office, London, 1962.

34. British Astronomical Association Handbook for 1971, British Astronomical Association, London.

35. Dunham, D.: Motions of the Satellites of Uranus. American Astron. Soc. Bull., vol. 3, no. 3, 1971, p. 415 (abstract).

36. Carr, T. D.; and Gulkis, S.: The Magnetosphere of Jupiter. Annual Review of Astronomy and Astrophysics, vol. 7, 1969, p. 577-618.

37. Warwick, J. W.: Particles and Fields Near Jupiter, NASA Contractor Report, CR-1685, 1970.

38. NASA SP-8069, The Planet Jupiter (1970). National Aeronautics and Space Administration, December 1971.

39. Berge, G. L.: Recent Observations of Saturn, Uranus, and Neptune at 3.12 cm. Astrophys. Letters, vol. 2, 1968, pp. 127-131.

40. Kern, J. W.; and Vestine, E. H.: Magnetic Field of the Earth and Planets. Space Science Review, vol. 2, no. 1, 1963, pp. 136-171.

41. Parker, E. N.: The Generation of Magnetic Fields in Astrophysical Bodies. IV. The Solar and Terrestrial Dynamos. Astrophys. J., vol. 164, no. 3, 1971, pp. 491-509.

42. Hide, R.: Dynamics of the Atmospheres of the Major Planets with an Appendix on the Viscous Boundary Layer at the Rigid Bounding Surface of an Electrically-Conducting Rotating Fluid in the Presence of a Magnetic Field. J. Atmospheric Sciences, vol. 26, 1969, pp. 841-853.

43. Pochtarev, V. I.: Magnetic Field of Planets According to a Study of the Magnetic Properties of Meteorites. Geomagnetism and Aeronomy, vol. 7, no. 4, 1967, pp. 609-611.

44. NASA SP-8005, Solar Electromagnetic Radiation. National Aeronautics and Space Administration, May 1971.

45. Appleby, J. F.; and Irvine, W. M.: Multicolor Photoelectric Photometry of Uranus. Astronomical J., vol. 76, no. 7, 1971, pp. 617-619.

46. Fix, J. D.; Neff, J. S.; and Kelsey, L. A.: Spectrophotometry of Pluto. Astronomical J., vol. 75, no. 8, 1970, pp. 895-896.

47. Dollfus, A.: Diametres Des Planetes Et Satellites. Surfaces and Interiors of Planets and Satellites, A. Dollfus (ed.), Academic Press, New York, 1970, pp. 45-139.

48. Younkin, R. L.; and Münch, G.: Spectrophotometry of Uranus from 3300 to 11000 A. Astronomical J., vol. 72, 1967, pp. 328-329 (abstract).

49. Newburn, R. L., Jr.; and Gulkis, S.: A Brief Survey of the Outer Planets Jupiter, Saturn, Uranus, Neptune, Pluto, and Their Satellites. Technical Report 32-1529, JPL, Pasadena, California, 1971.

50. Talley, R. L.; and Horak: The Phase Variation of Uranus. Astrophys. J., vol. 123, 1956, pp. 176-178.

51. Sinton, W. M.: The Albedos and Phase Variations of Uranus and Neptune. Lowell Obs. Bull., vol. IV, 1959, pp. 93-97.

52. Johnson, T. V.: Galilean Satellites: Narrowband Photometry 0.30 to 1.10 Microns. Icarus, vol. 14, 1971, pp. 94-111.

53. Pace, G.: UBV: Subroutine to Compute Photometric Magnitudes of the Planets and Their Satellites. Technical Report 32-1523, Jet Propulsion Laboratory, Pasadena, California, 1971.

54. Becker, W.: Der Physische Lichtwechsel Der Planeten Saturn Und Uranus. Astronomische Nachrichter, vol. 277, 1949, pp. 65-72.

55. Johnson, H. L.; and Iriarte, B.: The Sun as a Variable Star. Lowell Obs. Bull., vol. IV, no. 96, 1959, pp. 99-102.

56. Serkowski, K.: The Sun as a Variable Star II. Lowell Obs. Bull., vol. V, no. 157, 1961, pp. 116.

57. Jerzykiewicz, M.; and Serkowski, K.: The Sun as a Variable Star; III. Lowell Obs., Bull., vol. VI, no. 37, 1966, pp. 295-323.

58. Walker, M. F.; and Hardie: A Photometric Determination of the Rotational Period of Pluto. Astronomical Society Pacific Pub., vol. 67, 1955, pp. 224-231.

59. Brissenden, P.; and Erickson, W. C.: A Search for Decametric Radiation From Several Planets. Astrophys. J., vol. 136, 1962, p. 1140.

60. Smith, A. G.: Studies of Sporadic Radio Frequency Emission From the Planets. Final Report, No. DA-31-124-AROD-6903, Univ. of Florida, Physics and Astronomy Dept., 1969.

61. Low, F. J.: The Infrared Brightness Temperature of Uranus. Astrophys. J., vol. 146, no. 1, 1966, pp. 326-328.

62. Armstrong, K. R.: Infrared Photometry and Radiometry of the Planets. Thesis, Rice University, Department of Space Science, Houston, Texas, 1971.

63. Epstein, E. E.; Dworetsky, M. M.; Montgomery, J. W.; Forgarty, W. G.; and Schorn, R. A.: Mars, Jupiter, Saturn, and Uranus: 3.3-mm Brightness Temperatures and a Search for Variations with Time or Phase Angle. Icarus, vol. 13, no. 2, 1970, pp. 276-281.

64. Pauliny-Toth, I. I. K.; and Kellerman, K. I.: Millimeter-Wavelength Measurements of Uranus and Neptune. Astrophysical Letters, vol. 6, 1970, pp. 185-187.

65. Kuzmin, A. B.; and Losovsky, B. Ya.: Measurements of Uranus Radio Emission at 8.22 mm. Icarus, vol. 14, 1971, pp. 196-197.

66. Mayer, C. H.; and McCullough, T. P.: Microwave Radiation of Uranus and Neptune. Icarus, vol. 14, 1971, pp. 187-191.

67. Klein, M. J.; and Seling, T. V.: Radio Emission From Uranus at 8 Gc/s. Astrophys. J., vol. 146, no. 2, 1966, pp. 599-602.

68. Gerard, E.: Observations of Saturn, Uranus and Neptune at 11.13 cm. Astronomy and Astrophysics, vol. 2, 1969, pp. 246-248.

69. Kellermann, K. I.: The Thermal Emission from Mercury, Venus, Mars, Saturn, and Uranus. Icarus, vol. 5, 1966, pp. 478-490.

70. Kellermann, K. I.; and Pauliny-Toth, I. I. K.: Observations of the Radio Emission of Uranus, Neptune, and Other Planets at 1.9 cm. Astrophys. J., vol. 145, no. 3, 1966, pp. 954-957.

71. Aumann, H. H.; Gillespie, C. M., Jr.; and Low, F. J.: The Internal Powers and Effective Temperatures of Jupiter and Saturn. Astrophys. J. Let., vol. 157, 1969, L69-L72.

72. Kuiper, G. P.: "Limits of Completeness." Planets and Satellites. Kuiper, G. P. and Middlehurst, B. M. (eds.), Chapter 18, University of Chicago Press, Chicago, Ill., 1961, pp. 575-591.

73. Gurnette, B. L.; and Woolley, R. v.d. R.: Explanatory Supplement to the Ephemeris. Her Majesty's Stationery Office, London, 1961.

74. Kuiper, G. P.: "The Origin of the Satellites and the Trojans," Vistas In Astronomy. A. Beer (ed.), vol. 2, Pergamon Press, New York, 1956, pp. 1631-1666.

75. Sandner, W.: Satellites of the Solar System. Faber and Faber, London, 1965.

76. Steavenson, W. H.: The Satellites of Uranus. British Astronomical Association J., vol. 74, 1964, pp. 54-59.

77. Porter, J. G.: The Satellites of the Planets. British Astronomical Association J., vol. 70, 1959-60, pp. 33-59.

78. Alden, H. L.: The Mass of the Satellite of Neptune. Astronomical J., vol. 49, 1942, pp. 71-72.

79. Kuiper, G. P.: The Atmospheres of the Earth and Planets. University of Chicago Press, Chicago, Ill., 1952.

80. Spinrad, H.: Lack of a Noticeable Methane Atmosphere on Triton. Astronomical Society of the Pacific, Pub., vol. 81, no. 483, 1969, pp. 895-896.

81. NASA SP-8038, Meteoroid Environment Model – 1970 (Interplanetary and Planetary). National Aeronautics and Space Administration, October 1970.

82. Brandt, J. C.: Introduction to the Solar Wind. W. H. Freeman and Co., San Francisco, 1970.

83. Simpson, J. A.; and Wang, J.: Dimensions of the Cosmic Ray Modulation Region. Astrophys. J. Letters, vol. 149, 1969, pp. L73-L78.

84. Jokipii, J. R.; and Davis, L., Jr.: Long-Wavelength Turbulence and the Heating of the Solar Wind. Astrophys. J., vol. 156, 1969, pp. 1101-1106.

85. Haffner, J. W.: Radiation and Shielding in Space. Academic Press, New York and London, 1967.

86. Fanselow, J. L.: The Primary Cosmic-Ray Electron Spectrum Between 0.09 and 8.4 BeV In 1965. Astrophys. J., vol. 152, no. 3, 1968, pp. 783-798.

87. McDonald, F. B., (ed.): Solar Proton Manual, NASA TR R-169, 1963.

88. Dessler, A. J.: Solar Wind and Interplanetary Magnetic Field. Reviews of Geophysics, vol. 5, no. 1, 1967, pp. 1-44.

89. Parker, E. N.: Theoretical Studies of the Solar Wind Phenomenon. Space Science Reviews, vol. 9, 1969, pp. 325-360.

90. Hundhausen, A. J.: Composition and Dynamics of the Solar Wind Plasma. Rev. Geophys. and Space Physics, vol. 8, 1970, pp. 729-811.

91. Hundhausen, A. J.: Interplanetary Neutral Hydrogen and the Radius of the Heliosphere. Planetary and Space Science, vol. 16, 1968, pp. 783-793.

92. Semar, C. L.: Effect of Interstellar Neutral Hydrogen on the Termination of the Solar Wind. J. of Geophysical Research, vol. 75, 1970, pp. 6892-6898.

93. Blum, P. W.; and Fahr, H. J.: Interaction Between Interstellar Hydrogen and the Solar Wind. Astronomy & Astrophysics, vol. 4, 1970, pp. 280-290.

94. McDonough, T. R.; and Brice, N. M.: The Termination of the Solar Wind. Cornell Center for Radiophysics and Space Research, CRSR 437, 1971.

95. Law, S. E.; and Staelin, D. H.: Measurements of Venus and Jupiter Near 1-Cm Wavelength. Astrophys. J., vol. 154, 1968, pp. 1077-1086.

96. Gulkis, S.; McDonough, T. R.; and Craft, H.: The Microwave Spectrum of Saturn. Icarus, vol. 10, no. 3, 1969, pp. 421-427.

97. Dickel, J. R.: 6-Cm Observations of Jupiter. Astronomical J., vol. 148, 1967, pp. 535-540.

98. Berge, G. L.: An Interferometric Study of Jupiter's Decimeter Radio Emission. Astrophys. J., vol. 146, no. 3, 1966, pp. 767-798.

99. Branson, N. J. B. A.: High Resolution Radio Observations of the Planet Jupiter, Royal Astronomical Soc. Monthly Notices, vol. 139, 1968, pp. 155-162.

100. Braun, L. D.; and Yen, J. L.: Some Radio Observations at 35 GHz. Astronomical J., vol. 73, no. 10, 1968, p. S-168 (abstract).

101. Mayer, C. H.: "Radio Emission From The Moon and Planets," Planets and Satellites. Kuiper, G. P. and Middlehurst, B. M. (eds.), University of Chicago Press, Chicago, Ill., chapter 12, 1961, pp. 442-472.

102. Ginzburg, V. L.; and Syrovtaskii, S. I.: Cosmic Magnetobremsstrahlung. Annual Review of Astronomy and Astrophysics, vol. 3, 1965, pp. 297-350.

103. Gross, S. H.; and Rasool, S. I.: The Upper Atmosphere of Jupiter. Icarus, vol. 3, 1964, pp. 311-322.

104. Hunten, D. M.: The Upper Atmosphere of Jupiter. J. Atmospheric Sciences, vol. 26, 1969, pp. 826-834.

105. Shimizu, M.: The Upper Atmosphere of Jupiter. Icarus, vol. 14, 1971, pp. 273-281.

106. McGovern, W. E.: Exospheric Temperatures of Jupiter and Saturn. Journal of Geophysical Research, vol. 73, 1968, pp. 6361-6363.

107. Ratcliffe, J. A.: Physics of the Upper Atmosphere. Academic Press, New York, 1960.

108. De Marcus, W. C.: Planetary Interiors. Handbook der Physik, vol. 52, 1959, pp. 419-448.

109. Porter, W. S.: The Constitutions of Uranus and Neptune. Astronomical J., vol. 66, no. 5, 1961, pp. 243-245.

110. Reynolds, R. T.; and Summers, A. L.: Models of Uranus and Neptune. J. Geophysical Research, vol. 70, no. 1, 1965, pp. 199-208.

111. Ramsey, W. H.: On the Constitutions of Uranus and Neptune. Planetary and Space Science, vol. 15, 1967, pp. 1609-1623.

112. Herzberg, G.: Spectroscopic Evidence of Molecular Hydrogen in the Atmospheres of Uranus and Neptune. Astrophys. J., vol. 115, no. 3, 1952, pp. 337-340.

113. Spinrad, H.: Pressure-Induced Dipole Lines of Molecular Hydrogen in the Spectra of Uranus and Neptune. Astrophys. J., vol. 133, 1963, pp. 1242-1245.

114. Giver, L. P.; and Spinrad, H.: Molecular Hydrogen Features in the Spectra of Saturn and Uranus. Icarus, vol. 5, 1966, pp. 586-589.

115. Owen, T.: An Identification of the 6800-A Methane Band in the Spectrum of Uranus and a Determination of Atmospheric Temperature. Astrophys. J., vol. 146, 1966, pp. 611-613.

116. Owen, T.: Comparisons of Laboratory and Planetary Spectra IV: The Identification of the 7500-A Bands in the Spectra of Uranus and Neptune. Icarus, vol. 6, no. 1, 1967, pp. 108-113.

117. McElroy, M. B.: Atmospheric Composition of the Jovian Planets. J. of the Atmospheric Sciences, vol. 26, part 1, 1969, pp. 798-812.

118. Welsh, H. L.: The Pressure-Induced Infrared Spectrum of Hydrogen and its Application to the Study of Planetary Atmospheres. J. Atmospheric Sciences, vol. 26, 1969, pp. 835-840.

119. Belton, M. J. S.; McElroy, M. B.; and Price, M. J.: The Atmosphere of Uranus. Astrophys. J., vol. 164, no. 1, 1971, pp. 191-209.

120. Teifel, V. G.; and Kharitonova, G. A.: The Molecular Rotational Temperature of Uranus and an Upper Limit on the Pressure in Its Outer Atmosphere. Soviet Astronomy – AJ, vol. 13, no. 5, 1970, pp. 865-873.

121. Lewis, J. S.: Observability of Spectroscopically Active Compounds in the Atmosphere of Jupiter. Icarus, vol. 10, 1969, pp. 393-409.

122. Hauge, Ø.; and Engvold, O.: The Chemical Composition of the Solar Atmosphere. Report No. 31, Institute of Theoretical Astrophysics Blindern, Oslo, 1970.

123. Lewis, J. S.: The Clouds of Jupiter and the NH_3-H_2O and NH_3-H_2S Systems. Icarus, vol. 10, no. 3, 1969, pp. 365-378.

124. Ney, E. P.; and Maas, R.: Infrared Observation of Mercury and Uranus. American Astron. Soc. Bul., vol. 1, 1969, p. 202.

125. Gillett, F. C.; Low, F. J.; and Stein, W. A.: The 2.8-14 Micron Spectrum of Jupiter. Astrophys. J., vol. 157, 1969, pp. 925-934.

126. Trafton, L. M.: Model Atmospheres of the Major Planets. Astrophys. J., vol. 147, no. 2, 1967, pp. 765-781.

127. Fox, K.; and Ozier, I.: The Importance of Methane to Pressure-Induced Absorption in the Atmospheres of the Outer Planets. Astrophys. J., vol. 166, 1971, L95-L100.

128. Lewis, J. S.; and Prinn, R. G.: "Chemistry and Photochemistry of the Atmosphere of Jupiter," Theory and Experiment in Exobiology. A. W. Schwartz (ed.), 1970.

129. Guinan, E. F.; and Shaw, J. S.: The Diameter and Structure of the Atmosphere of Neptune from the Occultation of BD-17° 4388. American Astronomical Soc., Bull., vol. 2, no. 2, 1970, pp. 195-196, (abstract).

130. Urey, H. C.: The Atmospheres of the Planets. Handbuch der Physic, vol. 52, 1959, pp. 363-418.

131. NASA SP-8017, Magnetic Fields – Earth and Extraterrestrial. National Aeronautics and Space Administration, March 1969.

APPENDIX A.
DEFINITION OF SYMBOLS*

A_j	Saturation vapor pressure constant (B-2)
a	Semi-major axis of particle orbiting planet (3.1.2)
α_R	Right ascension of North rotational pole (2.1.3.2)
B_λ, B_υ	Planck function, intensity (per unit wave length or frequency) (3.1.4)
β	Atmospheric lapse rate (P/T)(dT/dP) (B-1)
β_o	Lapse rate constant (B-1)
c	Speed of light (3×10^{10} cm/s) (2.6.1)
C_p, C_v	Specific heats (at constant pressure or volume) (B-1)
γ	Ratio of specific heats (B-1)
Δ	Distance from object to observer (AU) (2.4.2.1)
Δm	Phase coefficient (magnitudes/degree) (2.4.2.1)
δ_R	Declination of North rotational pole (2.1.3.2)
δm	Uncertainty in absolute visual magnitude (2.4.2.1)
E	Charged particle kinetic energy (MeV) (2.6.1)
E_o	Local characteristic (kinetic) energy (MeV) (2.6.4.2)
ϵ	Planetary optical flattening (2.1.2)
F	Integrated flux of electromagnetic radiation (2.4.1)
F_λ, F_υ	Flux (per unit wavelength or frequency) (3.1.4)
G	Constant of gravitation ($6.673 \times 10^{-11} \frac{N \cdot m^2}{Kg^2}$) (2.2)
g	Acceleration of gravity (including rotation) (2.2)
H_p	Atmosphere pressure scale height (B-1)
H_ρ	Atmosphere density scale height (B-1)
H_λ	Solar spectral flux (per unit wavelength) (2.4.1)
$H_\odot$	Solar constant or solar irradiance at 1 AU (1.353×10^{-1} W/cm^{-2})(2.4.1)
I_λ, I_υ	Intensity (per unit wavelength or frequency) (3.1.4)
J_2	Coefficient of gravitational potential (2.2)
K	Constant (cosmic ray flux formula) (2.6.1)

*Numbers in parens give section where symbol used.

K_1	Lapse rate constant (K) (B-1)
K_2	Lapse rate constant (°K) (B-1)
L	Magnetic shell parameter (2.6.4.2)
λ	Wavelength of electromagnetic radiation (3.1.4)
λ_j	Latent heat of condensation (B-2)
M_p	Mass of planet including satellites, if any. Subscripts U, N, P, ⊕, and ∈ refer to Uranus, Neptune, Pluto, Earth and Sun, respectively (2.1.1)
M_o	Rest energy of particle (2.6.1)
$M_\odot$	Mass of the Sun (2.1.1)
$M_\oplus$	Mass of Earth (2.1.1)
m_V	Visual magnitude (2.4.2.1)
m	Mean opposition magnitude (visual) (3.1.4)
m_o	Absolute magnitude (visual) (2.4.2.1)
μ	Mean molecular weight (g/mol) (B-1)
N_o	Number density for charged particles (number per unit area) (2.6.5)
n_i	Mean motion of a satellite (degrees/day) (2.5.1.1)
υ	Wave frequency (3.1.4)
P	Atmospheric pressure (B-1)
P_2	Legendre polynominal (2.2)
p_λ	Geometric albedo (wavelength dependent) (2.4.2)
p_ε	Integrated geometric albedo (2.4.2)
Ψ	Phase angle (2.4.2.1)
R	Distance from center of planet to observer (2.2)
R_g	Universal gas constant (82.082 cm^3 atm/mol·K) (B-1)
R_s	R at reference ellipsoid (3.1.1)
R_{pe}	Polar radius of planet (2.1.2)
R_{eq}	Equatorial radius of planet (2.1.2)
R_p	Distance from planet to Sun (2.4.2)
ρ	Atmospheric gas density (g/cm^3) (B-1)
$\bar{\rho}$	Mean density of planet (2.1.2)

σ	Coefficient of rotational term in gravitational potential (2.2)
S	Observer to Sun distance (AU) (2.4.1)
T	Physical temperature of atmosphere (K) (B-1)
T_D	Disk brightness temperature (K) (2.4.3)
T_{eff}	Effective temperature of object (2.4.3)
T_o	Rotation period (3.1.1)
t	Dummy temperature variable (3.4.1)
U	Gravitational potential function (2.2)
w	Amount of cloud material per unit volume of gas (B-1)
z	Altitude (distance from correspondence level) (2.7.3)
z_o	Altitude of atmospheric reference level (2.7.3)
z_1	Nominal ionosphere altitude (2.6.5)
Φ_E	Flux of particles with energy $\geqslant$ E (2.6.1)
Φ_o	Flux parameter in energetic particle models (2.6.4.2)
Φ	Planetocentric latitude (2.2)
Φ'	Planetographic latitude (2.2)
ω_o	Angular rotation rate (3.1.1)

APPENDIX B.
ATMOSPHERE AND CLOUDS (MATHEMATICAL BASIS)

B-1 Atmospheric Structure

In terms of the symbols defined in appendix A, the model atmospheres of sections 2.7, 3.1.7, and 3.2.7 are governed for each atmospheric region by

hydrostatic equilibrium $$\frac{dP}{dz} = -\rho g \tag{B1}$$

the perfect gas law $$\rho = \mu P/R_g T \tag{B2}$$

a temperature-dependent gradient $$\frac{d \log T}{d \log P} = \beta = \beta_o \frac{T + K_1}{T + K_2} \tag{B3}$$

where values of the constants K_1 and K_2 are restricted by $K_2 \geq 0$ in general, by $K_1 = K_2 = 0$ for regions of constant $\beta = \beta_o \neq 0$, and by $K_1 = -T_A$ and $K_2 = 0$ for regions of $\beta = 0$ (at constant temperature $T = T_A$). Values of K_1 and K_2 can be chosen to ensure that β approximates the adiabatic value $(\gamma - 1)/\gamma$ for a real gas mixture whose specific heats are related by $\gamma = C_p/C_v$. (If C_p and C_v increase with temperature, $K_1 > K_2 > 0$ results.)

The solution of equations B1 through B3 requires that T and z at any value of P be related to those at T_A, z_A, and P_A in the same region by

$$\left(\frac{P}{P_A}\right)^{\beta_o} = \left(\frac{T}{T_A}\right)^{K_2/K_1} \left(\frac{T + K_1}{T_A + K_1}\right)^{(K_1 - K_2)/K_1} \tag{B4}$$

and

$$z = z_A - \frac{R_g}{ug}\left(\frac{T - T_A}{\beta_o} - K_1 \ln \frac{P}{P_A} + \frac{K_2}{\beta_o} \ln \frac{T}{T_A}\right) \tag{B5}$$

The lapse rate and scale heights are given by

$$\left.\begin{aligned} dT/dz &= -\beta ug/R_g \\ H_p &= R_g T/ug \\ H_\rho &= H_p/(1-\beta) \end{aligned}\right\} \tag{B6}$$

B-2 Clouds

It is assumed that clouds are formed by condensation of a species j in convective regions moving upward to lower temperature and pressure when the saturation vapor pressure P_{js} is exceeded by the partial pressure. Condensation of CH_4 results in a decrease in mean molecular weight μ. This decrease in μ is accounted for in the parameters affected (ρ, z, H_p, H_ρ) which are given in the atmosphere tables of sections 3.1.7 and 3.2.7. P_{js} is conventionally described by a form of the Clausius-Clapeyron equation

$$P_{js} = \exp\left[A_j - (\lambda_j / R_g T)\right]$$

where A_j and λ_j are constants, and λ_j is the latent heat of condensation. In this case P_{js} also specifies the partial pressure of the condensible gas in the cloud region above the lowest level of condensation, and the mass of the cloud per unit volume of gas is approximated by

$$w_j = \frac{\mu_j P_{js}}{R_g T}\left(\frac{\beta\lambda_j - R_g T}{\beta\lambda_j}\right) \tag{B7}$$

where β is given by equation B3 and μ_j is the mean molecular weight of the condensate.

Table B-1 lists the four species actually used in computing cloud properties and the appropriate constants.

TABLE B-1.

PARAMETERS OF CONDENSATES

	Liquid H_2O	Solid H_2O (ice)	Solid NH_3 (ice)	Solid CH_4 (ice)
μ_j (g/mol)	18	18	17	16
A_j (for P_{js} in $N \cdot m^2$)	25.485	28.948	28.637	23.543
λ_j (J/mol)	43,321.69	51,188.57	32,397.67	10,619.11

In establishing the location of the cloud bases, condensation to a pure (one molecular species) solution or solid was assumed. For NH_3 - H_2O solutions as dilute as those likely in the Warm Models, the liquid water constants were considered satisfactory approximations. For the Nominal and Cool Models, the existence of NH_3-H_2O solutions could result in the elimination of any solid H_2O phase. The change in mean molecular weight resulting from condensation was roughly accounted for above the base of the CH_4 clouds.

APPENDIX C.

GLOSSARY*

Adiabatic – Characteristic of processes in which heat is not transferred across system boundaries; in an atmosphere, such a system is a hypothetically rising or falling parcel of gas, and the adiabatic requirement must be satisfied when the parcel reaches equilibrium with the local pressure, temperature, and density.

Astronomical Unit (AU) – Approximately, the semi-major-axis of the Earth's orbit about the Sun, Gurnette and Woolley (ref. 73) provide a more precise definition, and a modern value cited by Melbourne et al. (ref. 12) is 1 AU = $1.49597893 \times 10^8 \pm 5$ km.

Bandwidth – The range of frequencies (or wavelengths) within which electromagnetic radiation is emitted or detected; the power or response distributions need not be uniform within this range (refs. 30 and 44).

Bolometric – Characteristic of an infinite **bandwidth**, and including electromagnetic radiation at all frequencies (or wavelengths) and polarizations (ref. 49).

Bond Albedo – The ratio of electromagnetic radiation reflected (in all directions) by an object to that incident on it in a collimated beam. This quantity depends on the **bandwidth** of interest. If the **bandwidth** is infinite, the term **Bolometric** Bond albedo is used.

Brightness Temperature – The temperature at which a blackbody would radiate an intensity of electromagnetic radiation identical to that of the source for the **bandwidth** and polarization considered.

Color – For a given light source, the difference in **magnitude** for two **bandwidths** centered on different wavelengths (ref. 30).

Decametric – Characteristic of electromagnetic radiation at those radio wavelengths between 10 and 100 meters; used here to cover a broader range extending to about 7 meters.

Decimetric – Characteristic of electromagnetic radiation at those microwave wavelengths between 10 and 100 cm; used here synonymously with **UHF** to cover a broader range extending to about 1 cm.

Declination (δ) – The celestial coordinate equal to the geocentric angle (north taken positive) between the direction to the object considered and the plane of the Earth's equator; the precession of the latter implies a slow variation of the declination even of fixed directions (ref. 73).

Disk Brightness Temperature (T_D) – The resulting **brightness temperature** when all radiation (excluding background sources) from a region surrounding an object is associated with the disk of that object; the disk brightness temperature may include a contribution from the radiation belts.

Effective Temperature (T_{eff}) – The temperature at which a black body would radiate a **bolometric** intensity of electromagnetic radiation identical to that of the source (ref. 23).

*Cross references within the glossary are indicated by bold face. These descriptions have been developed for this monograph. Additional information may be found in the references cited.

Flattening (ϵ) – The positive difference between unity and the ratio of the polar to the equatorial diameter of a planetary disk (optical), or the value for the same quantity which would be derived on the basis of hydrodynamic theory and the gravitational potential inferred from observed satellite motions (dynamic).

Flux of Electromagnetic Radiation (F, F_μ, or F_λ) – The power per unit area crossing an imaginary plane surface from one side to the other, either per unit bandwidth or integrated over all frequencies.

Flux of Charged Particles (ϕ_{E}) – The number of particles per unit area and per unit time with energy greater than E crossing an imaginary plane surface with positive or negative (but not both) velocity components perpendicular to the surface.

Geometric Albedo (p_λ) – The ratio of the reflected flux (power per unit detector area) from an astronomical object (observed at distance Δ, zero phase angle) to the quotient of the solar power intercepted by the object divided by $\pi\Delta^2$ in the bandwidth considered. Here the flux, power, and Δ must be expressed in consistent units, and Δ must be large compared to the dimensions of the object (ref. 49).

Intensity (I_μ or I_λ) – The flux of electromagnetic radiation per unit solid angle of the source for a defining imaginary surface whose normal intersects the source; intensity is independent of the source-surface separation.

Ionosphere – The atmospheric layer which includes the major maxima of electron and ion concentration.

Magnetopause – The outer boundary of the magnetosphere, determined by its interaction with the external charged particle and magnetic field environments, particularly the solar wind (ref. 131).

Magnetosphere – The region surrounding a planet in which the local magnetic field is dominated by planet-associated fields rather than by external environments (ref. 131).

Heliosphere – A region surrounding the Sun in which the combined energy density of solar-related particles and fields dominates that of interstellar particles and fields. This region likely extends well beyond the orbit of Jupiter.

Osculating Elements – The elements of a theoretical elliptic orbit in which the velocity and position are identical to those of a planet's actual orbit at a given time.

Magnitude (m) – Five-halves times the common logarithm (base ten) of the ratio of the power received per unit area within some bandwidth for a standard object to that for an astronomical object. The base of this logarithmic scale is $X = 2.512$, such that an increase of one magnitude corresponds to a decrease in power by a factor x^{-1} or an increase in distance by a factor $x^{½}$. Absolute magnitudes (m_o) are those assumed to occur in a standard geometrical configuration, namely, Sun-object distance 1 AU, object-observer distance $\Delta = 1$ AU and phase angle $\Psi = 0$ for solar system objects. Standard objects are commonly defined on the UBVRI system of magnitudes, corresponding to specific wavelength-dependent response characteristic of the observing equipment (refs. 30 and 49).

Phase Angle (Ψ) – The angle formed by the Sun, the point of reflection, and the observer (ref. 30).

Planetocentric – Referenced to the center of the planet.

Planetographic – Referenced to a line parallel to the direction of the zenith at the planet.

Plasma – A gas in which the concentration of charged particles has non-negligible effects on the properties of the gas.

Polodial – A field which has poles. In this context magnetic dipole or magnetic quadrupole fields are said to be polodial in structure.

Rayleigh Scattering – Scattering of electromagnetic radiation by particles whose characteristic size is small compared to the wavelength λ. The scattering cross-section and opacity are proportional to λ^{-4}.

Mean Opposition Distance – The average minimum separation distance between the Earth and an object whose orbit is wholly outside that of the Earth's.

Right Ascension (α) – The celestial coordinate equal to the angle (east taken positive) between the geocentric projection on the plane of the Earth's equator of the object considered and that of the **vernal equinox**: the precession of the Earth's rotation axis implies a slow variation of the right ascension even of fixed directions (ref. 73).

Scale Height (H_p, H_ρ) – A measure of the vertical gradient of a quantity x, e.g., pressure and electron concentration, such that if $H = x\,(dx/dz)^{-1}$ is constant with altitude z, the quantity x changes by a factor e within the altitude interval H.

Stratosphere – The atmospheric layer directly above the **troposphere** within which the temperature is constant or increases with altitude.

Trapped Radiation – Energetic charged particles whose trajectories in a planetary magnetic field are bounded in space. A particle travels nearly along the field line, "mirrors" or is reflected at equal north and south magnetic latitudes, and drifts in longitude.

Tropopause – The upper boundary of the **troposphere**, and the lower boundary of the **stratosphere**, characterized by a near-discontinuity in the temperature gradient.

Troposphere – The atmospheric layer within which major weather phenomena occur, characterized by decreasing temperature with increasing altitude.

Ultra High Frequency (UHF) – Characteristic of electromagnetic radiation at microwave frequencies between 300 and 3000 **Mhz**, used here synonymously with **decimetric** to cover a broader range extending to about 30,000 **Mhz**.

Vernal Equinox – The direction from the center of the Earth to the center of the Sun at the time when the latter lies in the plane of the Earth's equator in March of each year (ref. 73).

Zenith – The direction opposite to that of the local acceleration of gravity (including the centrifugal terms) and perpendicular to the local horizon.

Zenith Angle – The angle between the directions to the **zenith** and to an object observed.

NASA SPACE VEHICLE DESIGN CRITERIA MONOGRAPHS

ENVIRONMENT

SP-8005	Solar Electromagnetic Radiation, revised May 1971
SP-8010	Models of Mars Atmosphere (1967), May 1968
SP-8011	Models of Venus Atmosphere (1968), December 1968
SP-8013	Meteoroid Environment Model–1969 (Near Earth to Lunar Surface), March 1969
SP-8017	Magnetic Fields–Earth and Extraterrestrial, March 1969
SP-8020	Mars Surface Models (1968), May 1969
SP-8021	Models of Earth's Atmosphere (120 to 1000 km), May 1969
SP-8023	Lunar Surface Models, May 1969
SP-8037	Assessment and Control of Spacecraft Magnetic Fields, September 1970
SP-8038	Meteoroid Environment Model–1970 (Interplanetary and Planetary), October 1970
SP-8049	The Earth's Ionosphere, March 1971
SP-8067	Earth Albedo and Emitted Radiation, July 1971
SP-8069	The Planet Jupiter (1970), December 1971
SP-8084	Surface Atmospheric Extremes (Launch and Transportation Areas), May 1972
SP-8085	The Planet Mercury (1971), March 1972
SP-8091	The Planet Saturn (1970), June 1972
SP-8092	Assessment and Control of Spacecraft Electromagnetic Interference, June 1972

STRUCTURES

SP-8001	Buffeting During Atmospheric Ascent, revised November 1970
SP-8002	Flight-Loads Measurements During Launch and Exit, December 1964

SP-8003	Flutter, Buzz, and Divergence, July 1964
SP-8004	Panel Flutter, July 1964
SP-8006	Local Steady Aerodynamic Loads During Launch and Exit, May 1965
SP-8007	Buckling of Thin-Walled Circular Cylinders, revised August 1968
SP-8008	Prelaunch Ground Wind Loads, November 1965
SP-8009	Propellant Slosh Loads, August 1968
SP-8012	Natural Vibration Modal Analysis, September 1968
SP-8014	Entry Thermal Protection, August 1968
SP-8019	Buckling of Thin-Walled Truncated Cones, Septembe 1968
SP-8022	Staging Loads, February 1969
SP-8029	Aerodynamic and Rocket-Exhaust Heating During Launch and Ascent, May 1969
SP-8031	Slosh Suppression, May 1969
SP-8032	Buckling of Thin-Walled Doubly Curved Shells, August 1969
SP-8035	Wind Loads During Ascent, June 1970
SP-8040	Fracture Control of Metallic Pressure Vessels, May 1970
SP-8042	Meteoroid Damage Assessment, May 1970
SP-8043	Design Development testing, May 1970
SP-8044	Qualification testing, May 1970
SP-8045	Acceptance testing, April 1970
SP-8046	Landing Impact Attenuation for Non-Surface-Planing Landers, April 1970
SP-8050	Structural Vibration Prediction, June 1970
SP-8053	Nuclear and Space Radiation Effects on Materials, June 1970
SP-8054	Space Radiation Protection, June 1970
SP-8055	Prevention of Coupled Structure-Propulsion Instability (Pogo), October 1970

SP-8056	Flight Separation Mechanisms, October 1970
SP-8057	Structural Design Criteria Applicable to a Space Shuttle, January 1971
SP-8060	Compartment Venting, November 1970
SP-8061	Interaction with Umblicals and Launch Stand, August 1970
SP-8062	Entry Gasdynamic Heating, January 1971
SP-8063	Lubrication, Friction, and Wear, June 1971
SP-8066	Deployable Aerodynamic Deceleration Systems, June 1971
SP-8068	Buckling Strength of Structural Plates, June 1971
SP-8072	Acoustic Loads Generated by the Propulsion System, June 1971
SP-8077	Transportation and Handling Loads, September 1971
SP-8079	Structural Interaction with Control Systems, November 1971
SP-8082	Stress-Corrosion Cracking in Metals, August 1971
SP-8083	Discontinuity stresses in Metallic Pressure Vessels, November 1971
SP-8095	Preliminary Criteria for the Fracture Control of Space Shuttle Structures, June 1971

GUIDANCE AND CONTROL

SP-8015	Guidance and Navigation for Entry Vehicles, November 1968
SP-8016	Effects of Structural Flexibility on Spacecraft Control Systems, April 1969
SP-8018	Spacecraft Magnetic Torques, March 1969
SP-8024	Spacecraft Gravitational Torques, May 1969
SP-8026	Spacecraft Star Trackers, July 1970
SP-8027	Spacecraft Radiation Torques, October 1969
SP-8028	Entry Vehicle Control, November 1969
SP-8033	Spacecraft Earth Horizon Sensors, December 1969
SP-8034	Spacecraft Mass Expulsion Torques, December 1969

SP-8036	Effects of Structural Flexibility on Launch Vehicle Control Systems, February 1970
SP-8047	Spacecraft Sun Sensors, June 1970
SP-8058	Spacecraft Aerodynamic Torques, January 1971
SP-8059	Spacecraft Attitude Control During Thrusting Maneuvers, February 1971
SP-8065	Tubular Spacecraft Booms (Extendible, Reel Stored), February 1971
SP-8070	Spaceborne Digital Computer Systems, March 1971
SP-8071	Passive Gravity-Gradient Libration Dampers, February 1971
SP-8074	Spacecraft Solar Cell Arrays, May 1971
SP-8078	Spaceborne Electronic Imaging Systems, June 1971
SP-8086	Space Vehicle Displays Design Criteria, March 1972
SP-8098	Effects of Structural Flexibility on Entry Vehicle Control Systems, June, 1972

CHEMICAL PROPULSION

SP-8025	Solid Rocket Motor Metal Cases, April 1970
SP-8039	Solid Rocket Motor Performance Analysis and Prediction, May 1971
SP-8041	Captive-Fired Testing of Solid Rocket Motors, March 1971
SP-8048	Liquid Rocket Engine Turbopump Bearings, March 1971
SP-8051	Solid Rocket Motor Igniters, March 1971
SP-8052	Liquid Rocket Engine Turbopump Inducers, May 1971
SP-8064	Solid Propellant Selection and Characterization, June 1971

NASA-Langley, 1972 —— 30